To the Graduate Council:

I am submitting herewith a dissertation written by Seth Andrew Albright entitled "NMR Structural Studies of Endotoxin Receptor CD14 in Complex with Gram-Negative and Gram-Positive Endotoxin." I have examined the final electronic copy of this thesis for form and content and recommend that it be accepted in partial fulfillment of the requirements for the degree of Doctor of Philosophy, with a major in Biochemistry, Cellular, and Molecular Biology.

_____
Nitin U. Jain, Major Professor

We have read this dissertation
and recommend its acceptance:

_____
Gladys M. Alexandre

_____
Michael D. Best

_____
Engin H. Serpersu

_____
Pamela L. Small

Accepted for the Council:

_____
Carolyn R. Hodges
Vice Provost and Dean of the Graduate School

(Original signatures are on file with official student records.)

NMR Structural Studies of Endotoxin Receptor CD14 in Complex with Gram-Negative and Gram-Positive Endotoxin

A Dissertation Presented
for the Doctor of Philosophy
Degree
The University of Tennessee, Knoxville

Seth Andrew Albright
August 2011

ACKNOWLEDGEMENTS

First I must thank my patient and caring wife Cindy. I am deeply indebted to her for her support and patience through the long nights of caring for cultures and running experiments. She has supported me through the ups and downs of school and research, and for that I will always be grateful. Although she is too little to know, I am thankful to my daughter Laurel for putting a smile on my face every time I see her, and brightening many a long day. I also wish to thank all my family: The Albrights – Steve (Dad), Peggy (Mom), Austin, Misty, Kevin and Manju, The Tuckers – Raymond and Renee, and The Beasleys – Randy and Shirley. They have supported me all these years and forgiven me on numerous occasions for being late to the many family get togethers when I have gotten stuck in the lab completing experiments.

I want thank Dr. Jain for taking me into his lab and supporting and guiding my research. I have learned a great many skills through his willingness to let me learn things on my own. I have learned much from his tough questions and critiques, and I am extremely grateful to him for all this and more.

I am also grateful to the many undergrads that worked in the lab over the years. I could not have completed as much work as I did with out the faithful few that helped bear the *Pichia* culture and purification workload. I am especially grateful for the dedicated few that were kind enough to come into the lab during football season to feed the *Pichia* cultures. You kept me from having to spend hours fighting gameday traffic to do a 10 minute job, thank you.

I want to thank Dr. Carlos Steren for the friendship and advice he shared with me over many spectrometer helium fills. I also want to thank Dr. Wei Zhang who taught me the basics of using NMRPipe, and made the human CD14 homology model. I also must thank Dr. Prashansa Agrawal who taught me how to perform NMR assignments, and helped assign the Kdo_2-Lipid A structure.

ABSTRACT

Endotoxin recognition by the innate immune receptor CD14 is a critical part of the innate immune system's early detection and activation of the inflammatory response during microbial invasion. The differential recognition and high affinity binding of endotoxins from gram-negative and gram-positive bacteria is performed by the innate immune receptor CD14. Upon endotoxin binding, CD14 transfers the specific endotoxins to a Toll-like receptor signaling complex, which is responsible for initiating the intracellular signaling cascade. In the presence of overwhelming infection, the effects of CD14 lead to the over-activation of the inflammatory response, which results in the life threatening condition known as sepsis.

Preparation of a ^{15}N isotopically labeled truncated version of soluble CD14, using *Pichia pastoris*, allowed direct structural observation of the binding interaction between CD14 and two endotoxin ligands, lipopolysaccharide (LPS) and lipoteichoic acid (LTA), from gram-negative and gram-positive bacteria, respectively using solution NMR spectroscopy. These studies revealed that CD14 uses both a common set of residues, and endotoxin specific subsets of residues, to bind LPS and LTA.

To further investigate the structural features of each endotoxin recognized by CD14, ^{13}C ^{15}N isotopically labeled Kdo_2–Lipid A, a fully active chemically defined gram-negative endotoxin, and LTA lipid anchor, the minimal unit of LTA, were produced. This allowed detailed NMR spectral mapping of these agonist ligands bound to sCD14 which identified, for the first time, structural regions and features in each that are strongly affected during complex formation with sCD14.

Additionally, the presence of differential dynamic behavior was seen in both CD14 and the ligands upon complexation. This behavior suggests a likely role for dynamics in the mechanism of pattern recognition by CD14, which uses the dynamic ability of specific residue combinations to differentially affect endotoxin binding. Using NMR, the dynamic behavior of CD14 was further investigated using temperature and pH-dependence studies of isotopically labeled CD14. These studies clearly demonstrated the presence of multiple conformations for several residues, and may provide a possible explanation for the broad specificity of ligand binding by CD14.

In addition, the spin-labeling of isotopically labeled lipid A enabled the collection of intermolecular distances on CD14 bound lipid A.

TABLE OF CONTENTS

CHAPTER 1. BACKGROUND AND INTRODUCTION 1

1.1 THE IMPACT OF SEPSIS 1

1.2 SEPSIS AND THE INFLAMMATORY RESPONSE 2

1.2.1 THE INFLAMMATORY RESPONSE SIGNAL CASCADE 6

1.3 BACTERIAL ENDOTOXINS 10

1.3.1 GRAM-NEGATIVE ENDOTOXIN 10

1.3.2 GRAM-POSITIVE ENDOTOXIN 14

1.4 CD14 17

1.4.1 CD14 STRUCTURAL FEATURES 19

1.4.2 CD14 LIGAND BINDING 25

CHAPTER 2. EXPRESSION, PURIFICATION, CHARACTERIZATION, AND ISOTOPIC LABELING OF SOLUBLE CD14 AND THE ENDOTOXIN LIGANDS Kdo_2-LIPID A AND LIPOTEICHOIC ACID 32

2.1 INTRODUCTION 32

2.2 MATERIALS AND METHODS 39

2.2.1 DESIGN OF SOLUBLE CD14 CONSTRUCT 39

2.2.2 TRANSFORMATION OF *Pichia pastoris* 39

2.2.3 SCREENING OF *Pichia pastoris* CLONES FOR HIGH EXPRESSION 41

2.2.4 EXPRESSION AND PURIFICATION OF SOLUBLE CD14 42

2.2.5 GROWTH, EXTRACTION, AND PURIFICATION OF Kdo_2-LIPID A 43

2.2.6 PREPARATION OF Kdo_2-LIPID A AND LIPOTEICHOIC ACID STRUCTURAL VARIANTS 45

2.3 RESULTS AND DISCUSSION 48

2.3.1 EXPRESSION, PURIFICATION, CHARACTERIZATION, AND ISOTOPIC LABELING OF SOLUBLE CD14 IN *Pichia pastoris* 48

2.4.2 EXPRESSION, PURIFICATION, CHARACTERIZATION, AND ISOTOPIC LABELING OF Kdo_2-LIPID A AND LIPOTEICHOIC ACID 59

CHAPTER 3. SOLUTION NMR STUDIES PROVIDE A STRUCTURAL BASIS FOR ENDOTOXIN PATTERN RECOGNITION BY THE INNATE IMMUNE RECEPTOR CD14 64

3.1 INTRODUCTION 64

3.2 MATERIALS AND METHODS 66

3.2.1 EXPRESSION AND PURIFICATION OF ISOTOPICALLY LABELED RECOMBINANT SOLUBLE CD14 IN *Pichia pastoris* 66

3.2.2 BIOLOGICAL ACTIVITY ASSAYS ON RECOMBINANT SOLUBLE CD14-ENDOTOXIN BINDING DOMAIN 68

3.2.3 NMR STUDIES OF SOLUBLE CD14 — ENDOTOXIN INTERACTIONS 69

3.3 RESULTS AND DISCUSSION 69

3.3.1 EXPRESSION AND ISOTOPIC LABELING OF SOLUBLE CD14 IN *Pichia pastoris* 69

3.3.2 DETERMINATION OF BIOLOGICAL ACTIVITY OF SOLUBLE CD14 72

3.3.3 CHANGES IN NMR SPECTRA OF CD14 UPON ENDOTOXIN BINDING PROVIDES STRUCTURAL EVIDENCE FOR PATTERN RECOGNITION 74

CHAPTER 4. NMR SPECTRAL MAPPING OF THE LIPID A MOLECULAR PATTERNS AFFECTED BY INTERACTION WITH THE INNATE IMMUNE RECEPTOR CD14 83

4.1 INTRODUCTION 83

4.2 MATERIALS AND METHODS 86

4.2.1 PREPARATION AND ISOTOPIC LABELING OF Kdo_2-LIPID A IN *Escherichia coli* WBB06 86

4.2.2 NMR MEASUREMENTS ON Kdo_2 –LIPID A COMPLEXED WITH SOLUBLE CD14 87

4.3 RESULTS AND DISCUSSION 88

4.3.1 PREPARATION AND ISOTOPIC LABELING OF Kdo_2-LIPID A IN HEPTOSETRANSFERASE–DEFICIENT *Escherichia coli* STRAIN 88

4.3.2 NMR ANALYSIS OF THE Kdo_2-LIPID A COMPLEXED WITH CD14 93

CHAPTER 5. NMR SPECTRAL MAPPING OF LIPOTEICHOIC ACID MOLECULAR PATTERNS INTERACTING WITH THE ENDOTOXIN RECEPTOR CD14 106

5.1 INTRODUCTION 106

5.2 MATERIALS AND METHODS 108

5.2.1 GROWTH, EXTRACTION, AND PURIFICATION OF LIPOTEICHOIC ACID FROM *Bacillus subtilis* ATCC 6633™ 108

5.2.2 NMR MEASUREMENTS ON LTA LIPID ANCHOR BOUND TO SOLUBLE CD14 109

5.3 RESULTS AND DISCUSSION 110

5.3.1 PREPARATION AND ISOTOPIC LABELING OF LIPOTEICHOIC ACID IN *Bacillus subtillis* ATCC 6633™ 110

5.3.2 NMR ANALYSIS OF LIPOTEICHOIC ACID IN COMPLEX WITH SOLUBLE CD14 111

CHAPTER 6. THE ROLE OF DYNAMICS IN THE INTERACTION OF CD14 WITH ENDOTOXINS 118

6.1 INTRODUCTION 118

6.2 MATERIALS AND METHODS 120

6.2.1 EXPRESSION AND PURIFICATION OF ISOTOPICALLY LABELED SOLUBLE CD14 120

6.2.2 NMR STUDIES ON THE TEMPERATURE AND pH DEPENDENCE OF SOLUBLE CD14 120

6.3 RESULTS AND DISCUSSION 121
6.3.1 ENHANCEMENT OF SOLUBLE CD14 SOLUTION STABILITY 121
6.3.2 TEMPERATURE AND pH DEPENDENT CHANGES IN THE NMR SPECTRA OF CD14 122

CHAPTER 7. USE OF A SPIN-LABELED LIPID A TO MEASURE DISTANCE RESTRAINTS FOR LIPID A IN COMPLEX WITH CD14 129

7.1 INTRODUCTION 129

7.2 MATERIALS AND METHODS 131
7.2.1 PREPARATION, SPIN-LABELING, AND PURIFICATION OF ^{13}C LIPID A 131
7.2.2 CHARACTERIZATION OF SPIN-LABELED ^{13}C LIPID A BY EPR AND MALDI-TOF 132
7.2.3 NMR MEASUREMENTS OF SPIN-LABELED ^{13}C LIPID A IN COMPLEX WITH SOLUBLE CD14 134

7.3 RESULTS AND DISCUSSION 135
7.3.1 PREPARATION AND CHARACTERIZATION OF SPIN-LABELED ^{13}C ^{15}N LIPID A 135
7.3.2 NMR ANALYSIS OF SPIN-LABELED LIPID A IN COMPLEX WITH CD14 140
7.3.3 CALCULATION OF INTENSITY BASED DISTANCES FOR CD14 BOUND SPIN-LABELED LIPID A 142

CHAPTER 8. CONCLUSIONS 149

REFERENCES 152

APPENDICES 167

A.1 ^{1}H AND ^{13}C NMR ASSIGNMENTS FOR *Escherichia coli* Kdo$_2$-LIPID A 168

A.2 WESTERN BLOT PROCEDURES FOR ANALYSIS OF *Pichia pastoris* EXPRESSED SOLUBLE CD14 170

VITA 173

LIST OF TABLES

Table 1. Bacterial, Microbial, Viral, and Host derived CD14 ligands 28

Table 2: Intermolecular distances calculated for spin-labeled lipid A 146

Table A1. ^{1}H and ^{13}C NMR assignments for *E. coli* Kdo$_2$-Lipid A.....168

LIST OF FIGURES

Figure 1.1: General progression of sepsis from gram-negative bacterial infection.... 5

Figure 1.2: Toll-like Receptor MyD88-dependent and MyD88-independent signaling cascade. 9

Figure 1.3: Chemical schematic of Lipopolysaccharide, Lipid A, and antagonistic Lipid IVa. 13

Figure 1.4: Structural schematic of Lipoteichoic acid. 16

Figure 1.5: Crystal structure of full-length murine soluble CD14. 21

Figure 1.6: Homology Model of the 152-residue N-terminal truncation of human soluble CD14. 24

Figure 2.1: Agonist and Antagonist partial structures of Kdo_2-Lipid A, Lipid A, and Lipoteichoic acid partial structures. 37

Figure 2.2: Schematic for cloning of soluble CD14 into the pPICZαA vector. 49

Figure 2.3: SDS-PAGE and Western Blot analysis of soluble CD14 expressed in *Pichia pastoris*. 51

Figure 2.4: SDS-PAGE of soluble CD14 expressed in *Pichia pastoris* deglycosylated by PNGase F. 53

Figure 2.5: Far-UV Circular Dichroism spectra of soluble CD14. 53

Figure 2.6: Biological activity analysis of soluble CD14 with endotoxin ligands. 55

Figure 2.7: ^{1}H-^{15}N HSQC of isotopically labeled soluble CD14 expressed in *Pichia pastoris*. 58

Figure 2.8: ^{1}H-^{13}C HSQC spectrum of ^{13}C isotopically labeled Lipid A. 60

Figure 2.9: ^{1}H-^{13}C HSQC spectrum of ^{13}C isotopically labeled full-length Lipoteichoic acid. 63

Figure 3.1: Far-UV circular dichrosim spectra of soluble CD14 with and without ReLPS. 71

Figure 3.2 Biological activity analysis of soluble CD14 with endotoxin ligands. 73

Figure 3.3: Changes upon endotoxin addition to the ^{1}H-^{15}N HSQC spectra of soluble CD14. 77

Figure 3.4: ^{1}H-^{15}N HSQC spectrum of exchange rate changes in ReLPS bound soluble CD14. 81

Figure 4.1: Biological activity assay of endotoxin ligands with soluble CD14. 90

Figure 4.2: The ^{1}H-^{13}C HSQC spectrum of ^{13}C isotopically labeled Kdo_2-Lipid A. 92

Figure 4.3: Chemical schematic of Kdo_2-Lipid A structure. 94

Figure 4.4: Comparison of spectral characteristics in the ^{1}H–^{13}C HSQC spectra of ^{13}C labeled Kdo_2–Lipid A corresponding to the lower half of the acyl chain region. 95

Figure 4.5: Comparison of spectral changes in the upper acyl chain resonances of Kdo_2-Lipid A upon interaction with soluble CD14. 98

Figure 4.6: Comparison of spectral changes in the sugar headgroup and Kdo units of Kdo_2-Lipid A upon soluble CD14 binding. 101

Figure 4.7: Summary of Kdo_2-Lipid A features affected upon interaction with soluble CD14. 103

Figure 5.1: Structural schematic of LTA lipid anchor. 113

Figure 5.2: Comparison of ^{1}H-^{13}C HSQC spectra of the acyl chain region of LTA's lipid anchor upon interaction with soluble CD14. 115

Figure 6.1: Temperature-dependent changes in ^{1}H-^{13}C HSQC spectrum of CD14. 125

Figure 6.2: pH-dependent changes in ^{1}H-^{13}C HSQC spectrum of soluble CD14.... 127

Figure 7.1: EPR spectra of Spin-Labeled Lipid A in aqueous and organic solvent. 137

Figure 7.2: MALDI-TOF spectra of spin-labeled ^{13}C ^{15}N Lipid A. 139

Figure 7.3: Spin-labeled lipid A schematic indicating atoms for which distances were determined. 147

LIST OF ABBREVIATIONS AND SYMBOLS

5'AOX1	primer for the 5' direction of the alcohol oxidase 1 sequence in pPICZαA
3'AOX1	primer for the 3' direction of the alcohol oxidase 1 sequence in pPICZαA
$^{13}C_6$ glucose	Glucose labeled at all 6 carbon positions with C^{13} isotope
^{15}N ammonium sulfate	ammonium sulfate with nitrogen isotope N^{15}
Å	angstrom (10^{-10} m); unit of distance
α methylene	the first methylene after the hydroxyl in an acyl chain
α/β-fold	an overall protein fold containing a mixture of α helical and β sheet secondary structures
β methylene	the second methylene after the hydroxyl in an acyl chain
γ methylene	the third methylene after the hydroxyl in an acyl chain
μg/ml	microgram (10^{-6} grams) per milliliter
ºC	degrees Celsius; unit of temperature
Ala	alanine
Asn	asparagine
BMMY	buffered methanol-complex medium
CD	circular dichroism spectroscopy
CD14	cluster of differentiation 14 protein
CHO cells	Chinese hamster ovary cells
COSY	correlation spectroscopy
D_5-glycine	glycine with deuterium replacing all 5 protons
D-Ala	the uncommon optical isomer of L-Ala,
DHB	2,5-dihydroxybenzoic acid
DIC	disseminated intravascular coagulation
DTT	dithiothreitol
EPR	electron paramagnetic resonance spectroscopy
FLS2	flagellin-sensing 2
Glu	glutamic acid
GPI-anchor	glycosylphosphatidylinositol-anchor
HIC	hydrophobic interaction chromatography
HSQC	Heteronuclear Single Quantum Coherence
HRP	horseradish peroxidase
ICU	intensive care unit
IFN-β	interferon-β
IKK	inhibitor of nuclear factor-κB (IκB)- kinase
IKKα	inhibitor of nuclear factor-κB (IκB)- kinase α
IKKβ	inhibitor of nuclear factor-κB (IκB)- kinase β
IKKγ	inhibitor of nuclear factor-κB (IκB)- kinase γ
IκB	inhibitor of nuclear factor-κB (IκB
IL-1	interleukin-1
IL-6	interleukin-6

IL-8	interleukin-8
IL-12	interleukin-12
IMAC	immobilized metal ion affinity chromatography
IRAK	IL-1R-associated kinase
IRAK1	IL-1R-associated kinase 1
IRAK4	IL-1R-associated kinase 4
IRF3	interferon-regulatory factor 3
kDa	kilodalton (10^3Daltons); unit of mass
Kdo	3-deoxy-D-*manno*-oct-2-ulosonic acid
Kdo_2-Lipid A	Lipid A with two 3-deoxy-D-*manno*-oct-2-ulosonic acid units
L	liter
LBP	lipopolysaccharide-binding protein
LPS	lipopolysaccharide
LRR	leucine-rich repeat
LTA	lipoteichoic acid
Lys	lysine
M	molar
MAPK	mitogen-activated protein kinase
mCD14	membrane bound CD14
MD-2	myeloid differentiation protein 2
MALDI-TOF	matrix-assisted laser desorption/ionization time-of-flight mass spectrometry
MDa	megadalton (10^6) Daltons: unit of mass
MDP	muramyl dipeptide
mg/ml	milligrams (10^{-3} grams) per milliliter
MHz	megahertz (10^6 hertz); unit of frequency
mmol	millimole (10^{-3} moles); unit of concentration
mM	millimolar (10^{-3} moles per liter): unit of concentration
MyD88	myeloid differentiation primary-response protein 88
m/z	mass to charge ratio, X-axis units in mass spectrometry
NF-κB	nuclear factor- kappa B
N-linked glycosylations	asparagine linked glycan chains
NMR	Nuclear Magnetic Resonance
NOD1	Nucleotide-binding oligomerization domain-containing protein 1
NOD2	Nucleotide-binding oligomerization domain-containing protein 2
NOESY	nuclear Overhauser effect spectroscopy
N-terminal/terminus	the amine terminal end of a protein sequence
OD_{600}	optical density measured by the absorbance at 600nm
PAMP	pathogen-associated molecular pattern
PBS	phosphate buffered saline
PGN	peptidoglycan

PNGase F	peptide-N4-(N-acetyl-beta-glucosaminyl)asparagine amidase F; cleaves asparagine-linked glycosylations
pPICZαA	expression plasmid for *Pichia pastoris* vector containing zeocin resistance gene, and α-factor secretion signal
PRE	paramagnetic relaxation enhancement
PRR	pattern recognition receptor
ReLPS	*Salmonella Minnesota* strain Re 595 (Re mutant) LPS
rhCD14	recombinant human CD14
rhLBP	recombinant human LPS-binding protein
SacI	S*treptomyces achromogenes* restriction enzyme I
sCD14	soluble CD14
SDS-PAGE	sodium dodecyl sulfate-polyacrylamide gel electrophoresis
SEAP	secreted embryonic alkaline phosphate
TAB1	TAK1-binding protein 1
TAB2	TAK1-binding protein 2
TAK1	transforming-growth factor- β-activated kinase
TBK1	TRAF-family-member-associated NF-κB activator (TANK)-binding kinase 1
TBST	Tris buffered saline and Tween-20
THP1	Human acute monocytic leukemia cell line
THP1-Blue	Human acute monocytic leukemia cell line, stably transfected with NF-κB inducible SEAP reporter
TIR	Toll/IL-1 receptor domain
TIRAP	TIR-domain-containing adaptor protein
TLR	Toll-like receptor
TLR2	Toll-like receptor 2
TLR4	Toll-like receptor 4
TLR5	Toll-like receptor 5
TLR6	Toll-like receptor 6
TRAF6	tumor-necrosis-factor receptor-associated factor 6
TRAM	TRIF-related adaptor molecule
TRIF	TIR-domain-containing adaptor protein inducing IFN-β
TRIS-HCl	2-amino-2-(hydroxymethyl)propane-1,3-diol-hydrochloride
v/v	volume per volume solution mixture
X-33	a wildtype *Pichia pastoris* strain
YPD	yeast extract peptone dextrose medium
YPDS	yeast extract peptone dextrose sorbitol medium

CHAPTER 1. BACKGROUND AND INTRODUCTION

1.1 THE IMPACT OF SEPSIS

Sepsis is a condition resulting from overwhelming infection; the host's innate inflammatory response becomes over-activated causing dire physiological effects known collectively as sepsis or septic shock. The over-activation of the inflammatory response in sepsis can ultimately lead to multiple organ failure and death. Sepsis is one of the leading causes of death worldwide. During host infection, a wide variety of bacterial and microbial endotoxins such as lipopolysaccharide (LPS) and lipoteichoic acid (LTA) are responsible for activating the non-specific inflammatory response. In the past, gram-negative bacterial infections were the primary cause of sepsis, but since the late 1980's gram-positive bacteria have also become a leading cause of sepsis in the United States (*1*).

Sepsis is a growing global health threat requiring an increasing allocation of resources. Advances in medical treatments and technologies have lengthened the time that patients can survive with serious underlying medical issues, which compromise their immune systems, and often necessitate extended hospitalizations or immunosuppressive therapies. There are approximately 750,000 cases of sepsis in the US each year resulting in roughly 215,000 fatalities (*2*). The overall mortality rate for sepsis is 30%. In the elderly, the rate rises to 40% and in severe cases of sepsis, known as septic shock, the mortality rate exceeds 50% (*3*). As the US population continues to shift disproportionately towards an elderly populace the occurrence of severe sepsis is

projected to exceed the rate of population growth within 50 years (*2*). The rising incidence of sepsis is further compounded by the escalating occurrence of antibiotic resistant bacterial strains and their growing prevalence as a source of nosocomial infections (*4*).

In 2003 the Society of Critical Care Medicine, the European Society of Intensive Care Medicine, and the International Sepsis Forum launched the Surviving Sepsis Campaign with the objective of reducing severe sepsis mortalities by 25% over five years. While successful in improving patient outcomes and early sepsis identification and treatment, the campaign, which concluded in 2008, was only able to reduce the ICU mortality rate for participating hospitals by 20% (*5*). A major limitation in combating sepsis still remains the lack of effective treatments for sepsis in addition to treatment of the ensuing dysregulation it causes. At this time, drotrecogin alfa (activated), the only drug FDA approved to combat the effects of septic shock yields only a 6.1% reduction in absolute risk of death, and increases the risk of serious bleeding events (*6*). Understanding how the innate immune receptor CD14 recognizes endotoxins and facilitates the over-activation of the inflammatory response may hold the key to advancing the fight against sepsis.

1.2 SEPSIS AND THE INFLAMMATORY RESPONSE

There are three stages of sepsis, progressively increasing in both severity and mortality rate. The characterization of each stage was defined by the international sepsis definition conference with the first stage being sepsis, which is defined “by the presence

of both infection and a systemic inflammatory response". The second stage is severe sepsis, which is characterized as "sepsis complicated by organ dysfunction", and the most advanced stage is known as septic shock, which is "a state of acute circulatory failure characterized by persistent arterial hypotension unexplained by another cause" (*7*). Because these definitions do not describe individual disorders, but rather the differences between the escalating stages of severity in the same condition, for simplicity sake, the term sepsis will be used to refer to all three stages in this dissertation.

The inflammatory response is the non-specific, rapid response to general injury or infection in a host. This non-specific response allows a host to mount an immediate defense to an infection or injury much earlier than the pathogen specific adaptive immune response that follows. Inflammation also plays a critical role in many other biological processes from chronic inflammatory diseases such as rheumatoid arthritis, atherosclerosis, chronic pulmonary disease, and even contributes to increased insulin resistance in diabetics (*8-11*). In the case of infection, the innate immune system typically responds to a component of a bacterial invader's cell wall known as an endotoxin. In the case of a gram-negative bacterial infection, the endotoxin is the cell wall component LPS. In essence, the LPS molecule is first bound by the lipopolysaccharide-binding protein (LBP), followed by transfer of the LPS molecule to CD14, the primary innate immune receptor. CD14 is principally located on the surface of macrophages and monocytes (*12*). The CD14-bound LPS is then presented to the Toll-like receptor 4 transmembrane signaling complex resulting in the initiation of an inflammatory response (**Figure 1.1**). Activation of the inflammatory response leads to initiation of a signaling cascade,

described in greater detail later, which results in a massive mobilization of pro-inflammatory mediators, such as cytokines, chemokines, prostaglandins, lipid mediators, and reactive oxygen species (*3, 13*). In addition, this innate immune response triggers the activation and movement of several types of immune cells, including leukocytes, neutrophils, and macrophages, from the capillaries into the surrounding tissues (*13*). The recruitment of activated immune cells to a site of need introduces additional quantities of pro-inflammatory mediators stimulating the coagulation cascade. The influx of cytokines in combination with increased blood flow and activation of the coagulation cascade leads to a general "leakiness" of the tissues at and around the site(s) of inflammation (*13-15*). This vascular and endothelial compromise becomes increasingly severe as sepsis progresses, ultimately resulting in disseminated intravascular coagulation (DIC) and severe hypoperfusion. The ultimate consequences of this excessive inflammatory response are acute coagulopathies and the failure of multiple organ systems (**Figure 1.1**). Even if effective antimicrobial therapy is initiated, the inflammatory cascade will not abate. Its effects can be likened to a line of dominoes. The first domino to fall, injury or infection, will set a chain reaction in motion. Even if the first domino is set back up (treatment of the initial insult) the subsequent dominoes (the inflammatory cascade) continue to fall.

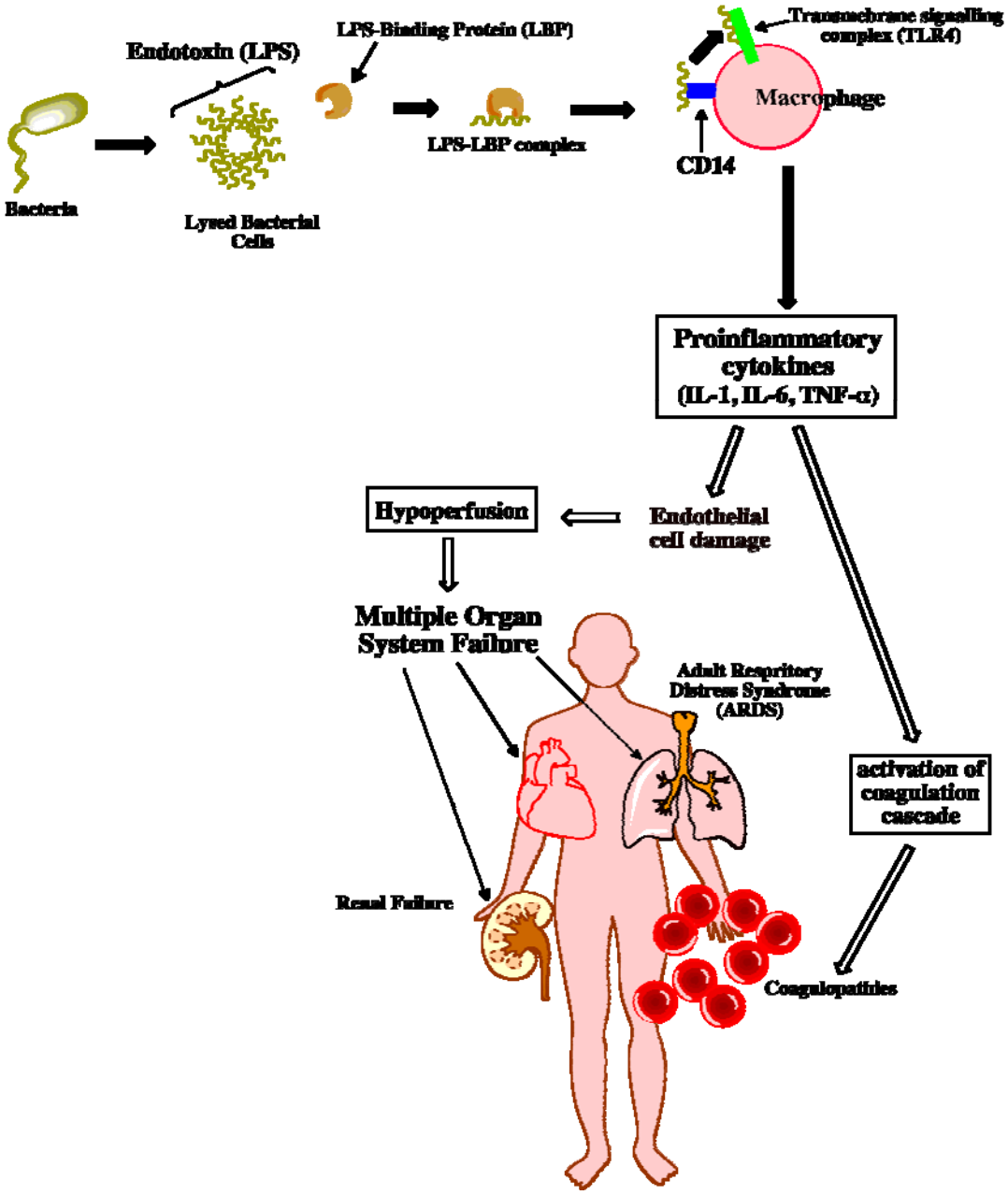


Figure 1.1: General progression of sepsis from gram-negative bacterial infection.

Infection via gram-negative bacteria leads to the release of its endotoxin LPS. LPS molecules are then bound by LPS-binding protein (LBP). The LPS molecule is transferred from LBP to CD14 on the surface of a macrophage. CD14 then presents the endotoxin to the transmembrane signaling complex, Toll-like receptor 4 (TLR4). This activates a signal cascade resulting in the release of cytokines. The action of cytokines and other inflammatory mediators cause hypoperfusion and full activation of the coagulation cascade. These disorders result in multiple organ system failure and severe coagulopathies.

1.2.1 THE INFLAMMATORY RESPONSE SIGNAL CASCADE

The effectiveness of the innate immune system's response is in part due to its ability to amplify its response to pathogens (*16*). The detection of pathogens by the innate immune system depends on a series of proteins, each performing specialized roles. These proteins include LBP, which functions as a carrier protein for LPS monomers, CD14, the key host cell surface receptor responsible for binding endotoxins and initiating the innate immune response, and the Toll-like receptors, which initiate the intracellular signaling cascade in response to specific endotoxins (*17-19*). Although CD14 is able to bind endotoxins with high affinity, it is unable to further transduce the signal since it is not a transmembrane protein. It must complex with one or more of the Toll-like receptors, which possess transmembrane domains, allowing it to stimulate the cell's immune response. Like CD14, Toll-like receptors (TLRs) recognize specific molecular patterns that are present in microbial and bacterial components. Currently, eleven human TLRs have been identified, all sharing several common features such as an extracellular domain consisting of multiple leucine-rich repeats and a cytoplasmic Toll/IL-1 receptor domain (TIR) (*20, 21*). Each TLR recognizes specific structural components of bacterial, microbial, or viral pathogens and induces an immune response (*22*). It has been observed that CD14 complexes with different TLRs depending on the endotoxin ligand bound and up-regulates the level of immune response (*20, 21*). Although TLRs can bind the endotoxins directly, CD14 is essential to increase the sensitivity of response to endotoxins by as much as 1000-fold (*20, 21*). In the case of gram-negative endotoxin, LPS, CD14 complexes with TLR4, and in the case of the gram-positive endotoxin, LTA,

it associates with a heterodimer of Toll-like receptor 2 (TLR2) and Toll-like receptor 6 (TLR6) (*23-27*). The differentiation between endotoxins by CD14, and therefore the TLR to which it delivers the endotoxin, is significant in that sepsis cases can present differently from a clinical standpoint based on whether the causative organism is gram-negative or gram-positive (*16*). The up-regulation of the immune response is accomplished in part by CD14's high affinity for endotoxin, which enables it to detect and bind endotoxins at concentrations significantly lower than those detected by the TLRs (*28*). As briefly described earlier, this response is initiated by the binding of endotoxin by CD14. The endotoxin LPS is first recognized by the high affinity LPS-Binding Protein, which disaggregates a single LPS molecule and transfers it to CD14. The CD14-LPS complex is then presented to TLR4 and its adaptor protein MD-2. In the case of LTA, CD14 binds it and presents it to a heterodimer of TLR2 and TLR6 to initiate the immune response (*25, 27, 29*). TLR2 is also able to respond to a variety of other bacterial lipoproteins, either on its own or by forming a heterodimer with another TLR (*22, 30*). Once CD14 has transferred the endotoxin to its specific TLR, the intracellular signal cascades are fairly similar.

Upon activation of a TLR, there are two main signaling pathways. These pathways differentiate after the initial activation of the highly conserved intracellular domain of the TLRs, the Toll/IL-1R (TIR) domain. The pathways are distinguished by the TIR adaptor proteins recruited to the activated TIR domain. The pathways are the MyD88 (myeloid differentiation primary-response protein 88)-dependent signaling pathway, which is common to all the TLRs, and the MyD88-independent signaling

pathway, which is specific to TLR4 and TLR3 (*31*).

The MyD88-dependent signal cascade leads to the activation of NF-κB (nuclear factor-κB) (**Figure 1.2**). Activation of NF-κB allows it to enter the nucleus and induce the expression of multiple target genes, such as tumor necrosis factor-alpha (TNF-α), interleukin-1 (IL-1), interleukin-6 (IL-6), interleukin-8 (IL-8), and interleukin-12 (IL-12), (*19, 31-34*). In addition, the MyD88-dependent signaling path leads to the activation of mitogen-activated protein kinases (MAPK), which leads to the production of nitric oxide and additional inflammatory mediators (*35*).

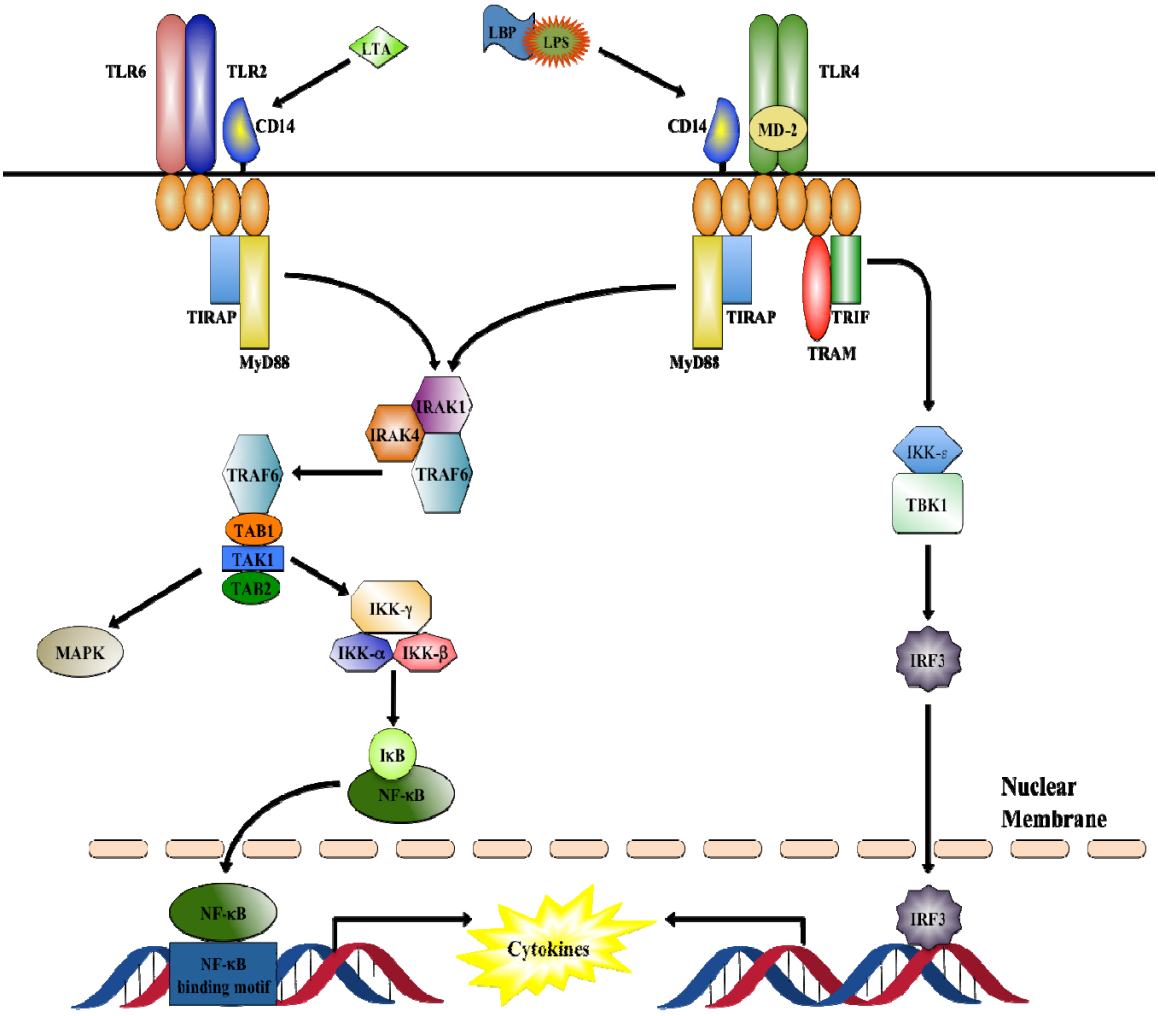


Figure 1.2: Toll-like Receptor MyD88-dependent and MyD88-independent signaling cascade.

In the MyD88-dependent signal path, the stimulation of TLR4 by LPS, begins with the transfer of LPS from LBP to CD14 then to the TLR4-MD-2 complex, triggering the association of MyD88 with the TLR's highly conserved cytoplasmic domain. This also occurs upon transfer of LTA from CD14 to the TLR2/TLR6 heterodimer. MyD88 activation causes association of TIRAP, and the recruitment of IRAK4 by MyD88. Activation of IRAK4 allows the association of IRAK1. IRAK4 then induces the phosphorylation of IRAK1. TRAF6 is then recruited to the receptor complex by associating with phosphorylated IRAK1. TRAF6 then dissociates from and forms a complex with TAK1, TAB1, and TAB2 translocates to the cytosol. This leads to the activation of TAK1. TAK1, in turn, phosphorylates both MAPK and the IKK complex, consisting of IKK-α, IKK-β and IKK-γ. The IKK complex then phosphorylates IκB, which is subsequently degraded. This allows NF-κB to translocate to the nucleus and induce the expression of its target cytokine genes. The MyD88-independent signal path starts with the association of TRIF and TRAM to stimulate TLR4's cytosolic domain. TRIF activates the non-typical IKKs IKK-ε and TBK1. IKK-ε and TBK1 mediate activation of IRF3, which moves into the nucleus and induce activation of IFN-β and type I IFN inducible cytokines.

Activation of the MyD88-independent signaling pathway leads to activation of interferon-β (IFNβ) and IFN-regulatory factor 3 (IRF3) resulting in the release of cytokines (**Figure 1.2**). Rather than MyD88, the adaptor proteins recruited to the activated TIR domain are TRIF (TIR-domain-containing adaptor protein inducing IFN-β) and TRAM (TRIF-related adaptor molecule) (*19*). This pathway also utilizes the non-typical IKKs IKK-ε and TBK1 (TRAF-family-member-associated NF-κB activator (TANK)-binding kinase 1) to mediate activation of IRF3, which upon translocation to the nucleus activates transcription of type I IFN genes (*31*).

The net affect of these signal cascades is activation of a robust inflammatory response, and as illustrated by the variety of alternate and complementary paths in this cascade, the response can be generated with ease. The initial rate-limiting step to the generation of an immune response is at the cell surface rather than at some point in the intracellular signal cascade. A TLR's ability to generate a response is restricted by its ability to locate and bind its respective ligand. This highlights the critical importance of CD14 in recognizing and presenting ligands to the appropriate TLR in a rapid and specific manner. CD14 can perform all these functions through its ability to bind a wide variety of ligands with high affinity as well as with specificity.

1.3 BACTERIAL ENDOTOXINS

1.3.1 GRAM-NEGATIVE ENDOTOXIN

The endotoxin from gram-negative bacteria is the amphipathic cell wall component lipopolysaccharide. LPS is found in the outer leaflet of the outer membrane,

and covers approximately 75% of the outer membrane of gram-negative bacteria (*36*). The LPS molecule is composed of the O-antigen polysaccharide, the core oligosaccharide, and the hydrophobic anchor known as lipid A (**Figure 1.3**) (*37*). The O-antigen is the most distal portion of the LPS molecule, and is exposed on the cell surface. The O-antigen is a heteropolysaccharide composed of multiple oligosaccharide units, containing a wide variety of both typical and atypical sugars as well as variants of those sugars (*38, 39*). The O antigen displays significant levels of variation in the types of sugar residues it contains, their organization within the repeating unit(s), and in the bonds within and between the repeating unit(s). This makes the O antigen polysaccharide the most variable portion of an LPS molecule (*39, 40*). Because of the inherent complexity and variability contained in the O-antigen, it is the basis of classification between serotypes in a bacterial species; some species have significant variation in the O antigen's polysaccharide composition and structure, such as *E. coli* which has ~170 different serotypes (*40*).

The core oligosaccharide consists of an inner and outer core region (**Figure 1.3**). It is much less variable in its composition than the O-antigen, and normally contains 15 or fewer sugar residues (*36*). The inner core is the portion forming the attachment point with the hydrophobic lipid A moiety, and the outer core is the portion to which the O-antigen polysaccharide is attached. The inner core retains a more highly conserved structure between bacteria serotypes. This is believed to result from the impact of lipid A and the inner core in membrane integrity (*40*). The outer core displays greater structural diversity. However, despite this diversity, the overall extent of structural differences seen

across the core oligosaccharides of a particular species or genus is still fairly limited (*36, 40*).

Lipid A is a glycophospholipid with a structure typified by that of *E. coli*'s lipid A structure. Lipid A is composed of a 1, 4'-bisphosphorylated D-glucosamine disaccharide backbone linked by a β(1'→6) glycosidic bond, with four ester linked R-3-hydroxymyristic acid substituents. The hydroxymyristic acid substituents are attached at the 2, 2', 3, and 3' positions with secondary acylation on the 2' and 3' acyl chains (**Figure 1.3**). The secondary acylation of the 2' and 3' anchored acyl chains form acyloxyacyl moieties with the 3' R-3-hydroxymyristic acid's secondary acylation being a myristic acid and the 2' R-3-hydroxymyristic acid having a lauric acid attached (*40, 41*). Lipid A is the smallest immunostimulatory portion of LPS required to elicit a full immune response from a host (*42*). In addition, the minimal LPS structure required for cell survival is lipid A plus the Kdo (3-deoxy-D-*manno*-oct-2-ulosonic acid) domains, which are the first two residues of the inner core (**Figure 1.3**) (*43, 44*). Lipid A has a much higher level of structural conservation throughout gram-negative bacteria than any other portion of LPS, regardless of whether a specific bacterium is considered pathogenic or not (*40*). Interestingly, lipid A in its standard hexaacylated form is a powerful agonist of the immune system, but removal of the secondary acyl chains from the acyloxyacyl moieties produces Lipid IVa, a tetraacylated lipid A precursor, which is a potent antagonist, blocking the response to LPS (**Figure 1.3**)(*45, 46*).

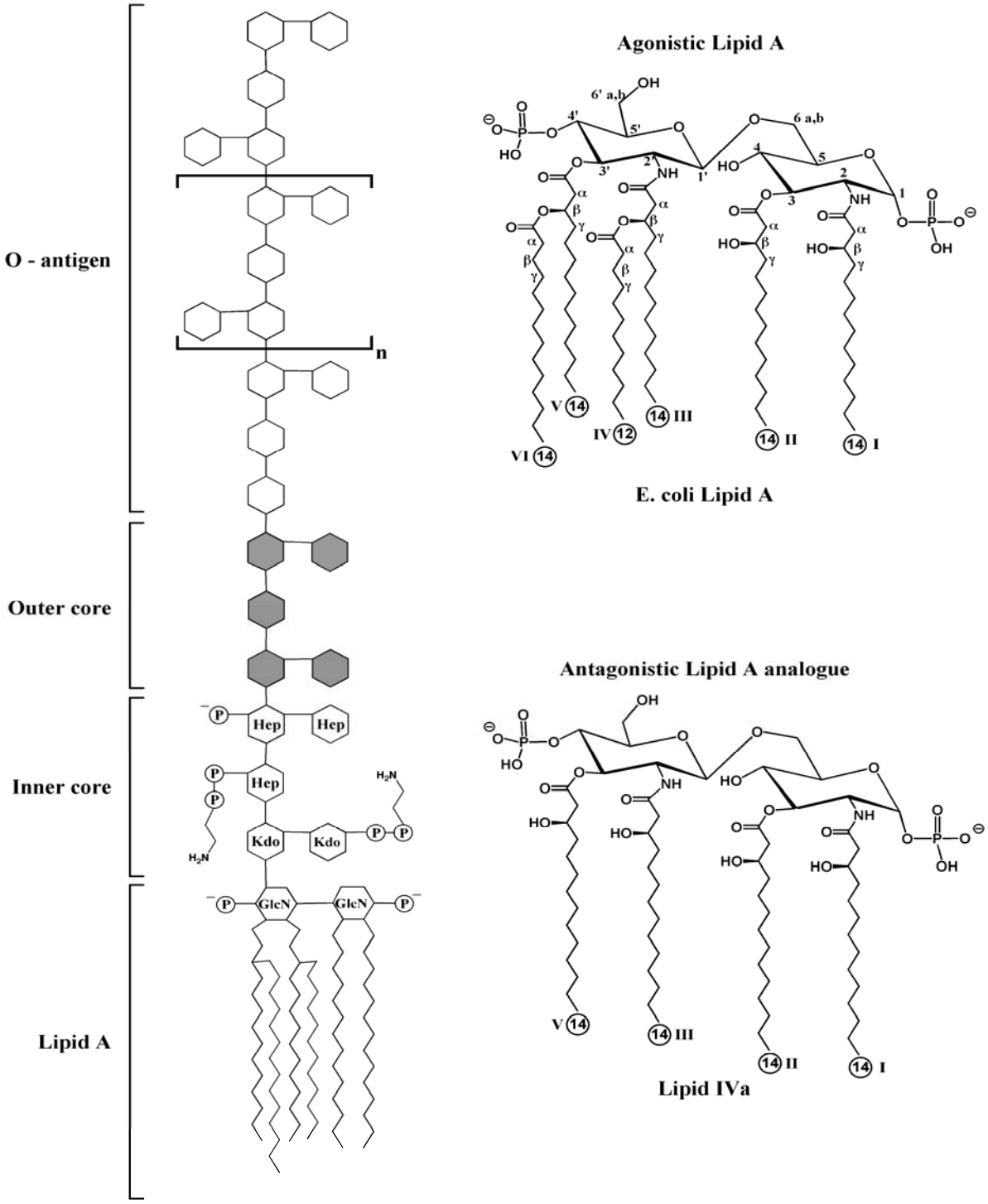


Figure 1.3: Chemical schematic of Lipopolysaccharide, Lipid A, and antagonistic Lipid IVa.

The numbering scheme for lipid A's headgroup and acyl chains is shown. The acyl chain numbering of lipid IVa is also shown. The circled numbers at the terminus of the acyl chains indicate the acyl chain length.

Atypical lipid A structures generally have alterations to the length of the acyl chain(s), loss or gain of acyloxyacyl groups, and in rare cases, derivatization of an acyl chain(s). In addition, atypical lipid A forms can also have extra sugar residues attached to the customary glucosamine disaccharide backbone of lipid A (*40*). However, whether a lipid A's structure is standard or atypical, the phosphate groups and acyloxyacyl groups are the key features giving lipid A its endotoxic ability to illicit an immune response (*37, 40, 47*).

1.3.2 GRAM-POSITIVE ENDOTOXIN

Gram-positive bacteria have no LPS, and the identity of an immunogenic molecule from gram-positive bacteria has, over the years, been a subject of debate, with the main candidates for the role being peptidoglycan (PGN), and lipoteichoic acid (LTA).

Lipoteichoic acid is an amphiphilic molecule found in gram-positive but not in gram-negative bacteria. LTA's structure is composed of a hydrophilic backbone consisting of polyglycerophosphate repeating units, and substituted with D-alanine, glucosamine, and hydroxyl groups. The polyglycerophosphate backbone is attached to a gentiobiosyl-diacylglycerol lipid anchor which secures the molecule in the membrane (**Figure 1.5**) (*48*). The number of glycerophophate units that make up the polyglycerophosphate backbone varies between bacterial species. For example, *Staphylococcus aureus* (*S. aureus*) averages 40-45 glycerophosphate units whereas *Bacillus subtilis* (*B. subtilis*) averages only 22-25. It has been shown that the more D-alanine substituents found on the polyglycerophosphate chain of an LTA the greater the immune response initiated. This is illustrated by the LTA of *S. aureus*, where D-alanine

represents 70% of the total substituents on the polyglycerophosphate chain, versus *B. subtilis*, with D-alanine accounting for only 25% of the substituents on its polyglycerophosphate chain (*49, 50*). Despite the variation in the number of repeating units in the polyglycerophosphate chains of *S. aureus* and *B. subtilis*, the structure of their lipid anchors is essentially identical. The lipid anchor of both species is composed of a gentiobiose headgroup, with two acyl chains linked to the headgroup through a glycerol (**Figure 1.4**). The lone difference in their lipid anchors is that on average *S. aureus*'s acyl chains are two carbons longer than those of *B. subtilis*, 16 versus 14 (*49, 50*).

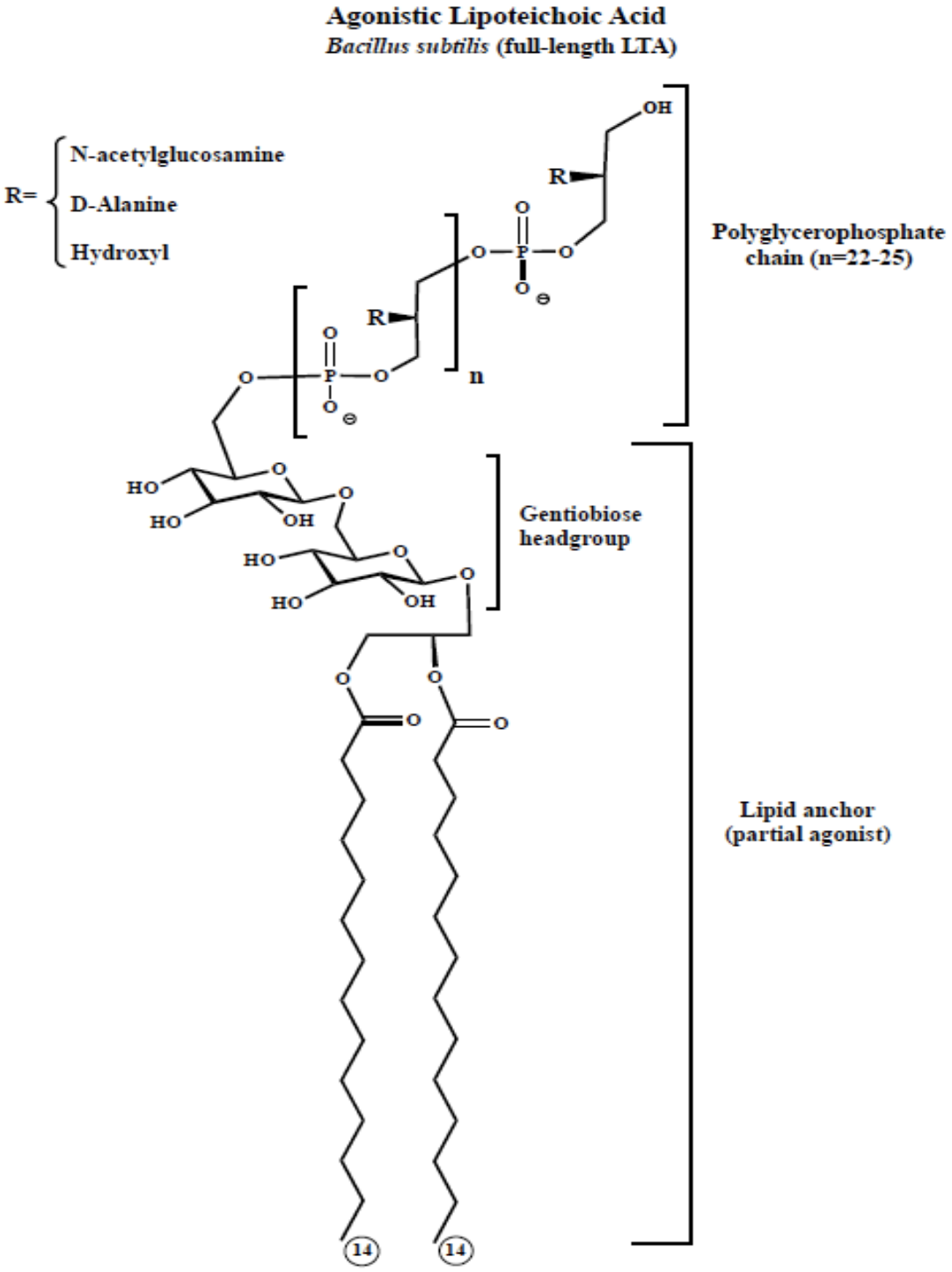


Figure 1.4: Structural schematic of Lipoteichoic acid.
The potential polyglycerophosphate substituent's sites are indicated by R. The circled numbers at the terminus of the acyl chains indicate the acyl chains length.

In recent years, there has been progress towards resolving the controversy over which gram-positive cell wall component is the source of immunostimulation. Peptidoglycan has been excluded as a ligand for any TLR pathway. It was proven that the early identification of PGN binding by TLR2 was due to sample contamination with significant levels of lipopeptide, teichoic acid, and lipoteichoic acid left behind by the methods employed to extract PGN from native cell membranes (*50, 51*). It has now been conclusively proven that PGN is not a ligand for TLR2 or any of the TLR2 heterodimer (*51-54*). The argument against LTA being the immunostimulator from gram-positive bacteria was established based simply on conflicting results of immune response generation in cell based assays (*51, 53*). The failure of LTA to produce a strong immune response was traced back to the extraction and purification of the LTA from native cell walls. It was discovered that traditional extraction of LTA using a 68 ºC phenol-water mixture resulted in the release of the labile D-alanine substituents off of the backbone, and could even result in the loss of multiple glycerophosphate units (*49, 50*). Production of synthetic LTA has confirmed that LTA generates an immune response through TLR2/6 (*26, 52*). In addition, it was shown that the LTA lipid anchor with five glycerophophate units and carrying four D-alanine substituents and a single N-acetylglucosamine is the minimum LTA structure necessary for initiating an innate immune response (*55, 56*).

1.4 CD14

CD14 is the key high-affinity receptor for bacterial endotoxins and serves a critical role in endotoxin-induced activation of innate immune cells (*57*). CD14 is a

necessity to achieving rapid activation and up-regulation of the immune response to bacterial or microbial incursion. It has been hypothesized that CD14 recognizes/binds LPS and LTA via recognition of pathogen-associated molecular patterns, which are common structural elements found in endotoxins (*58*). CD14 is required for the response to low concentrations of LPS (*57, 59*). This is illustrated by the fact that CD14-deficient mice are insensitive to LPS and are essentially unaffected by LPS doses lethal to wild-type mice (*59*).

In humans, CD14 is a glycoprotein constitutively expressed in a 55 kDa membrane bound form (mCD14), found mainly on the cell surface of monocytes and macrophages anchored to the membrane through a glycosylphosphatidylinositol anchor (GPI-anchor) (*60*). Additionally, mCD14 is found to a lesser extent on the surface of a variety of other immune cells including polymorphonuclear neutrophils, chondrocytes, B cells, and dendritic cells (*12*). CD14 is also present in a 48 kDa soluble form (sCD14) typically found in serum and body fluids of healthy adults at concentrations in the range of 2-6 μg/ml. In patients with sepsis, the circulating levels of sCD14 in the plasma can exceed 7 μg/ml (*61-64*). The soluble form of CD14 is nearly identical to mCD14, the exception being its lack of a GPI anchor (*61*). It is thought that sCD14 is produced *in vivo* either by cleavage of mCD14 via proteases and phospholipases from the cell surface of monocytes and macrophages, or as a secreted protein without the necessary post-translational modification needed for attachment of the GPI-anchor (*60, 62, 63*). The GPI-anchor is not required for CD14 function or signaling. It is thought that the

anchoring of CD14 to the membrane may simply facilitate the localization of mCD14 in close proximity to the membrane spanning TLRs (*65, 66*).

Both the soluble and membrane bound forms of CD14 signal through the same TLR pathways. A significant difference is that the presence of sCD14 allows cells that do not express mCD14, such as some endothelial and epithelial cells, to respond to lower levels of endotoxin than could be detected by the cell's endogenous TLRs alone (*67-69*). Another difference between the mCD14 and sCD14 initiated response to endotoxin was seen in the sensitivity of LPS detection. Wild-type murine monocyte cells, which express mCD14, are capable of inducing pro-inflammatory cytokine production with only 1 ng/ml concentrations of LPS present. In contrast, CD14-deficient murine monocytes supplemented with 20 μg/ml recombinant full-length sCD14 did not induce cytokine production until the LPS concentration was at least 100 ng/ml. This difference is insignificant considering that with no CD14 present it takes over 1 μg/ml of LPS to see even minor activation of cytokine production (*59*). This decrease in sensitivity is likely due to the fact that mCD14 is generally located in very close proximity to TLR4 signaling complexes, allowing a speedy transfer LPS to TLR4 and a rapid triggering of the response (*35*). However, sCD14 has the additional task of first locating a TLR4 signaling complex then transferring the LPS to it before the cytokine induction can be initiated.

1.4.1 CD14 STRUCTURAL FEATURES

The full-length *cd14* gene codes for 375 amino acids, the first 19 amino acids compose a transport signal sequence that is cleaved off in the endoplasmic reticulum to

yield the mature 356 amino acid mCD14 protein. In addition, the mature soluble form of CD14 also lacks the last eight C-terminal amino acids, which are lost in the cleavage of the GPI anchor (*61*). Since both mature forms of CD14 lack the signal peptide, it is customary to number the amino acid sequence at the first N-terminal residue after the secretion signal. As a member of the leucine-rich repeat family of proteins, which also includes the TLRs, CD14 contains 10 leucine-rich repeats spanning from residue 67-312 (*70*). The leucine-rich repeat (LRR) motif is typically a 20 to 29-residue sequence with characteristically positioned hydrophobic residues (*71*). As implied by its name, the predominant hydrophobic amino acid being repeated in an LRR is leucine. However, isoleucine, valine, and phenylalanine can also occupy the role of "leucine" in the repeating pattern of an LRR (*72*). In the case of human CD14, the repeated pattern is LXXLXLX, where X is any amino acid and L is Leu, Val, Phe, or Ile (*73*).

CD14 also has four N-linked glycosylation sites. Cleavage of the glycosylations using glycosidases results in a ~12 kDa decrease in molecular weight, indicating that glycosylations account for roughly 20% of CD14's total molecular weight (*74*). Within the last several years, a crystal structure of full-length murine sCD14 without a ligand has been solved (**Figure 1.5**) (*75*).

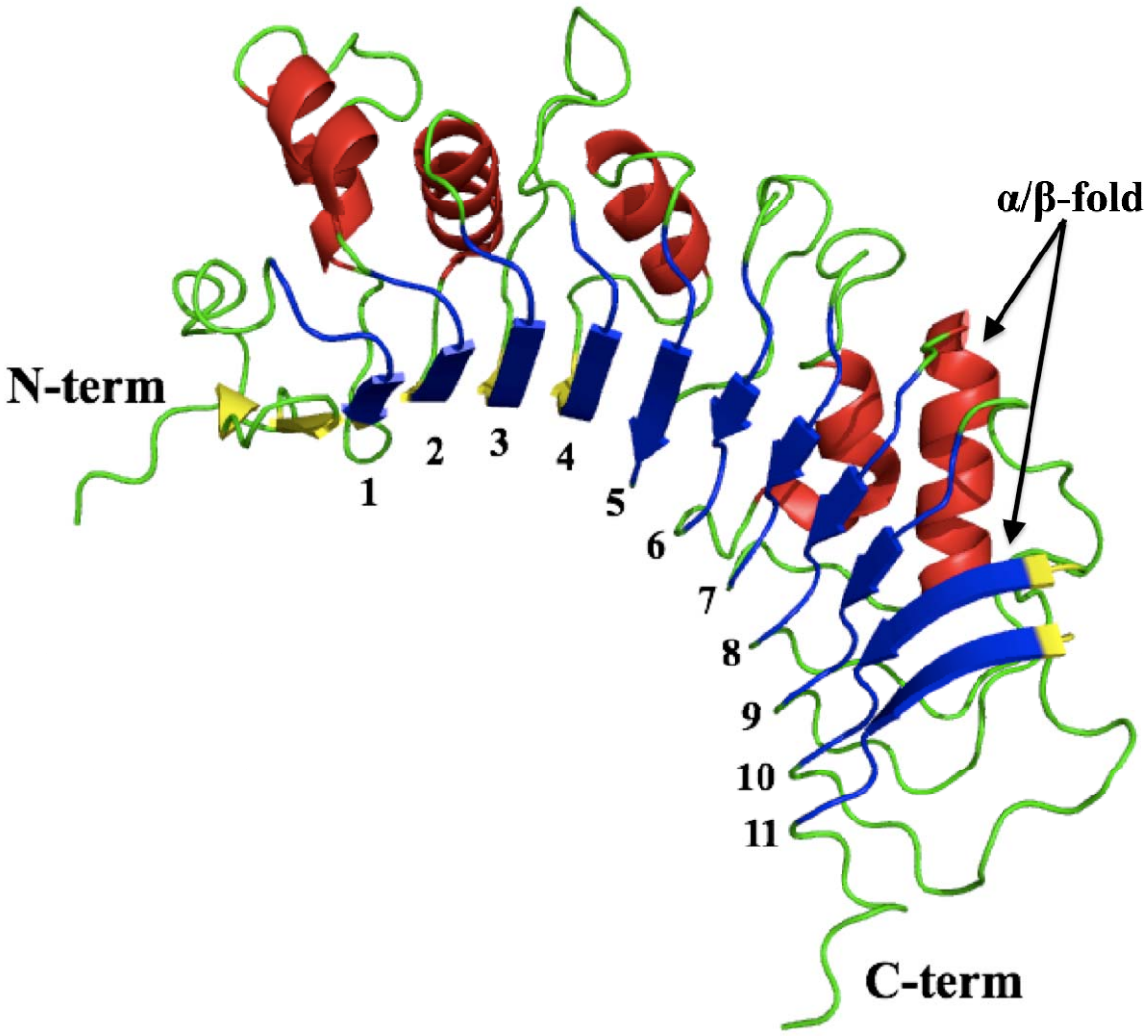


Figure 1.5: Crystal structure of full-length murine soluble CD14.
Ribbon view of secondary structural elements in full-length murine sCD14 (Protein Data Bank code 1WWL) (*75*). A representative region of the α/β-fold is indicted by the arrows. The 11 leucine-rich repeats (LRR) found in mouse CD14 are numbered, and the hydrophobic amino acid repeating sequence (LXXLXLX) is colored blue for each LRR. Figure generated using PyMol (Delano Scientific, San Carlos, CA).

The X-ray crystal structure shows that CD14 has an overall α/β-fold containing a mixture of α-helical and β-sheet secondary structure connected by loops of varying length; the vast majority of the protein's secondary structural elements are β-sheets. In addition, the crystal structure has a general shape reminiscent of half a horseshoe with a series of β-sheets forming the concave inner edge, and a combination of loops and a few α-helices forming the outer convex edge. This general architecture is typical of leucine-rich repeat proteins as has been shown by the crystal structures for several other members of the LRR-protein family, such as the *Yersinia pestis* cytotoxin YopM and more recently the structures of several TLRs and TLR complexes (*29, 76-78*). The crystal structure also revealed a large hydrophobic pocket surrounded by a largely hydrophilic rim at the N-terminus (*75*). Murine CD14 shares ~66% sequence identity with human CD14 which makes the mouse crystal structure a useful structural reference for comparison to human CD14 (*73*). An important finding made while investigating the functional roles of the leucine-rich repeats was that a 152 residue N-terminal truncation, which eliminated all but the first 3 repeats, still retained the ability to bind LPS as well as full biological activity on par with that of wild-type sCD14 (**Figure 1.6**). The fact that even when lacking repeats 4 through 10 CD14 retained wild-type function suggests that the last 7 repeats are not critical for CD14 binding or activity (*70, 79*). At this time the biological function of these repeats is not known. It has been hypothesized that the presence of all 10 repeats serve as a structural scaffold to orient or position membrane bound CD14 in such a way that facilitates ligand transfer to the transmembrane TLRs, which have the same general structure as CD14 but contain from 19 to 25 LRRs in their extracellular

domains (*71*). LRRs are known to play a role in protein-protein interactions, as illustrated by the recent crystal structures of the TLR1-TLR2 heterodimer, and the TLR3 homodimer complexes (*29, 80*). Though both CD14 and the TLRs contain LRRs, their contribution to the formation of a CD14-ligand-TLR complex is not known. This complex is so transient that it has yet to be stably isolated for any CD14-TLR complex, preventing detailed characterization of its protein-protein interactions (*28, 81*). In addition, LRRs are also involved in ligand binding interactions (*82*). However, given the thousands of protein sequences identified as containing LRRs the primary function of LRRs appears to be as a versatile framework, facilitating protein-protein interactions (*72*). In the time since murine CD14's structure was solved, the structures of LRR-protein family member's TLR3, the TLR4/MD-2 complex, and the TLR1-TLR2 heterodimer, all of which are receptors in the innate immune response, have had their structures solved and each display a similar overall architecture to that of murine CD14 (*29, 77, 78, 83, 84*).

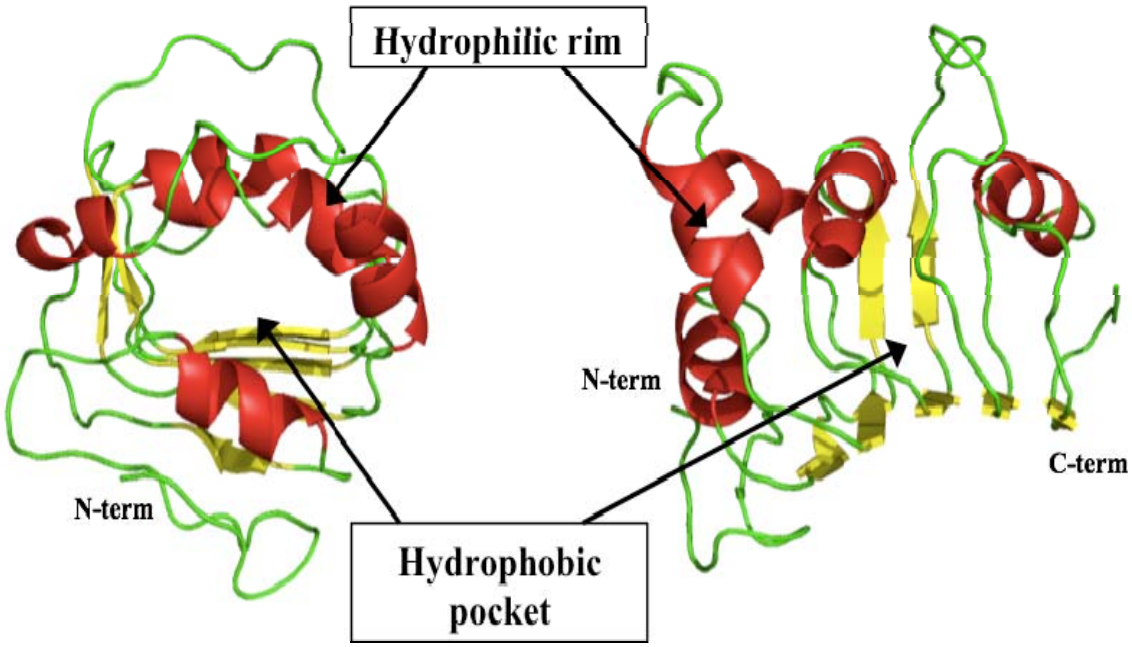


Figure 1.6: Homology Model of the 152-residue N-terminal truncation of human soluble CD14.

Ribbon view of secondary structures of human sCD14 illustrating the hydrophilic rim and hydrophobic pocket. β-sheets are shown in yellow, and α-helices are in red. Homology model made by Wei Zhang. Figure generated using PyMol (Delano Scientific, San Carlos, CA).

1.4.2 CD14 LIGAND BINDING

CD14's ability to recognize a wide assortment of ligands led to the hypothesis that CD14 is a pattern recognition receptor, which recognizes its ligands via pathogen-associated molecular patterns (PAMPs) (*17*). The utilization of pattern recognition receptors to recognize and initiate an innate immune response is well conserved even among different species, from plants and insects to mammals (*22*). Pattern recognition receptors are thought to recognize molecules and structures unique to bacteria and microbes that are not associated with a host's cells. These unique molecules share common structural features and are termed pathogen-associated molecular patterns. PAMPs consist primarily of microbial cell wall components that are essential for the microorganism's survival. The essential nature of a PAMP to cell survival means that its general structural characteristics are conserved, as changes to the structure would be difficult without detrimentally influencing an organism's survivability (*22*). This critical role in the organism's survival is illustrated by well-characterized PAMPs from several organisms as illustrated by lipid A in gram-negative bacteria and lipoteichoic acid in gram-positive bacteria, both of which are critical for membrane integrity (*85*). This is also seen for the viral PAMP, double stranded RNA, which is produced by RNA viruses during their replication (*86*). The essential and conserved role of PAMPs in cell survival is true even for PAMPs recognized by the plant innate immune system. In plants, the best-characterized PAMP is flagellin, the principal building block of the bacterial flagella (*87*). Flagellin is recognized by flagellin-sensing 2 (FLS2) in *Arabidopsis* and by TLR5 in mammals (*88*). The direct interaction of flagellin with a LRR in TLR5 relies strongly

on electrostatic interactions as indicated by mutagenesis studies (*89-91*). The direct interaction of flagellin with FLS2 from *Arabidopsis thaliana*, has been shown to be sensitive to salt concentrations, which is indicative of ionic interactions (*92*). At this time, these investigations represent the most detailed structural studies carried out to date on the flagellin binding interactions of FLS2 and TLR5. The role of ionic/electrostatic interactions in ligand binding has also been seen in the binding of LPS by CD14, as evidenced by charge reversal mutagenesis studies, which caused CD14 to become unable to bind LPS (*93, 94*).

CD14 is capable of binding well over a dozen ligands (**Table 1**), and with its ability to bind atypical structural variants of lipid A and LTA, this number could be even larger (*25, 95-106*). While the binding affinities for most of the ligands in Table 1 hasve not been determined, the affinity of those that have been determined range from 27 nM for LPS to 5.7 μM for a synthetic triacyl lipopeptide (Pam3CSK4) (*98, 102*). CD14's ligand binding and recognition is all the more remarkable in that identification and characterization of CD14's binding site revealed that it possesses a single binding pocket.

The residues/regions identified in CD14 as necessary for the binding of LPS are primarily located within a region spanning from the N-terminus to residue 100. Introduction of a combination of single and multiple deletions into CD14's N-terminus revealed that several hydrophilic regions and amino acids are required for serum dependent binding of LPS (*107*). Additionally, a group of amino acids spanning residues 57–64 was found to be protected from protease digestion when LPS was bound by CD14. Deletion of this group of amino acids resulted in a loss of binding ability as well as the

ability to initiate a response to LPS (*108, 109*).

Another region of amino acids, residues 39–44, was found to function in LPS binding through an alanine scanning mutagenesis study (*110*). The contributions of individual hydrophilic amino acids in the N-terminus were further examined by means of serine replacement mutagenesis and charge reversal mutations (*93, 94*). Only the charge reversal mutations resulted in a loss of LPS binding ability by CD14. Another study identified an LPS-binding domain in CD14 located in the region adjacent to the N-terminal 66 amino acids, by mapping the full-length 356 amino-acid CD14 protein using 20-amino-acid peptides. This study found that a peptide containing amino acids 81-100 was sufficient to bind and neutralize LPS (*111*).

Table 1. Bacterial, Microbial, Viral, and Host derived CD14 ligands

Interacting Molecule	Source Organism	Reference
Tri-acyl lipopeptides	gram-positive bacteria, mycobacteria	(*95*)
Di-acyl lipopeptides	*Mycoplasma salivarium* (FSL-1)	(*96*)
Lipoprotein/Lipopeptides	gram-positive and gram-negative bacteria	(*96*)
polymeric Peptidoglycan	gram-positive bacteria	(*97*)
Lipoteichoic acid	gram-positive bacteria	(*25*)
Lipomannan	mycobacteria	(*98*)
Lipoarabinomannan	mycobacteria	(*98, 112*)
Glycoinositolphospholipids	*Trypanosoma cruzi*	(*99, 113*)
Glycolipids	*Treponema maltophilum*	(*100*)
fungal cell wall components	*Aspergillus fumigatus*	(*101*)
Lipopolysaccharide	gram-negative bacteria	(*97, 102*)
Atypical LPS	*Helicobacter pylori*	(*103*)
Atypical LPS	*Porphyromonas gingivalis*	(*103*)
double-stranded RNA	viruses	(*104*)
Fusion protein	Respiratory syncytial virus	(*105*)
Heat Shock Protein 60	Host	(*106*)

Based on these studies, it was concluded that the binding site was located at the N-terminus of CD14. This was confirmed by a large hydrophobic pocket rimmed by charged residues at the N-terminus of the mouse CD14 crystal structure (*75*). These studies shed significant light on CD14's binding mechanism(s), revealing that binding interactions take place using a number of broad overlapping residues and regions, but they did not examine whether the interactions were ligand specific. It bears noting that many of the ligands CD14 binds contain fatty acids and negatively charged phosphate groups, and that many of the amino acids identified as being involved in CD14's binding interactions are charged amino acids. The surrounding of the binding site by charged residues strongly implicates ionic interactions as a critical ingredient in the binding and recognition of endotoxins. This is validated by the fact that charge reversal mutations resulted in a loss of function by CD14 (*93, 94*). This also correlates with the fact that dephosphorylated lipid A is not bound by CD14, and that monophosphoryl lipid A has reduced binding affinity to CD14; both of these variants result in reduced to negligible biological activation of an immune response (*114, 115*). The fact that full-length CD14 has a large hydrophobic cavity created by the LRRs makes it ideally suited for sequestering the multiple acyl chains of LPS and LTA. In combination with the charged amino acids rimming the hydrophobic pocket (**Figure 1.6**), this suggests that placement of the acyl chains in the hydrophobic pocket would result in the positioning of an endotoxin's sugar headgroup and its charged moieties in proximity to hydrophilic rim's charged amino acids. However, atomic level structural information about CD14's binding interactions and its differential recognition of endotoxins is limited by the fact that the

CD14 crystal structure has no ligand.

Recently, the crystal structure of the TLR4/MD-2 co-complex has been solved with an agonist and antagonist bound, providing a wealth of new information into TLR4's interaction with LPS (*78*). However, it is CD14's role upstream that is central to the enhancement of the immune responses of TLR4 and TLR2. In addition, CD14's mechanism of differential ligand binding has yet to be fully characterized, yet remains of great importance.

In addition to being a pattern recognition receptor, CD14 has been proposed to have a broader physiological role in lipid exchange mechanisms, where it catalyzes the exchange of different phospholipids including phosphatidylcholine, phosphatidylinositol and phosphatidylethanolamine (*116*). CD14 on the surface of human macrophages is also important in the recognition and clearance of apoptotic cells (*117*). Due to its multifunctional role, CD14 is now viewed as a key pattern recognition receptor in the initiation of the innate inflammatory response. Capable of recognizing shared structural features of microbial cell surface components, CD14 enables the host to respond to pathogenic bacteria, but not to a great variety of other non-microbial polysaccharides. However, the specific molecular patterns recognized by CD14 had not been determined, as no structure for a CD14-endotoxin complex is available. This is likely because of the many challenges associated with structural determination of co-complexes. Crystallization is further complicated by the micelle forming characteristics of LPS and LTA, and the highly flexible nature of their glycolipid structures. This has prevented detailed molecular level characterization and comparison of various CD14-endotoxin

ligand complexes. NMR spectroscopy is an excellent method for characterizing interactions between protein and ligands in complex with each other, and can provide residue-level observation of interactions between protein and ligand.

This dissertation focused on characterizing the interactions between CD14 and the primary gram-negative and gram-positive endotoxins, LPS and LTA, using solution NMR spectroscopy. In this project, NMR structural studies were carried out on isotopically labeled LPS- and LTA-based ligands to determine the structural features of these endotoxins which interact with CD14. It is hoped that these studies will enable further understanding of differential recognition of these endotoxins by CD14 and shed light on the mechanistic aspects of how ligand pattern recognition by CD14 translates into specificity of TLR selection. These studies will also benefit the design of new ligands that can antagonize the pro-inflammatory effects of CD14 and reduce inflammatory over-activation. Targeting of CD14 may, therefore, offer the possibility of safely interrupting the process of systemic inflammation in response to bacterial infection early on, slowing or preventing the severe over-activation of the inflammatory response. This could avert the onset of sepsis, allowing serious infections to be treated without the inflammation induced complications of sepsis.

CHAPTER 2. EXPRESSION, PURIFICATION, CHARACTERIZATION, AND ISOTOPIC LABELING OF SOLUBLE CD14 AND THE ENDOTOXIN LIGANDS Kdo_2-LIPID A AND LIPOTEICHOIC ACID

2.1 INTRODUCTION

NMR spectroscopy is an excellent method for characterizing interactions between a protein and its ligand(s) in complex with one another. The use of NMR can enable residue-specific information to be collected regarding the interaction of the ligand on the protein, and conversely the protein on the ligand. When a substrate or ligand is bound by its receptor, such as a large protein, several NMR parameters can be affected. These include the chemical shifts and the relaxation times of both the ligand and the protein. The local environment of the bound ligand is different from the environment it experienced in its free state; this causes the chemical shifts of its protons to change. Because, chemical shifts are very sensitive to changes in a residue's environment, they can be used to detect even weak interactions, as evidenced by observable changes in the chemical shifts. The same is true for the chemical shifts of the protein's residues that are affected by either direct binding interactions or indirectly as a result on other neighboring residues involvement in the binding. Specific types of interactions can also be observed an example being ionic or electrostatic interactions, which can correlate to chemical shift changes in relation to pH changes, or also evidenced by the loss or gain of proton signals

due to deprotonation of protonation of residues as the sample pH reaches their respective pKa (*118, 119*). NMR can also reveal whether a binding interaction is dynamic, which is indicated by changes in the linewidth and shape of a chemical shift relative to the rate at which it is transitioning between various possible conformational states. These detailed methods for examination of binding interactions and structural changes makes NMR ideal for investigating the binding and differential recognition of endotoxins by CD14. The projects described in this dissertation focused on characterizing the interactions between CD14 and the primary gram-negative and gram-positive endotoxins, LPS and LTA, using solution NMR spectroscopy.

In order to perform NMR studies of CD14, it is necessary to obtain milligram quantities of isotopically labeled protein. For a study to be biologically relevant, it is critical that the production of any recombinant protein for use in the research be in a functional form with a native fold. To that end, a fully functional fragment of sCD14 consisting of the first 152 residues of the N-terminus of the protein, which includes the region for endotoxin binding, was chosen for expression and use in these studies (*70*). Throughout the remainder of this dissertation, sCD14 will refer to the soluble N-terminal 152-residue truncation of full-length sCD14 containing the endotoxin-binding domain, unless indicated otherwise. Expression of human proteins in glycosylated forms is inherently difficult in any system. In the case of CD14, the problem is compounded by the fact that it has high affinities for endotoxin, and as such must be produced in a system which contains minimal amounts of endotoxin (*25, 102*). In addition, to allow for NMR studies and assignments, CD14 must be isotopically labeled. These constraints made it

critical to select an appropriate system to express sCD14.

E. coli is capable of producing recombinant proteins in large quantities, and is a well characterized source for the cost-effective production of isotopically labeled samples. However, it is not capable of post-translational modification of expressed proteins, and any CD14 produced using *E. coli* would have considerable endotoxin contamination. Mammalian expression systems have been used to produce many glycosylated human proteins. However, mammalian expression systems are unable to produce the large quantities of isotopically labeled samples needed in a cost effective manner. With these issues in mind, the yeast system of *Pichia pastoris* was chosen. As a eukaryotic system, *Pichia pastoris* is capable of post-translational modifications, and minimizes the potential endotoxin contamination. In addition, the glycosylations attached by *Pichia* are short for a eukaryote consisting of only 8-14 mannose residues, making it more amenable to solution NMR studies (*120*). While *Pichia*'s glycosylations might be shorter they are still functional, which is important for CD14 because the N-linked glycosylation at Asn^{132} is necessary for proper function. The other three N-linked glycosylation sites can be mutated with little affect to CD14's function (*121*), though we have observed a significant decrease in the lifespan of CD14 in its folded form after removal of all glycosylations. *Pichia* produced proteins can be isotopically labeled with relative ease by simple substitution of the media with a ^{13}C carbon source, such as methanol, and/or a ^{15}N nitrogen source, such as ammonium sulfate. Another advantage *Pichia* affords is that it can be readily scaled up from shake flask to fermentation. This combination of features made *Pichia pastoris* the most advantageous system for

recombinant expression of sCD14.

In order to unravel the structural features of the endotoxin ligands necessary for interaction with CD14, it is essential to produce pure, isotopically labeled ligands directly from gram-negative and gram-positive bacterial sources. Given the size and inherent heterogeneity of the O-antigen and core oligosaccharide, native LPS is undesirable for use in detailed structural studies (*40*). For this reason, a minimal endotoxic portion of LPS, Kdo_2-Lipid A (**Figure 1.3**), was chosen for use. Kdo_2-Lipid A is a well-characterized sub-structure of LPS capable of eliciting a strong immune response comparable to that of whole LPS (*122*). The heptosyltransferase-deficient *Escherichia coli* K-12 mutant, W3110 *δ(rfaCF)::tet6* (WBB06), which is unable to attach the outer core oligosaccharide and consequently also lacks the O-antigen, has only Kdo_2-Lipid A as its LPS (*44*). The WBB06 strain, (a gift from Christian Raetz, Duke University) was utilized to produce the Kdo_2-Lipid A samples for use in investigating the sCD14 interactions with gram-negative endotoxin. Starting from pure Kdo_2-Lipid A, several lipid A and Kdo_2-Lipid A structural variants were produced (**Figure 2.1**) to aid in the comprehensive investigation of the binding interactions of Kdo_2-Lipid A with sCD14. These variants include creation of lipid A through cleavage of the Kdo units from Kdo_2-Lipid A. Dilute acid hydrolysis of the 1-phosphate group produces the partial agonist monophosphoryl lipid A, and complete dephosphorylation, using hydrofluoric acid, produces a non-binding variant. Removal of the O-linked acyl chains from Kdo_2-Lipid A creates the partial agonist de-O-acylated Kdo_2-Lipid A (*45, 46, 123*). Lipid IVa was produced from the *E. coli* K-12 mutant, W3110 (*kdtA::kan*) pWMsbA (CMR300)

(another generous gift from Christian Raetz, Duke University). This mutant produces Lipid IVa as its LPS via the deletion of *kdtA* gene, which encodes the Kdo transferase in conjunction with over-expression of MsbA, the inner membrane flippase for core-lipid A. This over-expressed flippase combined with the deletion of the Kdo transferase results in the premature flipping of Lipid IVa, which is produced normally by *E. coli* as a precursor in LPS production, to the outer leaflet and prevents Kdo attachment (*124*). The lipid A and Kdo_2-Lipid A variants have been previously characterized as an agonist, or partial agonist based on their ability to induce production of the pro-inflammatory cytokines IL-1, IL-6, and TNF-α. In the case of Lipid IVa, it was classified as an antagonist based on its ability to almost completely inhibit cytokine induction by LPS (*125, 126*).

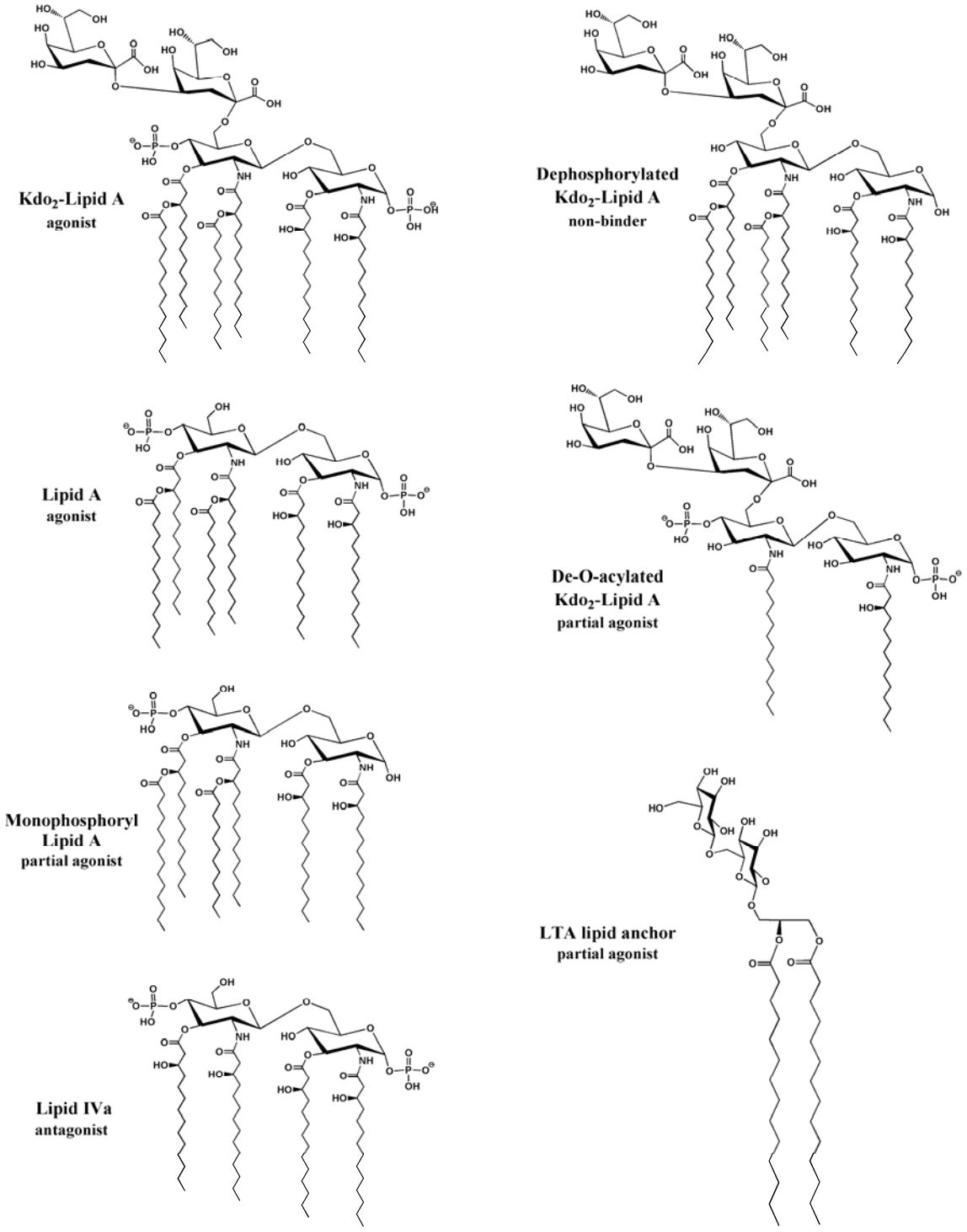


Figure 2.1: Agonist and Antagonist partial structures of Kdo_2-Lipid A, Lipid A, and Lipoteichoic acid partial structures.

LTA was produced using *Bacillus subtilis,* whose LTA shares many features in common with the highly immunogenic LTA of *Staphylococcus aureus*, but as a biosafety level 1 organism, *B. subtilis* does not require any additional safety procedures while *S. aureus*, a level 2 organism, does. The LTA of *S. aureus* is considered to be the structural archetype of immunogenic LTA, but *B. subtilis* differs in only two ways from that of *S. aureus*. These differences are limited to the polyglycerophosphate chain, which in *S. aureus* has 40 to 45 glycerophosphate repeating units versus *B. subtilis*'s 25 to 28. The second difference is in the percentage of polyglycerophosphate substituents that are D-alanine. In *S. aureus* D-alanine represents 70% of the total substituents on the chain, but in *B. subtilis* D-alanine accounts for only 25% of its total (*49, 50*). However, the lipid anchor portion of both *S. aureus* and *B. subtilis*'s LTA are identical, and both species full-length LTAs induce very similar levels of TNF-α production in human whole blood (*50*). For these reasons, and because of the ease of culturing *B. subtilis* in minimal mediums in isotopically labeled forms, *B. subtilis* was selected for production of LTA samples. In addition to producing full-length *B. subtilis* LTA, the polyglycerophosphate chain was cleaved to produce the partial agonist LTA lipid anchor. The LTA lipid anchor is characterized as a partial agonist based on its lower levels of TNF-α induction compared to the levels induced by full-length LTA (*56*).

2.2 MATERIALS AND METHODS

2.2.1 DESIGN OF SOLUBLE CD14 CONSTRUCT

The gene sequence encoding the N-terminal endotoxin binding domain of human sCD14, consisting of the 152 residues after the signal peptide sequence (20–171), was synthesized with codon-optimization for yeast and inserted into the *Pichia* expression vector pPICZαA (Invitrogen, Carlsbad, CA) by BIO S&T (Montreal, Canada). The pPICZαA vector contains a zeocin antibiotic resistance gene, the α̃factor secretion signal, to allow secretion of the inserted gene product into the culture medium, and a 6x histidine tag to aid in purification. Additional plasmid was produced using *E. coli* BL21 cells from Promega (Madison, WI). *E. coli* growth, plasmid isolation, and purification were all carried out using standard molecular biology techniques and miniprep and reaction clean-up kits from Qiagen (Valencia, CA). Plasmid DNA was sequenced by the Molecular Biology Research Facility (MBRF) on the University of Tennessee campus to confirm the sequence, proper insertion, and location of the 152-residue CD14 gene sequence within pPICZαA. Sequencing was preformed in both the 5' and 3' directions using the 5' *AOX1* and 3' *AOX1* sequencing primers described in the Easyselect™ Pichia Expression Kit manual (Invitrogen).

2.2.2 TRANSFORMATION OF *Pichia pastoris*

The purified pPICZαA-CD14 construct must be linearized prior to transformation into *Pichia*. Linearization was carried out using the restriction enzyme *SacI* (Promega, Madison, WI), and was performed per the manufacturer's guidelines. The linearization

was checked via gel electrophoresis on a 1.2 % agarose gel containing 0.48 μg/ml of ethidium bromide.

The lineraized pPICZαA-CD14 construct was transformed into the wild type *Pichia pastoris* strain X-33 (Invitrogen) using an optimized electroporation method developed in our lab, combining portions of the protocols described in Wu and Letchworth (*127*), De Backer *et al.* (*128*), and the Easyselect™ Pichia Expression Kit manual. X-33 was streaked out from a stab onto Yeast Extract Peptone Dextrose Medium (YPD) plates containing 100 μg/ml ampicillin and allowed to grow overnight at 30 °C. The next day, a single colony from the plate was inoculated into YPD liquid medium containing ampicillin and allowed to grow until it reached an OD_{600} of between 1.3 and 1.5. Then 50 ml of culture was spun down at 1500*g* for 5 minutes in a chilled tube and resuspended in 50 ml of ice-cold sterile water. Following a second centrifugation step, the cell pellet was resuspended in 25ml of cold water and spun again. The cell pellet was then resuspended in 4 ml of a solution containing 100mM lithium acetate, 10 mM DTT, 0.6 M sorbitol, 10 mM Tris-HCL pH 7.5, and incubated for 30 minutes at room temperature. After this incubation, the cells were centrifuged and resuspended in 2 ml of ice-cold sterile 1M sorbitol, followed again by centrifugation and resuspension in 150 μl of 1 M sorbitol. An 80 μl volume of cells were placed in a chilled 1.5 ml microtube and 0.5-1 μg of linearized DNA was added to the cells. The cells and DNA were incubated on ice for 5 minutes before being transferred into an electroporation cuvette with a 2 mm gap. This was immediately placed into a BioRad micropulser electroporator and pulsed with 2 kV using the preset Pichia parameters in the instrument. Immediately post

electroporation, 0.9 ml of 1 M sorbitol was added to the cuvette. The contents of the cuvette were then transferred to a sterile 1.5 ml microtube and allowed to recover for 1 hour at 30 ºC. After recovery, the cells were inoculated onto Yeast Extract Peptone Dextrose Sorbitol Medium (YPDS) plates containing 100 µg/ml of zeocin and allowed to incubate at 30 ºC for 3-5 days or until colonies appeared.

2.2.3 SCREENING OF *Pichia pastoris* CLONES FOR HIGH EXPRESSION

Pichia transformants express protein at differing levels based on the number of copies of the transformed construct integrated into the *Pichia's* genome. The higher the number of copies, the higher the expression levels of recombinant protein as well as the higher the resistance to zeocin. Initial screening for high expressing transformants was carried out by spotting of 52 individual colonies onto gridded YPD plates containing 1 mg/ml zeocin. After two days of growth at 30 ºC, each colony was analyzed for its ability to grow on the 1 mg/ml zeocin plates. Colonies showing the healthiest/most robust growth were selected for secondary screening.

Secondary screening consisted of growing the colony in 12 ml of YPD medium overnight, followed by transfer into 4 ml of the expression medium, buffered methanol-complex medium (BMMY) containing 0.5 % methanol (v/v). The culture was allowed to grow for 72 hours with a total of 0.75 % methanol added approximately every 24 hours. After 3 days of growth in expression media, the cultures were spun down and a 2 µl portion of unconcentrated supernatant from each colony was run on an SDS-PAGE gel. The SDS-PAGE was silver stained, and the best expressing colony was identified based on which colony had the largest sCD14 band. The position of the sCD14 band in the

SDS-PAGE was initially confirmed via western blotting. The sCD14 band in subsequent SDS-PAGE screening gels was identified by position as it was the dominant band on the gel, and distinctly positioned in relation to the molecular weight marker.

2.2.4 EXPRESSION AND PURIFICATION OF SOLUBLE CD14

Large-scale shake-flask expression of sCD14 took place using 2.8 L Fernbach flasks. A single loop from a glycerol stock of the highest expressing sCD14 colony was streaked onto a 200 mg/ml zeocin YPD plate and allowed to grow for two days. Several individual colonies were then selected and inoculated into 15 ml of YPD. After growth overnight, the 15 ml culture was used to inoculate a 125 ml of YPD. This 125 ml culture was grown overnight, and the following day used to inoculate 1L of YPD. The 1 L YPD growths were allowed to grow to an OD_{600} of 5-8, approximately 20-24 hours, at which time the cultures were spun down. The cell pellet was then resuspended in 250 ml of the expression media, BMMY, and 0.75 % (v/v) of methanol was added every 24 hours. After ~96 hours in BMMY media, the culture supernatant was harvested via a multistep centrifugation process. Isotopic labeling was accomplished by simply substituting the unlabeled methanol and ammonium sulfate in BMMY for ^{13}C methanol, and ^{15}N ammonium sulfate.

The culture media supernatant was passed through an IMAC column packed with ~3 ml of Talon Cobalt Metal Affinity Resin (Clontech, Mountain View, CA). The column was washed with 100 ml of PBS, pH 7.4 containing 1M NaCl to remove nonspecific binders. Then 40 ml of 20 mM imidazole in PBS pH 7.4 was used to elute weakly binding proteins, followed by 40 ml of 125 mM imidazole in PBS pH 7.4 to elute

tightly bound proteins. The imidazole elutes were then concentrated down to 1.5 ml and loaded onto a HiPrep S-100 Sephacryl column (GE Healthcare). The column was run at 0.5 ml/min in PBS pH 7.4. The resulting pure sCD14 peak eluted from the column at ~65 ml and individual 1 ml fractions were stored at -80 °C.

2.2.5 GROWTH, EXTRACTION, AND PURIFICATION OF Kdo_2-LIPID A

Production of Kdo_2-Lipid A was accomplished by use of the *E. coli* mutant WBB06, which was grown in M9 minimal medium at 37 °C with agitation. One liter of M9 medium contained 7 g Na_2HPO_4, 3.5 g KH_2PO_4, 0.5 g NaCl, 1 ml trace metals solution, 4 g D-glucose, 1 g NH_4Cl, and 12 μg/ml tetracycline. To obtain isotopically labeled samples $^{13}C_6$ D-glucose and $^{15}NH_4Cl$ were substituted in place of their unlabeled versions. After 22-24 hours the cell pellet was harvested by centrifugation, and the cell pellet was then stored at -80 ºC until needed.

Prior to extraction of the Kdo_2-Lipid A, the cell pellet was resuspended and washed with endotoxin-free water and then washed twice with anhydrous ethanol. The washed pellet was inverted and allowed to drain for ~10 minutes. A monophasic extraction solution containing liquid phenol, chloroform, and petroleum ether in a ratio of 2:5:8 (v/v) was added to the cell pellet in a ratio of 4 ml extraction solution per 1 gram of cell pellet. The cell pellet-extraction solution mixture was then vortexed and sonicated until a fine solution was produced. The cell pellet-extraction solution mixture was then sealed tightly and left stirring overnight at room temperature. Next, the extraction mixture was centrifuged at 15,000 rpm for 10 minutes, and the supernatant was saved. The pellet was re-extracted once more for 2-3 hours and centrifuged again. The supernatant from

both extractions was pooled and filtered into a round bottom flask. Petroleum ether and chloroform were removed via rotary evaporator; deionized water was added dropwise to the remaining liquid phenol in the round bottom flask to precipitate the Kdo_2-Lipid A (*129*).

The precipitate was collected by centrifugation and resuspended by vortexing and sonication in 0.2 M NaCl, which causes Kdo_2-Lipid A to aggregate; the round bottom flask was also washed and sonicated with several ml of 0.2 M NaCl and this was pooled with the resuspended precipitate. The supernatant was then ultracentrifuged at 30,000 rpm for 15 minutes to concentrate the Kdo_2-Lipid A. The resulting supernatant was poured off the pelleted Kdo_2-Lipid A before being resuspended in 1.5 ml of fresh 0.2 M NaCl. This sample was then loaded on a HiPrep Sephacryl S-100 column, using 0.2 M NaCl running buffer, and with UV detection at 254 nm (*130*). The Kdo_2-Lipid A micelle eluted as a single peak in the void volume of the column. The center peak fractions were combined, placed in an ultracentrifuge tube, and diluted with endotoxin-free water. The combined fractions were then centrifuged at 50,000 rpm for 15 minutes. This was followed by repeated resuspension and centrifugation steps, until the Kdo_2-Lipid A pellet was a uniform hazy, clear-white color. The sample's identity and purity were then confirmed by NMR using 1D and 2D ^{1}H-^{13}C HSQC experiments, with a final purity of >90 %. In instances demanding even higher purity, the Kdo_2-Lipid A samples were subjected to hydrophobic interaction chromatography (HIC) using a column packed with octyl-Sepharose CL-4B (Sigma Aldrich). Samples were eluted using a linear gradient from of *n*-propanol in 0.1M ammonium acetate, pH 4.7 (*131*). Confirmation of the

identity and purity of Kdo_2-Lipid A was achieved by collecting a one dimensional ^{1}H-^{13}C HSQC spectrum in the mixed deuterated solvent mixture, CD_3OD:$CDCl_3$:D_2O (3:2:1 v/v), which was compared to the published spectrum and assignments in Qureshi et al. (*41*). Experiments were performed at 25 ºC on either a cold probe equipped Varian VNMRS 600 MHz spectrometer or a Varian VNMRS 500 MHz equipped with a Varian OneNMR™ probe.

2.2.6 PREPARATION OF Kdo_2-LIPID A AND LIPOTEICHOIC ACID STRUCTURAL VARIANTS

LIPID A

Production of lipid A from Kdo_2-Lipid A was accomplished by addition of 1% acetic acid to the sample and incubation at 70 ºC for 2 hours (*132*). The sample was then diluted with endotoxin-free water and centrifuged at 14,000 rpm to pellet the lipid A. The pelleted lipid A was resuspended in endotoxin-free water aided by sonication; this process was repeated five times. This sample was then resuspended in a three solvent mixture of CH_3OH:$CHCl_3$:H_2O (3:2:1 v/v); the lipid A micelle is soluble in this solvent, where as any residual Kdo_2 units or trace salts are not. The lipid A in the three solvent mixture was centrifuged for 20 minutes at 14,000 rpm to pellet any remaining impurities. The supernatant containing the lipid A was saved, and evaporated to dryness. The dried sample was then resuspended, with the aid of sonication, in 2 ml of endotoxin-free water, and loaded onto a NAP-25 column (GE Healthcare). The column was washed with 2 ml of endotoxin-free water and the pure lipid A was eluted with an additional 3.5 ml of endotoxin-free water, per the manufacturer's recommendations.

MONOPHOSPHORYL LIPID A

Monophosphoryl lipid A was obtained by hydrolysis of pure lipid A with 0.1 M HCl at 100 ºC for 45 min (*123*). The reaction solution was neutralized with 1M NaOH, and the cleaved 1-phosphate group was washed away from the lipid A by repeated washing/centrifugation steps. The three solvent mixture CH_3OH:$CHCl_3$:H_2O (3:2:1 v/v) was used for the final wash as described above for lipid A.

DEPHOSPHORYLATED Kdo_2-LIPID A

Dephosphorylated Kdo_2-Lipid A was prepared from Kdo_2-Lipid A by acid hydrolysis with 48 % aqueous HF for 72 hours at 4 ºC with continuous stirring. The HF was neutralized using saturated sodium bicarbonate. The neutralized solution was then centrifuged at 35,000 rpm for 25 minutes, and resuspended in endotoxin-free water; this step was repeated 5-8 times. The final washed sample was then resuspended in a three solvent mixture of CH_3OH:$CHCl_3$:H_2O (3:2:1 v/v), and centrifuged and evaporated as described above for lipid A.

DE-O-ACYLATED Kdo_2-LIPID A

De-O-acylated Kdo_2-Lipid A was prepared by overnight incubation in 0.25 N NaOH at 37 ºC. After centrifuging at 10,000 rpm for 20 minutes to clarify the solution, the supernatant was saved and the pH adjusted to 3.5 with the addition of 4 M HCl. The de-O-acylated Kdo_2-Lipid A was precipitated from the acidified supernatant by addition of 5 volumes of chilled isobutanol, and then allowed to stand for 12 hours at -20 ºC. The resulting precipitate was recovered by centrifugation and washed twice with the chilled alcohol. The precipitate was washed with ice-cold ether-acetone (1:1), and the solvents

were removed by evaporation under a stream of nitrogen gas (*123*).

LIPID IVa

Lipid IVa was produced using the *E. coli* mutant CMR300, which was grown as described earlier for the mutant strain WBB06. The Lipid IVa was extracted by re-suspension of the cell pellet in a single-phase Bligh/Dyer solution (chloroform:methanol:PBS, 1:2:0.8 v/v), which was stirred for 1 hour at room temperature. The single-phase supernatant was then converted to an acidic two-phase Bligh/Dyer (chloroform:methanol:0.1N HCl, 2:2:1.8 v/v) solution by addition of the proper volumes of chloroform and water. The two-phase solution was centrifuged and the lower phase saved and evaporated under nitrogen gas. The dried lower phase was then re-suspended in 5 ml of chloroform/methanol/water (2:3:1, v/v), and applied to a 2 ml DEAE cellulose column (acetate form) equilibrated with the same solvent mixture. The column was washed with 20 column volumes of chloroform/methanol/water (2:3:1, v/v). The Lipid IVa was eluted with successive 10 ml steps of chloroform/methanol/aqueous ammonium acetate (2:3:1, v/v), with increasing ammonium acetate concentrations of 60, 120, 240, and 480 mM (*133*). The fractions of the 240 and 480 mM eluates were checked by NMR for the presence of Lipid IVa. The Lipid IVa was detected in the 480 mM ammonium acetate fractions, and in the last 240 mM fraction.

All structural variants were analyzed for identity and purity by NMR spectroscopy using one and/or two dimensional ^{1}H-^{13}C HSQC experiments using the three solvent system with deuterated solvents CD_3OD:$CDCl_3$:D_2O) (3:2:1 v/v). All

experiments were carried out at 25 ºC on either a cold probe equipped Varian VNMRS 600 MHz spectrometer or a Varian VNMRS 500 MHz equipped with a Varian OneNMR™ probe.

2.3 RESULTS AND DISCUSSION

2.3.1 EXPRESSION, PURIFICATION, CHARACTERIZATION, AND ISOTOPIC LABELING OF SOLUBLE CD14 IN *Pichia pastoris*

Considerable enhancement of *Pichia* expression levels was achieved by significant modification and optimization of the parameters for the transformation of the sCD14 construct into *Pichia*. Additional optimization of the screening process to identify clones with the highest protein expression levels led to more efficient identification of colonies with high expression levels. Furthermore, altering the composition of the standard culture medium, and fine-tuning of the methanol levels in the cultures led to a significant enhancement of protein expression. The final transformation, screening, and expression methods we developed have evolved far beyond the standard protocols and optimizations suggested by the supplier, Invitrogen (Carlsbad, CA). Additionally, a robust fermentation protocol for expression was developed yielding large quantities of unlabeled sCD14. Secretion of sCD14 into the expression medium was accomplished via the α-factor secretion signal contained in the pPICZαA expression vector from Invitrogen (Carlsbad, CA), and in conjunction with a 6x Histidine tag on the C-terminus greatly simplified purification (**Figure 2.2**).

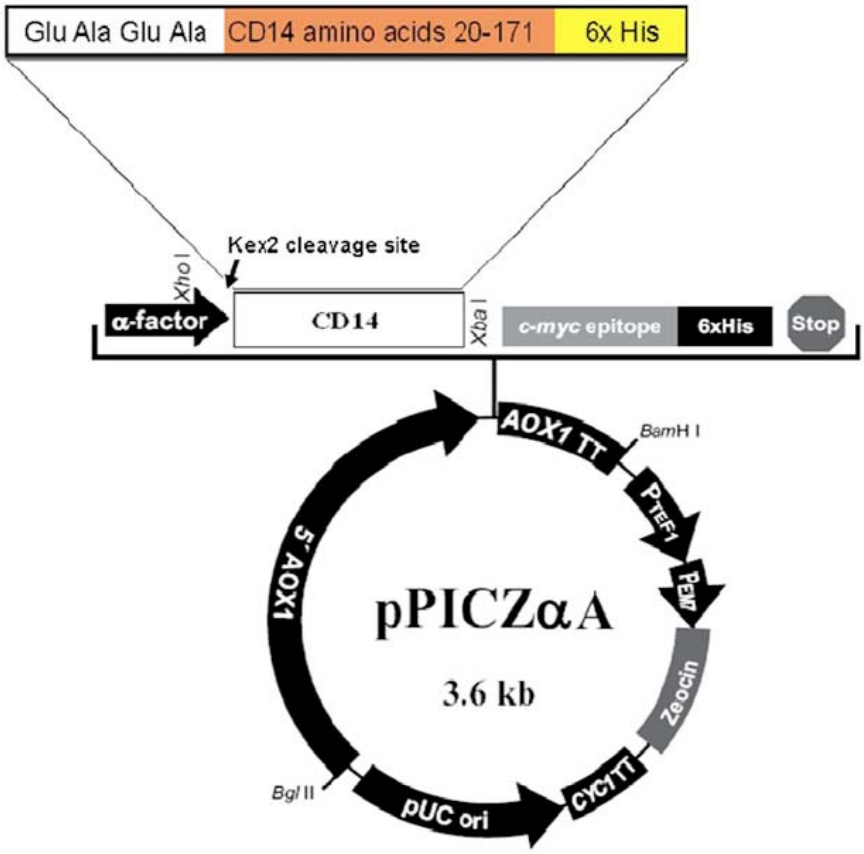


Figure 2.2: Schematic for cloning of soluble CD14 into the pPICZαA vector.
Schematic for cloning of sCD14 sequence (residues 20–171) in pPICZαA vector along with a 6x His-tag for expression in *Pichia pastoris*. Recombinant sCD14 is secreted into the extracellular medium by the yeast α-factor secretion signal via cleavage at the Kex2 protease site.

Immobilized metal-affinity chromatography (IMAC) was employed to recover sCD14 from the expression media and yielded a partially pure product. The concentrated eluate from the IMAC column was then subjected to size-exclusion chromatography yielding a single band with an approximate molecular weight of ~32 kDa as shown by SDS-PAGE gel analysis (**Figure 2.3**). The observed ~32 kDa molecular weight is higher than the calculated molecular weight of ~18 kDa, which is likely due to the presence of glycosylation at the two potential N-glycosylation sites, Asn^{18} and $Asn1^{32}$, contained in the sCD14 152 residue truncation (*74*). Deglycosylation studies using the enzyme PNGase F (New England BioLabs), which cleaves N-linked glycosylations, resulted in the disappearance of the 32 kDa band and appearance of a single band at ~20 kDa (**Figure 2.4**), supporting the presence of N-linked glycosylations.

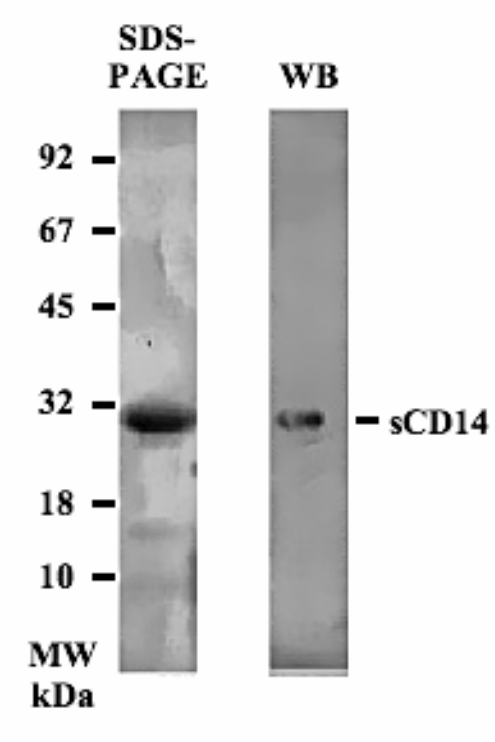


Figure 2.3: SDS-PAGE and Western Blot analysis of soluble CD14 expressed in *Pichia pastoris*.
(SDS-PAGE) Coomassie stained SDS-PAGE showing a single band for sCD14. (WB) Western blot of sCD14 with the monoclonal CD14 antibody, Mem-18, confirming the band's identity.

The identity of the purified sCD14 was confirmed via western blot using the monoclonal antibody MEM-18 (Abcam), which binds within the endotoxin-binding domain of CD14 (**Figure 2.3**) (*110, 134*). N-terminal sequencing (Dana-Farber Cancer Institute) provided additional confirmation that the purified protein was CD14.

Proper folding of the *Pichia* expressed sCD14 was confirmed through circular dichroism spectroscopy (**Figure 2.5**). The circular dichroism (CD) spectra of our *Pichia* produced 152-residue CD14 truncation matched that of CD spectra collected on the 152-residue truncation by previous groups (*135*). The biological activity of the sCD14 was confirmed using a cell-based assay utilizing THP-1 human monocyte cells. THP-1 cells naturally express human TLRs 1-10 but not CD14.

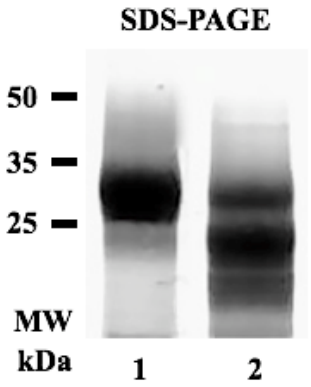


Figure 2.4: SDS-PAGE of soluble CD14 expressed in *Pichia pastoris* deglycosylated by PNGase F.
SDS-PAGE of pure sCD14 (1) and deglycosylated sCD14 (2) after cleavage of N-linked glycosylations by PNGase F. Sample shows some residual glycosylated sCD14 present, likely due to inadequate incubation time, while the majority was deglycosylated. The low molecular weight streak is cleaved glycosyl chains.

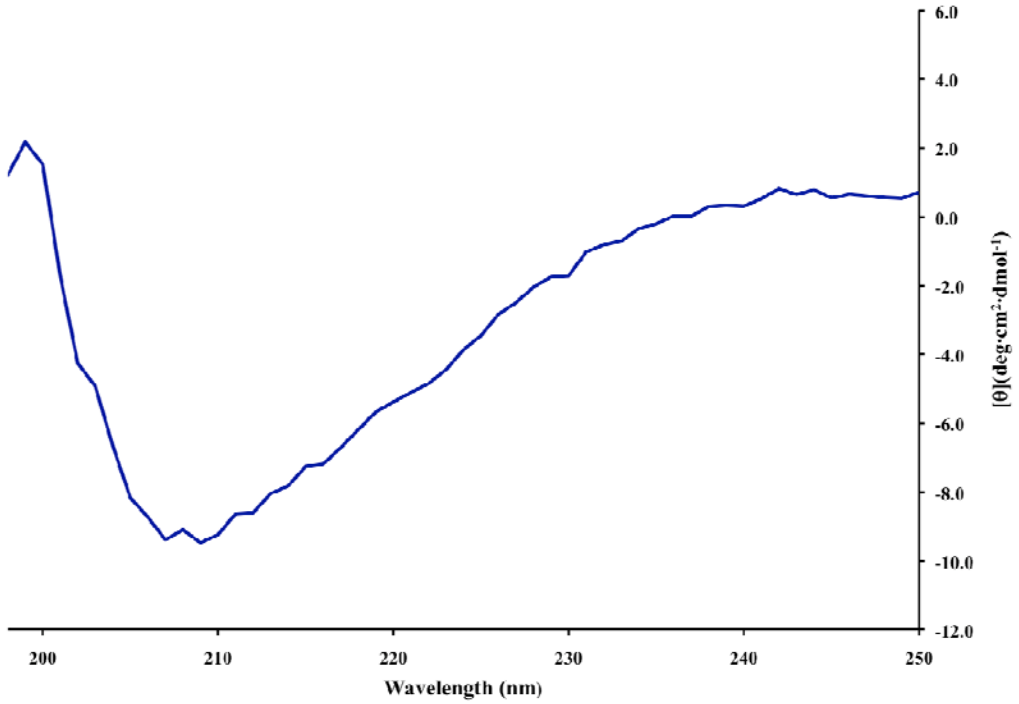


Figure 2.5: Far-UV Circular Dichroism spectra of soluble CD14.
Circular dichroism spectra is the average of five scan collected on a 1μM sCD14 sample in PBS buffer, pH 7.4 at 25ºC.

The absence of endogenous CD14 allows the biological activity of our recombinant sCD14 to be monitored by its ability to up-regulate production of the inflammatory mediator NF-kB. This assay was performed using THP1-Blue cells (Invivogen, San Diego, CA) containing a stably transfected NF-κB-inducible reporter, secreted embryonic alkaline phosphatase (SEAP), whose levels can be quantitatively measured using the QUANTI-Blue colorimetric reagent (Invivogen). The THP1-Blue cells were incubated singly or in varying combinations with sCD14, recombinant human LBP (R&D Systems, Minneapolis, MN), recombinant human CD14 (R&D Systems), *E.coli* K-12 full-length LPS (Invivogen), Kdo_2-Lipid A, dephosphorylated Kdo_2-Lipid A, lipid A, monophosphoryl lipid A, or LTA. Up-regulation of the THP-1 cell's production of NF-κB, is indicative of an up-regulation of the inflammatory response by sCD14. The level of NF- κB was quantified via detection of SEAP. An upsurge in NF-κB induces expression of the NF-κB-regulated inflammatory cytokines, such as IL-1, IL-6, and IL-8 which are associated with increased activation of the inflammatory response (*136*). The sCD14 was found to be biologically functional in this assay, as it was able to up-regulate the production levels of NF-κB over that of cells incubated without CD14 (**Figure 2.6**).

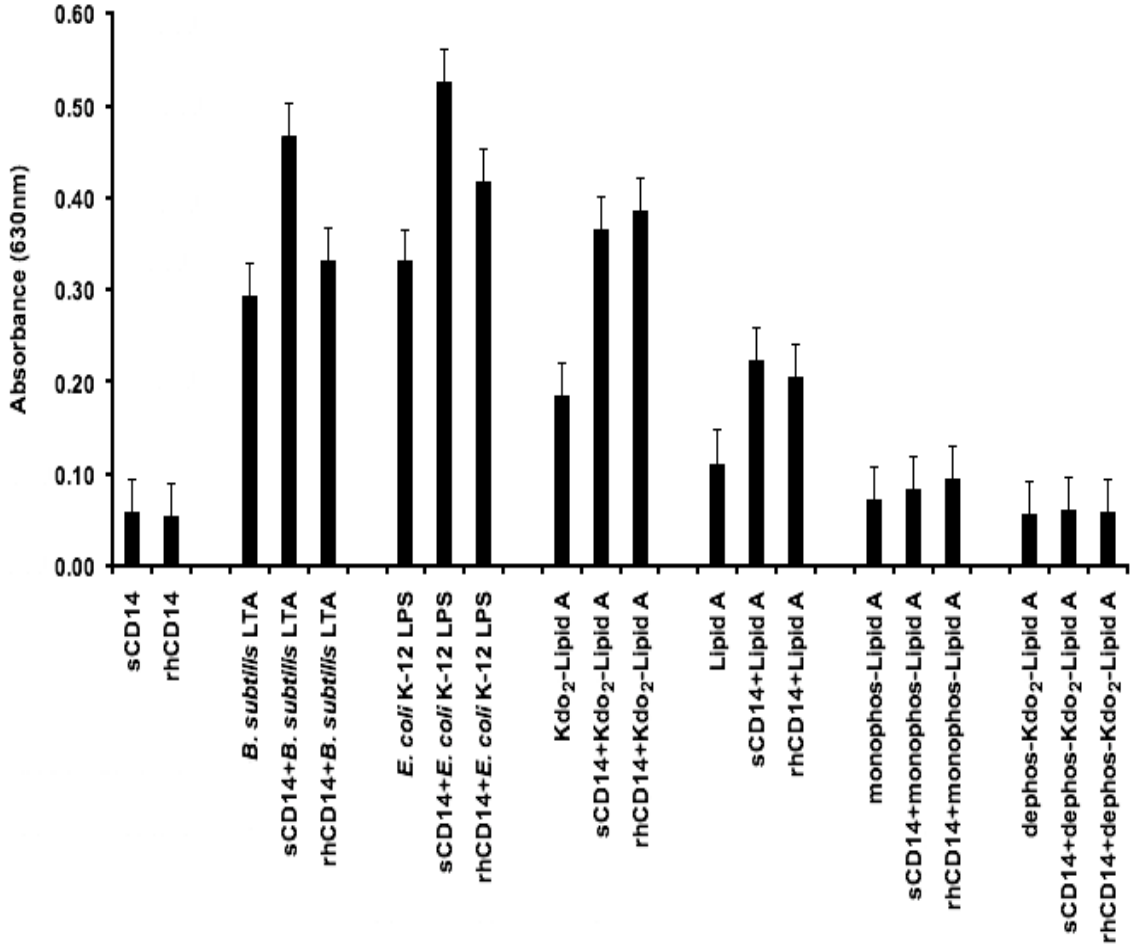


Figure 2.6: Biological activity analysis of soluble CD14 with endotoxin ligands.
Responses of THP1-blue cells-mediated by full-length wild-type sCD14 (8nM) and pure *Pichia pastoris* produced sCD14 (8nM). Upon stimulation with ~1μM of one of five agonist, *E. coli* K-12 full-length LPS, *B. subtilis* LTA, Kdo_2-Lipid A, Lipid A, the partial agonist monophosphoryl Lipid A, or the non-binder dephosphorylated-Kdo_2-Lipid A stimulation was assessed by measuring the levels of NF-κB, which was quantified by its induction of the reporter secreted embryonic alkaline phosphatase (SEAP). SEAP levels were detected via absorbance readings at 630 nm of culture supernatants in SEAP detection medium. Control experiments are the responses generated by rhCD14 and sCD14 alone. The values shown represent an average of three separate measurements. Error bars represent average standard deviation across all three experiments.

The sCD14 produced in this work using *P. pastoris* showed essentially the same level of NF-κB up-regulation as the rhCD14 (R&D Systems), which was produced using Chinese hamster ovary (CHO) cells. The NF-κB levels induced by sCD14 were substantially higher than the background levels generated through the endogenous NF-κB response of the THP-1 cells, demonstrating that our sCD14 is capable of up-regulating production of NF-κB in human monocytes. Results from these experiments demonstrate that the sCD14 produced using *Pichia pastoris* is capable of binding a variety of endotoxins, and initiating the increased production of NF- κB, which is indicative of biological activity. Additionally, the *Pichia* expression system allowed us to produce uniformly labeled sCD14 samples for use in NMR studies.

Other groups have previously reported the expression and purification of recombinant sCD14 from *P. pastoris* (*135, 137*). However, production of endotoxin-free, isotopically labeled sCD14 for use in NMR investigations was not demonstrated in their studies. For the first time, isotopic labeling of sCD14 was carried out using ^{15}N ammonium sulfate and ^{13}C methanol to produce both single and double labeled versions of sCD14, as evidenced from the ^{1}H-^{15}N HSQC spectra of sCD14 (**Figure 2.7**). Approximately half of the 152-residues in sCD14 are clearly visible in the ^{1}H-^{15}N HSQC spectrum of sCD14. The high degree of spectral overlap in the ^{1}H-^{15}N HSQC spectrum is primarily due to the high number of aliphatic amino acids present in sCD14, ~42% of the total amino acid content. These overlapping resonances form broad multiplets, which impede accurate identification/ determination of the total number of residues visible. Some of the missing peaks could be due to deprotonations in the pH 8.9 buffer. Other

missing peaks might be a result of exchange broadening lowering the intensity levels below the threshold of detection. Additionally, the truncated sCD14 sequence contains 12 prolines, which do not produce a signal ^{1}H-^{15}N HSQC spectra.

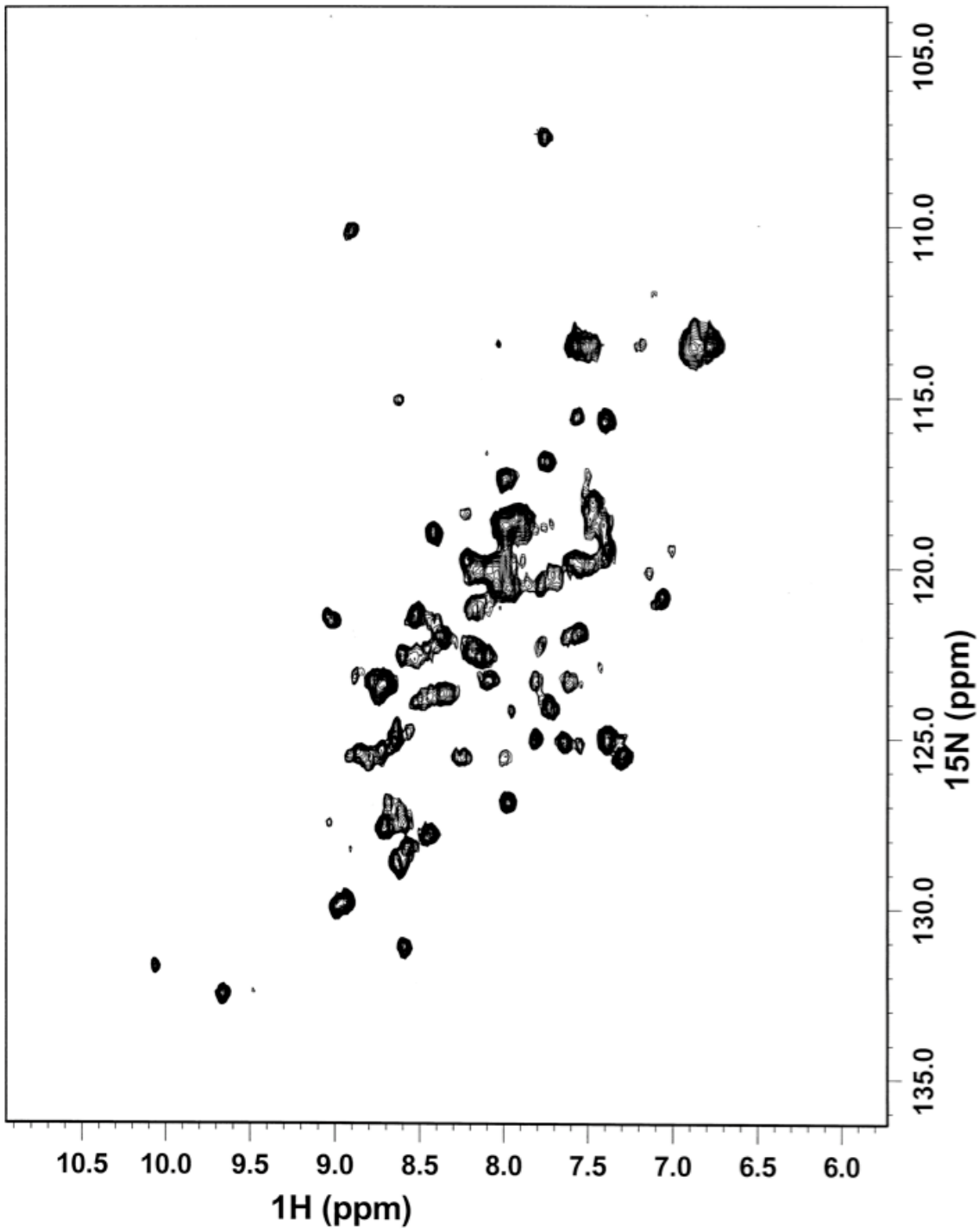


Figure 2.7: ^{1}H-^{15}N HSQC of isotopically labeled soluble CD14 expressed in *Pichia pastoris*.
^{15}N-labeled sCD14 N-terminal 152-residue truncation in PBS buffer, pH 8.9, containing 2M D_5-glycine collected at 37 ºC.

2.3.2 EXPRESSION, PURIFICATION, CHARACTERIZATION, AND ISOTOPIC LABELING OF Kdo_2-LIPID A AND LIPOTEICHOIC ACID

An extensive panel of LPS- and LTA-based ligands with varying partial structures corresponding to agonists, partial agonists, antagonists, and non-binders has been generated in ^{13}C, ^{15}N isotopically labeled forms. Successful production and purification of Kdo_2-Lipid A has been accomplished through growth of *E. coli* WBB06 in minimal medium, and labeled samples were produced by supplementing the media with $^{13}C_6$-glucose and ^{15}N ammonium chloride. Purification of Kdo_2-Lipid A directly from cell membranes was achieved using a multi-step process resulting in pure hexaacylated Kdo_2-Lipid A samples, and removing any residual traces of undesired underacylated forms and contaminating lipoproteins and peptides. Lipid IVa was produced by growth of *E. coli* mutant CMR300 in minimal media, and labeling was accomplished in the same manner as described for *E. coli* mutant WBB06.

The resulting samples were of high-purity and produced in milligram quantities in both unlabeled and labeled versions, as shown by the ^{1}H-^{13}C HSQC of Lipid A (**Figure 2.8**).

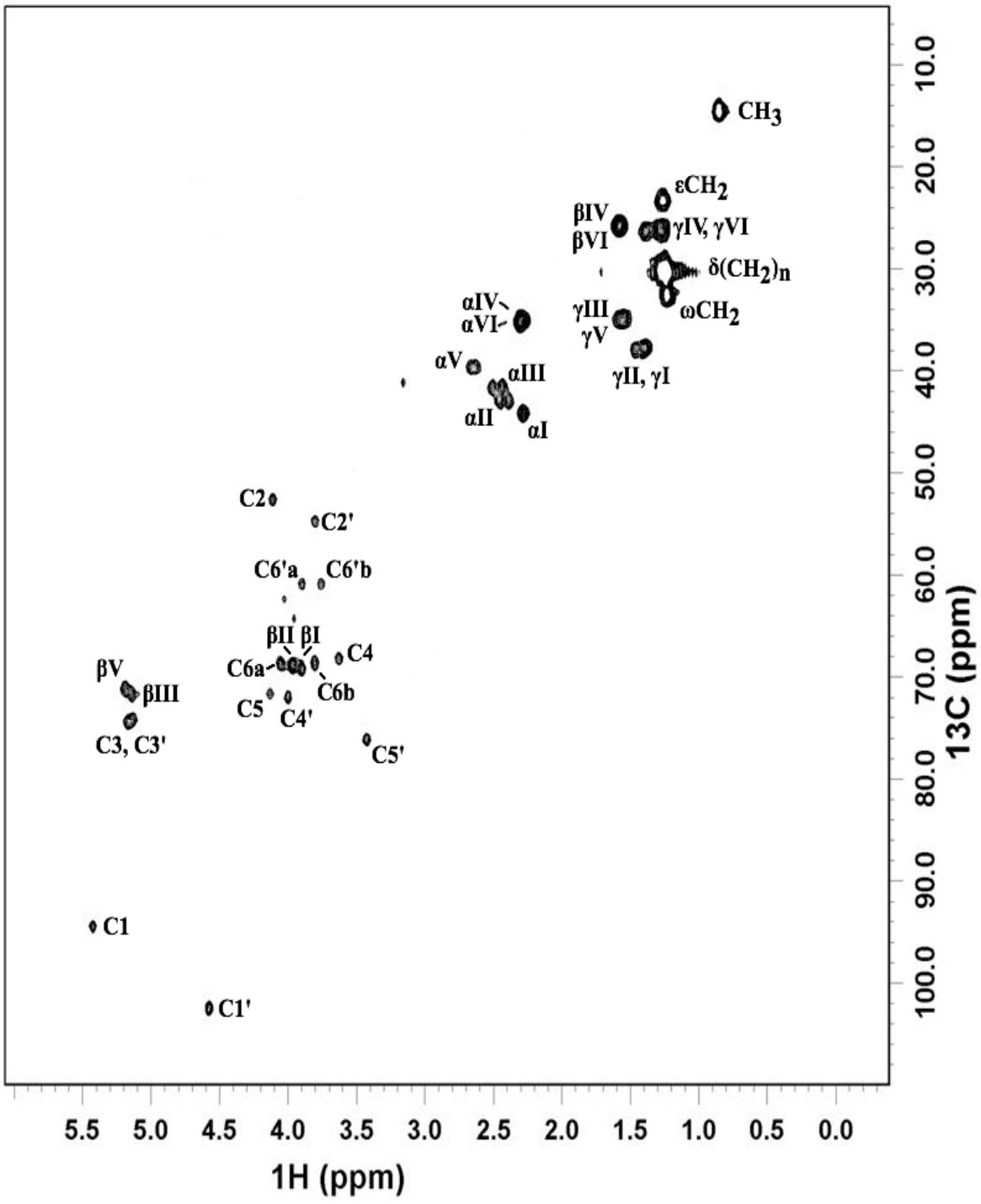


Figure 2.8: ^{1}H-^{13}C HSQC spectrum of ^{13}C isotopically labeled Lipid A.
The two-dimensional ^{1}H-^{13}C HSQC spectrum of isotopically labeled Lipid A in $CDCl_3$:CD_3OD:D_2O (2:3:1, v/v) mixed solvent system showing correlations within the sugar headgroup and acyl chain regions.

Additionally, the Kdo_2-Lipid A and lipid A structural variants were also produced in pure milligram quantities in both labeled and unlabeled forms. Since the overall lipid A-like character is maintained in these partial structures, it is likely that they bind to a similar region on CD14. The specific structural interactions of individual features and motifs can be distinguished from the fully intact agonist ligands. The ability of the agonistic ligands to elicit an immune response was confirmed through the THP-1 human monocyte cell based assay (**Figure 2.6**). These highly purified, well characterized ligands serve as aids in the dissection of the sCD14 binding interactions, revealing the features necessary for recognition and binding by CD14 as described in Chapter 4. . Not all Kdo_2-Lipid A and lipid A variants we prepared were used in NMR binding studies. The structural variants, Kdo_2-Lipid A, lipid A, dephosphorylated Kdo_2-Lipid A, and monophosphoryl lipid A were used in the THP-1 cell based assay and for NMR studies. Lipid IVa was also use in NMR binding studies. The only variant not used in either a cell based assays or for NMR studies was de-O-acylated Kdo_2-Lipid A, which was the most difficult to produce. However, the high-quality NMR data collected using the other structural variants did not require the use of de-O-acylated Kdo_2-Lipid A for structural information

The gram-positive endotoxin LTA was produced and extracted from *Bacillus subtilis* ATCC 6633™ using n-butanol in order to prevent the structural decomposition associated with traditional phenol extraction methods (*50*). We were able to successfully

produce milligram quantities of ^{13}C, ^{15}N labeled LTA ligands as demonstrated by the ^{1}H-^{13}C HSQC spectra of LTA (**Figure 2.9**). The effects of CD14 binding of the ^{13}C-isotopially labeled LTA lipid anchor is described in Chapter 5.

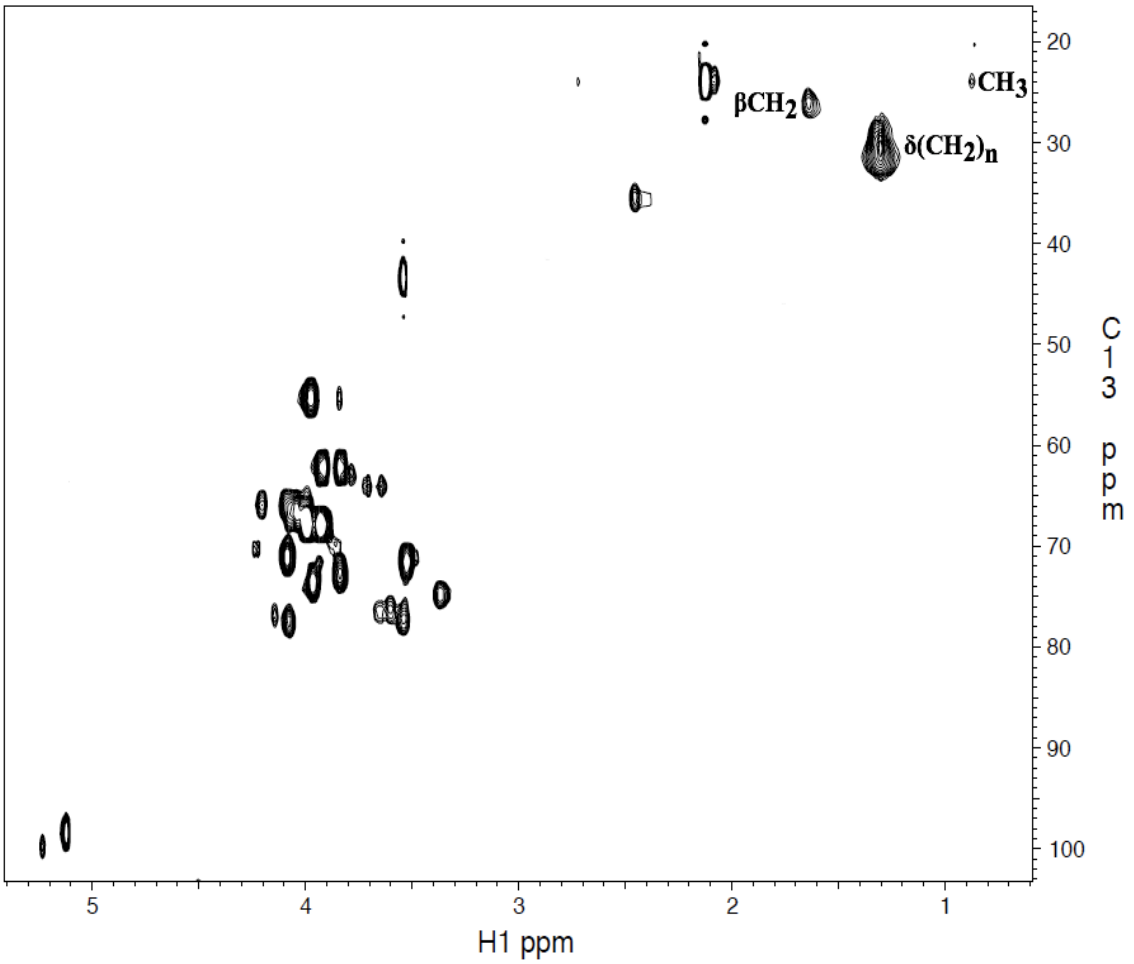


Figure 2.9: ^{1}H-^{13}C HSQC spectrum of ^{13}C isotopically labeled full-length Lipoteichoic acid.
Partially annotated two-dimensional ^{1}H-^{13}C HSQC spectrum of ^{13}C isotopically labeled LTA from *B. subtilis* in PBS buffer pH 8.9 containing 2M D_5-glycine.

CHAPTER 3. SOLUTION NMR STUDIES PROVIDE A STRUCTURAL BASIS FOR ENDOTOXIN PATTERN RECOGNITION BY THE INNATE IMMUNE RECEPTOR CD14

This chapter is a modified version of a paper first published in *Biochemical and Biophysical Research Communications* in 2008:

"Reprinted from *Biochemical and Biophysical Research Communications*, Vol. 368, Albright, S., Chen, B., Holbrook, K., and Jain, N. U., Solution NMR studies provide structural basis for endotoxin pattern recognition by the innate immune receptor CD14, 231-237, (2008), with permission from Elsevier."

As first author, I performed a majority of the experimental work and sample preparations. Nitin Jain carried out the NMR spectroscopy experiments, processed, and analyzed the NMR data. Bin Chen, and Kristen Holbrook assisted in the *Pichia pastoris* growth and purifications of CD14.

3.1 INTRODUCTION

To date, several studies have confirmed interactions of CD14 with a variety of microbial ligands such as lipopolysaccharide (LPS) from gram-negative bacteria, lipoteichoic acid (LTA), and peptidoglycan (PGN) from gram-positive bacteria, lipoproteins, lipoarabinomannan, polymannuronic acids, and even synthetic molecules (*17, 57, 97, 138-140*). The ability of CD14 to interact with such structurally diverse endotoxins has led to the hypothesis that CD14 functions as a pattern recognition receptor by recognizing and binding to different pathogen-associated molecular patterns (*17*). It is believed that this pattern recognition may be important for the high selectivity of CD14-mediated cellular activation, and the distinctiveness of the signaling pathway in response to specific ligands (*141*). However, the mode of recognition of these structurally distinct

patterns by CD14 is not clear, since structural details for CD14 in complex with any of its ligands is not available. Deletion mutagenesis experiments and epitope mapping with monoclonal antibodies and proteases have previously identified several broad regions (residues 39–44, 57–64, 81– 100) on CD14 that are crucial for the binding of various microbial ligands and possess overlapping sites of interaction for these ligands (*93, 109-111, 138*). More recently, the high-resolution X-ray crystal structure for mouse sCD14 without any ligand has been determined (*75*), in which a potential endotoxin binding pocket can be seen at the N-terminus. Clustered around this pocket are the binding regions identified previously from the mutagenesis experiments. However, apart from these general interpretations, no direct structural evidence for differential binding to specific residues of CD14 is available.

In order to confirm the role of CD14 as a pattern recognition receptor, and provide a structural basis for endotoxin recognition and binding by CD14, direct structural evidence is critical. In order to determine the potential contribution of CD14 residues to endotoxin pattern recognition, we have analyzed the binding of various endotoxin ligands to CD14 at a molecular level using solution NMR spectroscopy. NMR spectral changes were mapped out for the binding interactions between the residues of a fully functional 152-residue N-terminal domain of CD14 and the cell-wall components from gram-negative and gram-positive bacteria. The CD14 was expressed and isotopically labeled in *Pichia pastoris*. The gram-negative and gram-positive cell wall components differ from one another both structurally and with respect to their ability to stimulate innate host responses via CD14. Comparison of the pattern of residues in CD14

affected upon binding of each ligand reveals differential changes in the NMR spectra of CD14 for each ligand. However, the pattern of residues affected by binding of these ligands utilizes both a similar set of residues as well as a subset of different residues specific to the ligand bound. This provides, for the first time, direct structural evidence for endotoxin specific differential recognition by CD14 and supports the pattern recognition hypothesis. Another interesting finding from the observed spectral changes is that the mode of binding may be dynamically modulated, which may provide a mechanism for pattern recognition.

3.2 MATERIALS AND METHODS

3.2.1 EXPRESSION AND PURIFICATION OF ISOTOPICALLY LABELED RECOMBINANT SOLUBLE CD14 IN *Pichia pastoris*

As described in detail in the preceding chapter, the gene sequence encoding the N-terminal endotoxin-binding domain of human sCD14, consisting of 152 residues after the signal peptide sequence (20–171), was codon-optimized for expression in yeast, and was cloned into the pPICZαA vector (Invitrogen) by BIO S&T (Montreal, Canada). The sCD14 pPICZαA construct was transformed into wild-type X-33 *P. pastoris* cells, and the individual colonies were screened using small-scale cultures to select the best sCD14-expressing clone. Expression levels were determined by SDS–PAGE analysis of secreted sCD14 protein in the medium.

At the time of original publication, the protocol used for large-scale shake flask expression of sCD14 was as follows. In a 2.8 liter baffled shake flask, 1 liter of BMD medium (Invitrogen) was inoculated with the best expressing colony and grown for ~24

hrs to an OD_{600} of ~12. The culture was then spun down and the cells resuspended in 250 ml of BMMY medium (Invitrogen). The yeast extract and peptone used in the BMMY medium was filtered through acrodisc mustang E filters (Pall) to reduce the endotoxin levels in the media. Isotopic labeling was accomplished by substituting the primary nitrogen source ammonium sulfate with ^{15}N labeled ammonium chloride. Protein expression was carried out for 4 days with addition of methanol everyday at 0.5 % of the culture volume. At the end of the expression period the cells were spun down, and the sCD14 was purified from the supernatant using a column containing Talon cobalt metal-affinity resin (Clontech). The column was washed with 20 column volumes of PBS buffer (pH 7.4), and washed with 1 column volume of PBS containing 20 mM imidazole, and the bound CD14 eluted with PBS containing 200 mM imidazole.

The protein eluted from the IMAC column was further purified by size exclusion chromatography using a HiPrep Sephacryl S-100 column (GE Healthcare) equilibrated with PBS. Pure endotoxin-free fractions of sCD14 were pooled, concentrated, and used for characterization via SDS–PAGE and Western blot analysis. Samples of sCD14 (~1 μg) were loaded, in duplicate, on Novex 18 % tris–glycine gels (Invitrogen) and run following the manufacturer's recommendations. One half of the gel was then coomassie-blue stained and de-stained overnight, while the other half of the gel was transferred onto a PVDF membrane (Pierce) for Western blot analysis. The membrane was incubated with the monoclonal antibody for CD14, MEM-18, and developed using metal-enhanced DAB (Pierce) per manufacturer's directions (see western blotting protocol in the Appendix).

Circular dichroism (CD) spectra in the far-UV region (190–250 nm) were

collected for 10μM samples of sCD14 at 25 ºC in PBS buffer, pH 7.4, on an AVIV Model 202 spectrometer with and without endotoxins. The circular dichroism spectrum were displayed by calculating the molar ellipticity values and plotted against the wavelength.

3.2.2 BIOLOGICAL ACTIVITY ASSAYS ON RECOMBINANT SOLUBLE CD14-ENDOTOXIN BINDING DOMAIN

For the activity assay, THP1-Blue cells (Invivogen) stably transfected with an NF-κB-inducible reporter, secreted embryonic alkaline phosphatase (SEAP), were cultured in supplemented RPMI 1640 medium at 37 ºC in a 5 % CO_2 environment. Cells were spun down and resuspended at $1x10^6$ cells/ml in fresh growth media. 100 μl of cell suspension was added to each well of a 96-well plate along with sCD14 or recombinant human CD14 (rhCD14) (R&D Systems), recombinant human LBP (rhLBP) (R&D Systems), and one of three individual ligands. The three ligands used were ReLPS (List Biological Laboratories), *S. aureus* LTA (Invivogen), or the peptidoglycan derivative MDP (Sigma Aldrich). The ligands or proteins alone served as positive controls with endotoxin-free water and growth media as negative controls. After incubation for 20–24 hours at 37 ºC under 5 % CO_2, the 96-well plate was spun down, and 10 μl of supernatant from each well was added to 200 μl of Quanti-Blue reagent (Invivogen) in a new 96-well plate to quantitate the amount of SEAP present. This plate was then incubated at 37 ºC, and readings at 630 nm were made every hour for 6 hours using a Biotek Synergy2 plate reader. A final reading of the plate was taken after 18–20 hours.

3.2.3 NMR STUDIES OF SOLUBLE CD14 — ENDOTOXIN INTERACTIONS

CD14 protein samples for the NMR experiments were prepared in PBS buffer pH 7.4 with typical protein concentrations of ~0.2 mM. Stock solutions of endotoxin ligand compounds, ReLPS, a rough strain form of LPS from *Salmonella minnesota* Re595 (List Biological Laboratories), LTA from *Staphylococus aureus* (Invivogen), and MDP (Sigma–Aldrich) were prepared at a 5 mg/ml concentration in D_2O to ensure minimal dilution of protein upon addition of the ligand. The endotoxin stock solutions were extensively sonicated to ensure complete solubilization of the ligands. NMR samples of protein:ligand were prepared in a molar ratio of 1:1, except for MDP, where a ratio of 1:10 was used. Also present in each sample was rhLBP at a concentration of 5μM. Protein:ligand samples were incubated for 30 minutes at 37 ºC to ensure complete binding of ligand (*142*). Sensitivity-enhanced $^{1}H–^{15}N$ HSQC spectra (*143*) were recorded for each sample with and without the ligand. Data was collected with 1024 complex points in the direct dimension and 128 complex points in the indirect dimension. All NMR experiments were carried out on a Varian VNMRS 600 MHz spectrometer at 17 ºC equipped with a cold probe. NMR data was processed and analyzed with the Felix software package (Molecular Simulations).

3.3 RESULTS AND DISCUSSION

3.3.1 EXPRESSION AND ISOTOPIC LABELING OF SOLUBLE CD14 IN *Pichia pastoris*

We were able to accomplish ^{15}N isotopic labeling in *P. pastoris* in an inexpensive manner using ^{15}N ammonium chloride as the nitrogen source. This allowed us to produce

milligram quantities of uniformly ^{15}N labeled samples of the fully functional sCD14 fragment, which includes the region for endotoxin binding (*70*). Both the SDS-PAGE and Western blot indicate that the protein is expressed as a single isoform and in an endotoxin-free form, which is quite valuable for high-resolution NMR structural studies (**Figure 2.3)**.

In order to evaluate whether the purified protein was correctly folded, Circular Dichroism (CD) spectroscopy was used to study the solution secondary structure of sCD14. The far-UV CD spectrum of purified sCD14 is shown in **Figure 3.1**. As seen from the CD spectrum, sCD14 contains a mixture of α-helical and β-sheet type structures. This is confirmed by a recent X-ray structure of mouse sCD14, which depicts an α/β-fold for the protein (*75*). The spectrum of sCD14 changes minimally upon addition of the endotoxin ligand ReLPS, a close structural relative of Kdo_2-Lipid A produced by *Salmonella minnesota* Re959. The lack of significant changes in the CD spectrum suggests that there are no global conformational changes in the protein upon ligand binding (*108*).

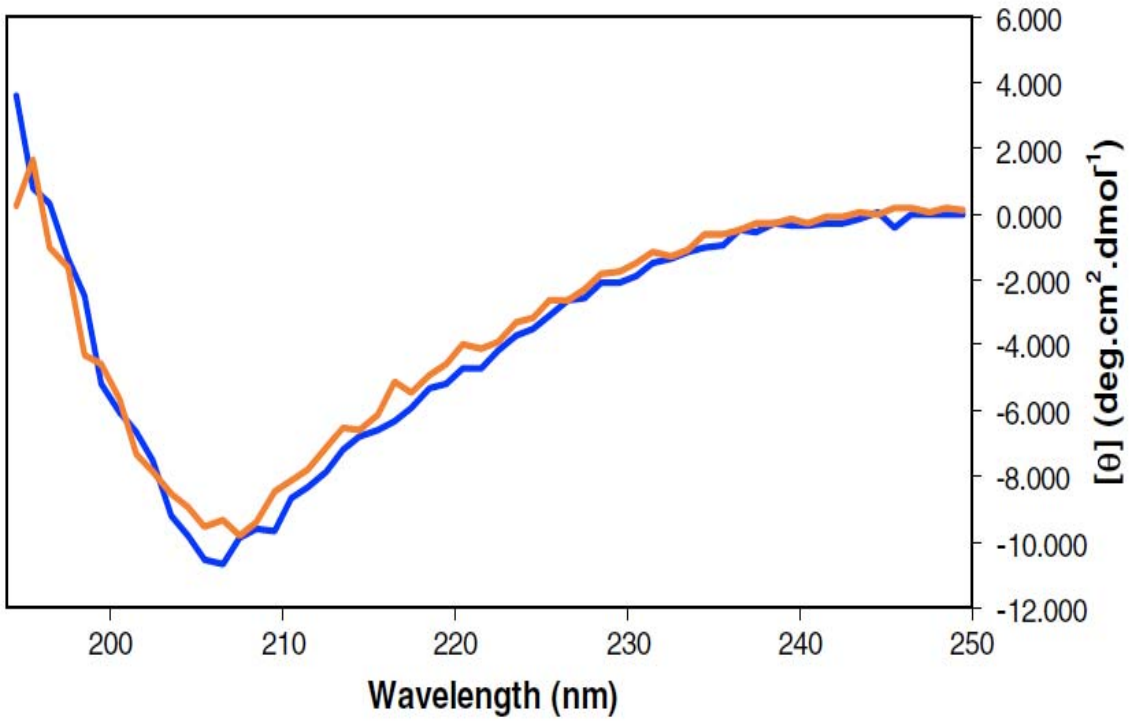


Figure 3.1: Far-UV circular dichrosim spectra of soluble CD14 with and without ReLPS.

sCD14 (blue line) and ReLPS complexed sCD14 (red line). Both spectra are average of five scans.

3.3.2 DETERMINATION OF BIOLOGICAL ACTIVITY OF SOLUBLE CD14

To test the biological activity of sCD14 a cell-based assay was used. The ability of sCD14 to enhance the NF-κB-induced cytokine production from various endotoxin ligands, such as ReLPS, *S. aureus* LTA, and the PGN-derived MDP was monitored. This assay relies on detection of the NF-κB-induced reporter, SEAP, upon activation of an established cell line such as THP1-Blue by endotoxins in presence of CD14 (**Figure 3.2**). Compared to the activation of THP1-Blue cells by the protein or ligands alone, addition of ReLPS to sCD14 and rhLBP produced an almost 3-fold increase in production of NF-κB, while LTA showed an almost 5-fold increase. This is consistent with the observation that LPS and LTA are highly potent activators in mammals. On the other hand, PGN-derived ligand, MDP, showed only a small activation compared to protein or ligand alone. It has been reported previously that sCD14 shows low levels of cellular responsiveness to MDP and only at saturating concentrations (*97*).

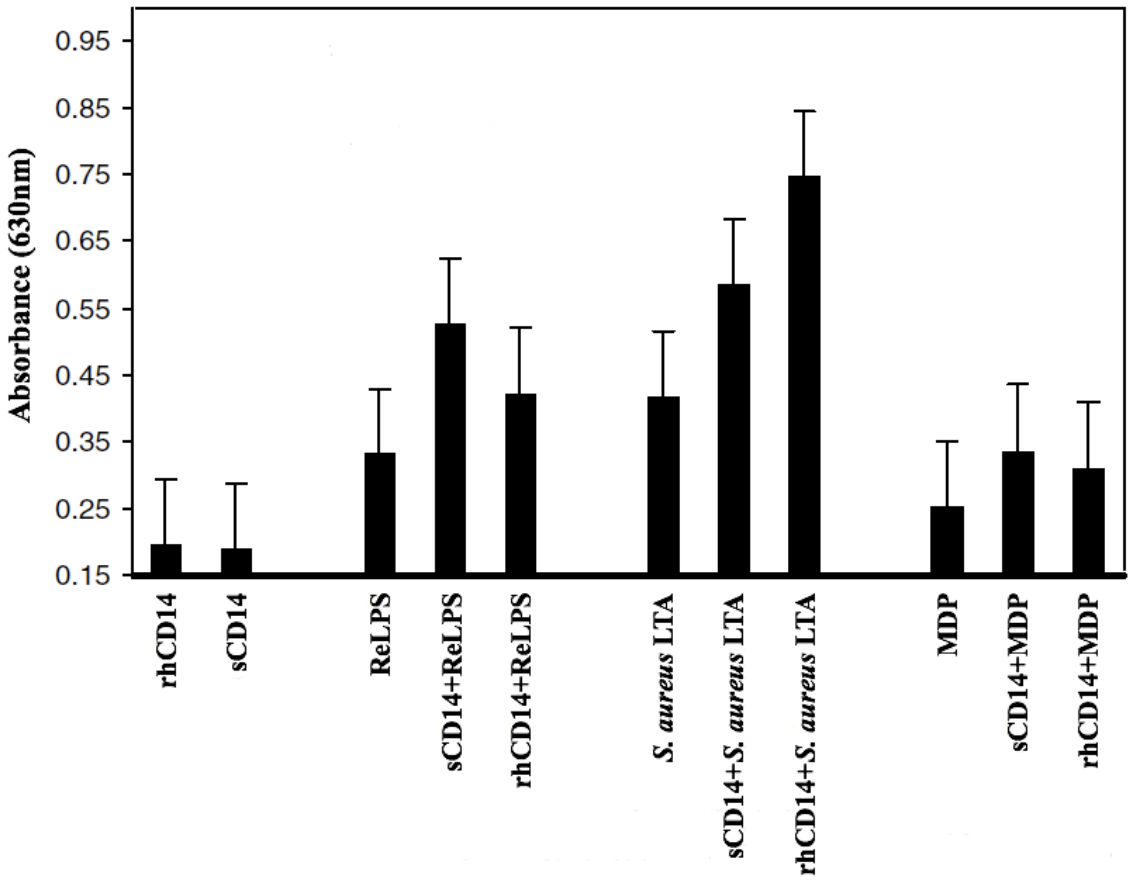


Figure 3.2 Biological activity analysis of soluble CD14 with endotoxin ligands.
Responses of THP1-blue cells-mediated by full-length wild-type sCD14 (rhCD14, 400 ng/ml) and purified sCD14 (sCD14, 200 ng/ml) upon stimulation with three endotoxins, ReLPS (1 μg/ml), *S. aureus* LTA (1 μg/ml), and MDP (200 ng/ml). After 24 hours incubation, endotoxin stimulation was assessed by measuring the levels of NF-κB inducible reporter alkaline phosphatase (SEAP) using a SEAP detection medium with absorbance values at 630 nm. Control experiments in form of responses to rhCD14 and gCD14 alone are shown as well. The values shown represent an average of three separate measurements and the error bars show the range.

However, another possibility that cannot be ruled out is that this small activation is not due to MDP, but due to contamination of this commercial MDP sample with minute traces of LTA and/or lipopeptides. Commercial PGN samples are commonly known to suffer from contamination by residual cell wall components such as teichoic acids, lipopeptides, lipoproteins, and lipoteichoic acid (*144*). Because MDP is derived from PGN, it is entirely possible that it too suffers some level of residual contamination. This is illustrated by the extensive purification techniques applied to PGN in order to obtain pure MDP samples to test the binding and activation of another intracellular immune receptor (*145*). In these circumstances, the multi-step acid hydrolysis needed to produce MDP from PGN should have significantly reduced the residual level of contamination.

Based on the similar levels of NF-κB response observed for each ligand in the presence of sCD14 and rhCD14, it can be inferred that both possess similar abilities to induce NF-κB release by human monocytes (*102*). Therefore, results from these experiments indicate that our recombinant soluble CD14 can bind and induce cellular effects in response to different endotoxins similar to wild-type protein, confirming its biological activity.

3.3.3 CHANGES IN NMR SPECTRA OF CD14 UPON ENDOTOXIN BINDING PROVIDES STRUCTURAL EVIDENCE FOR PATTERN RECOGNITION

In order to gain a structural perspective regarding the mechanism by which CD14 is able to recognize and differentially bind a diverse array of endotoxin patterns through a common binding site(s), we have investigated the interaction of the endotoxins ReLPS,

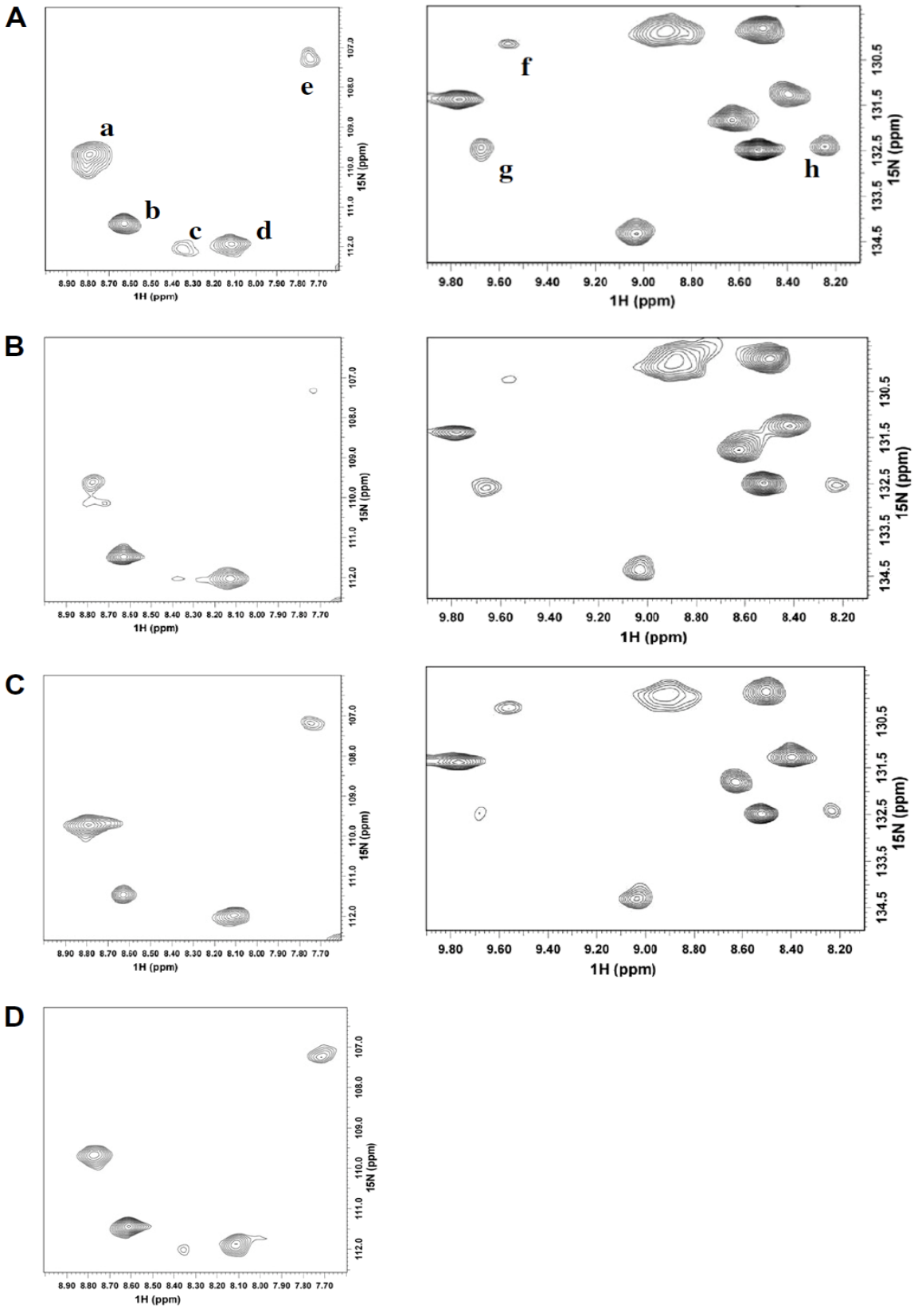
LTA, and MDP using $^{1}H–^{15}N$ HSQC NMR spectroscopy. The endotoxin ligands ReLPS and LTA represent the primary endotoxins of gram-negative and gram-positive bacteria, and are potent activators of the inflammatory response in mammals. MDP is the minimal PGN structure observed in past studies necessary for adjuvant activity (*97*). For many years PGN was thought to be the gram-positive endotoxin. However, it has only been in the last few years that PGN and its derivatives have been excluded as the gram-negative endotoxin. As mentioned above, the immunostimulatory effects attributed to MDP and PGN are likely due to trace contamination of the samples with other gram-positive cell wall components, such as LTA. In the NMR binding studies performed using ^{15}N-labeled CD14, we chose to include the PGN-derivative ligand, MDP, in order to evaluate structurally whether binding by CD14 could be occuring.

The binding studies described here constitute the first molecular level NMR characterization of structural interactions between an innate immune system receptor and endotoxins. Analysis of NMR spectra with and without the endotoxin ligands reveals no drastic overall change in the protein's HSQC spectra. This is in line with the circular dichroism analysis, which also showed no major global structural changes. However, a number of CD14's ^{1}H and ^{15}N backbone amide peaks show specific changes in their resonances with the addition of each ligand, possibly from local structural changes. Both line-broadening and chemical shift changes are observed in the spectra with ReLPS and LTA, but in the case of MDP, only minor chemical shift perturbations can be seen. A comparison of selected regions in the HSQC spectra exhibiting the largest changes upon ligand addition is shown in **Figure 3.3 A–D**. The most striking characteristic observed in

these regions is the pattern of sCD14 resonances affected by each ligand. It is evident from the spectra that ReLPS and LTA affect similar resonances in the CD14 spectra. However, the identity of resonances affected by individual ligands differs. For example, ReLPS and LTA both affect peaks ‘‘c” and ‘‘h” in the spectra, with all three ligands affecting peak ‘‘c”. However, peaks ‘‘e” and ‘‘f” are affected only by ReLPS, while LTA affects only peaks ‘‘b” and ‘‘g” in the regions shown. It is worth noting that the minor changes seen in the spectra of MDP and CD14 appear quite similar to that of LTA bound sCD14 (**Figure 3.3 C & D**). While this could be due to sCD14 binding MDP, we believe this indicates that MDP is not being bound by CD14. The similarity between the changes seen in the MDP spectra and the changes in the bound LTA spectra could be an indication that traces of some gram-positive cell wall component(s) remained as a trace impurity in the MDP sample (*144*). In addition, it has now been shown that sCD14 does not bind any low molecular weight PGN fragments such as MDP (*97, 146, 147*).

Figure 3.3: Changes upon endotoxin addition to the ^{1}H-^{15}N HSQC spectra of soluble CD14.

Comparison of changes upon endotoxin ligand addition for a representative set of resonances in the 600 MHz ^{1}H-^{15}N HSQC spectra of ^{15}N labeled sCD14 in PBS pH 7.4. (A) sCD14 only, (B) sCD14 in 1:1 complex with ReLPS, (C) sCD14 in 1:1 complex with LTA and (D) sCD14 in 1:10 complex with MDP.


A
a
b
c
d
e
f
g
h
1H (ppm)
15N (ppm)
B
C
D

Our observation of the ability of specific residues to differentially affect endotoxin binding demonstrates previously unobserved residue level binding characteristics for CD14 and provides a structural basis for pattern recognition. It is possible that each endotoxin may, either directly or indirectly, individually affect different sets of residues. The set of individual residues affected upon binding of a ligand may depend on the characteristic molecular pattern possessed by the ligand. Given CD14's broad ligand specificity, several of the structural features affected in CD14 are likely shared between the different endotoxins in order to maintain spatial and functional similarity within the interaction site. Because assignments for CD14 are not currently available, it is not possible to locate the exact regions affected by ligand binding in the sequence of CD14. However, it is probable that the affected regions shown are the binding sites of the ligands, as the chemical shift perturbations and broadening seen upon binding of ReLPS or LTA are much smaller in other regions of the sCD14 spectra. However, at this stage, spectral changes caused by conformational changes in other regions of the protein due to ligand binding cannot be ruled out. Regardless of whether the spectral changes are a result of direct binding interactions or are caused indirectly, it is clear that recognition of endotoxin ligands depends on specific contributions of select CD14 residues. The use of specific groups of residue may have implications for pattern recognition.

Another significant feature observed in the NMR spectra of CD14, particularly

when either ReLPS or LTA were bound, is that in a number of cases the resonances affected by binding split into multiple peaks (**Figure 3.4**). We interpret this splitting as a result of changes in the dynamics of CD14's flexible regions from fast to slow exchange on the NMR chemical shift time scale.

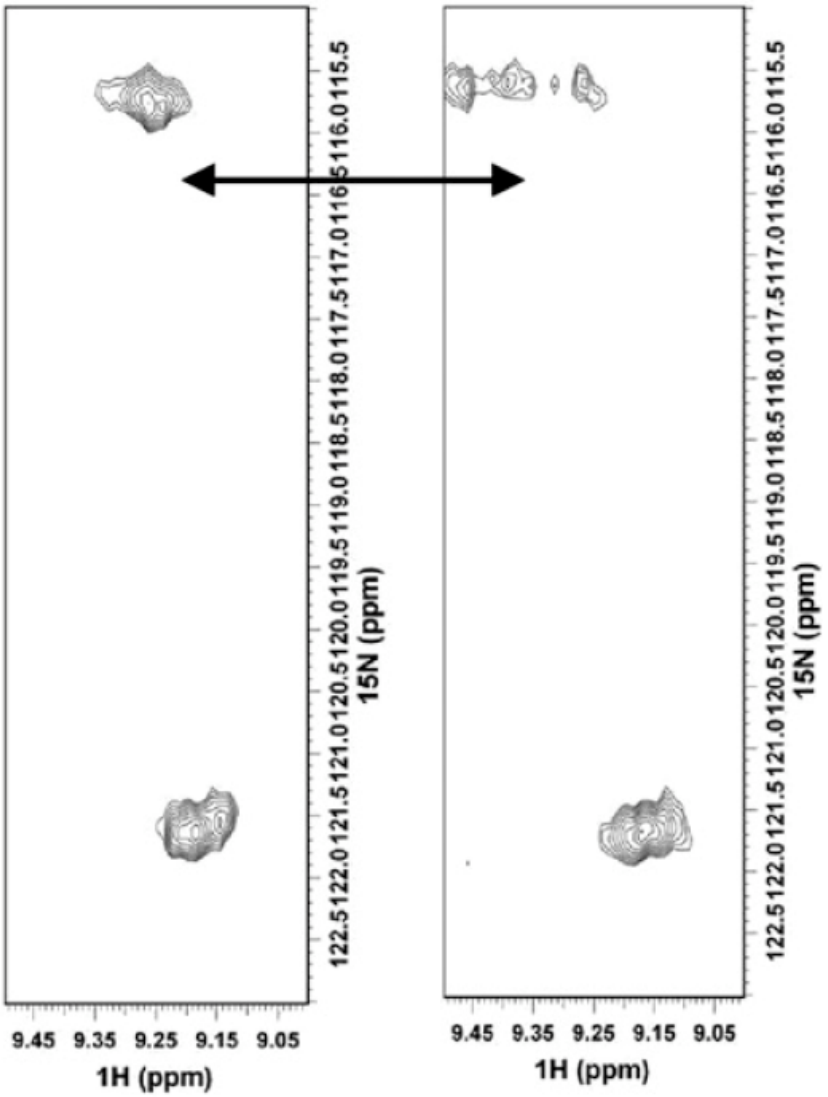


Figure 3.4: ^{1}H-^{15}N HSQC spectrum of exchange rate changes in ReLPS bound soluble CD14

Splitting of a representative resonance in sCD14 in PBS pH 7.4 (left sub-spectrum) into multiple peaks upon complexation with ReLPS (right sub-spectrum), indicating change in dynamics to slower exchange on the NMR time scale.

This signifies that various conformational sub-states can be occupied, from within a dynamic ensemble of interconverting populations, in order to specifically select for binding. Interestingly, based on the crystal structure of mouse sCD14, the regions previously identified as acting in endotoxin binding map to a highly flexible hydrophilic rim and also the bottom of the large hydrophobic pocket (*75*). In the CD14 crystal structure, the hydrophobic pocket is fairly rigid, while the residues on the hydrophilic rim exhibit multiple conformations in addition to having high average temperature factors. In addition, the electron density for this region is rather poorly defined in the crystal structure. Based on these observations, we conclude that the flexibility of the hydrophilic rim allows it to interact with structurally diverse sugar moieties. At the same time, the rigid but large nature of the hydrophobic pocket would allow it to accommodate ligands with structural variations in the hydrophobic portion, such as LPS and LTA. Therefore, we propose that the structural characteristics of CD14's binding site help impart its broad specificity in ligand recognition, through the use of specific residue combinations. The dynamic modulation of CD14 may also play an important role in providing a mechanism by which structurally diverse endotoxin ligands can be bound in a common binding site. The NMR observed structural and dynamic changes presented here lend credence to this possibility.

CHAPTER 4. NMR SPECTRAL MAPPING OF THE LIPID A MOLECULAR PATTERNS AFFECTED BY INTERACTION WITH THE INNATE IMMUNE RECEPTOR CD14

This chapter is a modified version of a paper first published in *Biochemical and Biophysical Research Communications* in 2009:

"Reprinted from *Biochemical and Biophysical Research Communications*, Vol. 378, Albright, S., Agrawal, P., and Jain, N. U., NMR spectral mapping of lipid A molecular patterns affected by interaction with the innate immune receptor CD14, 721-726, (2009), with permission from Elsevier."

As first author, I performed a majority of the experimental work and produced all of the samples used. I also carried out some of the NMR spectroscopy. Prashansa Agrawal aided in the processing and analysis of NMR spectra, and I assisted her in making the heteronuclear assignments for Kdo2-Lipid A. Nitin Jain performed a number of the NMR experiments, and was responsible for the final analysis of all NMR data.

4.1 INTRODUCTION

Bacterial endotoxins such as lipopolysaccharide (LPS), which comprises part of the outer cell-wall of gram-negative bacteria, are potent immunostimulators and causative agents for the pathogenesis of gram-negative bacterial sepsis in higher organisms. Chemically, LPS is composed of a variable polysaccharide region covalently linked to a conserved phospholipid known as lipid A, the source of biological potency in LPS. Studies using lipid A, synthetic analogs, as well as preparations of lipid A variants from a variety of different bacterial strains, have been previously carried out to evaluate the structural features of lipid A necessary for endotoxic activity (*126, 148*). Results from

these studies point to the length and number of acyl chains as well as the phosphorylation state of the disaccharide backbone to be major contributing factors to lipid A's endotoxicity. Additionally, by conformational analysis of lipid A aggregates, it was deduced that the molecular shape of lipid A and nature of its aggregate structures can be correlated to the level of endotoxicity (*149*). An emerging consensus is that the requirement of particular structural characteristics may be embodied in specific interactions of lipid A with host cell receptors. In receptors such as LBP, CD14, MD-2, and TLR4 these interactions may function in modulating the bioactivity of lipid A in the inflammatory response pathway. Structural studies of lipid A interactions with these receptors are therefore necessary to understand how they enable cells to respond to lipid A.

A better understanding of CD14–lipid A interactions could be facilitated through detailed structural characterization of lipid A in complex with CD14. It is known that CD14 functions similarly in both its membrane-bound (mCD14) and soluble (sCD14) forms as a pattern recognition receptor, recognizing various pathogen-associated molecular patterns (PAMPs) with high affinity (*17, 138, 139*). This recognition is accomplished through an endotoxin binding and functional region of CD14 that is contained in the first N-terminal 152 residues of the molecule (*70*). A recent crystal structure of murine sCD14 revealed within this N-terminal region, a large hydrophobic pocket surrounded by a hydrophilic rim to which endotoxins like lipid A can potentially bind (*75*). However, since this crystal structure was solved without a bound ligand, information regarding the identity of specific lipid A structural motifs involved in

interacting with CD14 is not available. Such information is crucial to the rational design of CD14 targeted LPS antagonists.

NMR structural studies of lipid A in complex with CD14 and other host cell receptors offer a viable option to obtain detailed structural information on their interactions. However, the lack of availability of isotopically labeled lipid A ligands has been a limiting factor to undertaking such studies. In the present study, we have overcome this difficulty by preparing Kdo_2–Lipid A, a lipid A variant, in a highly pure ^{13}C, ^{15}N isotopically labeled form. While lipid A is the minimal structural unit needed for biological activity, addition of a 3-deoxy-D-manno-octulosonic acid disaccharide unit (Kdo_2) to lipid A results in a molecule which sCD14 binds with high, lipid A-like, affinity. Kdo_2-Lipid A has the additional benefit of being a chemically well-defined endotoxin making it quite suitable for solution NMR studies (*122*). In an effort to determine the potential contributions of various structural elements of lipid A in its recognition by CD14, we have performed detailed NMR spectral mapping of isotopically labeled Kdo_2–lipid A bound to sCD14. We now report, for the first time, the identity of structural regions in this agonist ligand strongly affected by complex formation with sCD14, as well as their differential dynamic behavior. These studies constitute the first direct structural observations of interactions of an LPS agonist ligand with a host cell receptor in solution, and provide valuable insights into the mechanism of lipid A pattern recognition by sCD14.

4.2 MATERIALS AND METHODS

4.2.1 PREPARATION AND ISOTOPIC LABELING OF Kdo_2-LIPID A IN *Escherichia coli* WBB06

Kdo_2-Lipid A was prepared from the heptosyltransferase-deficient *E. coli* mutant WBB06 (kindly provided by Christian Raetz, Duke University). WBB06 was cultured in M9 minimal medium at 37 ºC for 22–24 hours. One liter of M9 medium contained 7 g Na_2HPO_4, 3.5 g KH_2PO_4, 0.5 g NaCl, 1 mL trace metals solution, 4 g D-glucose, 1 g NH_4Cl, and 12 μg/ml tetracycline. For isotopic labeling, $^{13}C_6$ D-glucose and $^{15}NH_4Cl$ were used in place of their unlabeled versions. Extraction of Kdo_2-Lipid A from the harvested cell pellet was performed using a chloroform–methanol mixture, followed by purification with normal phase and reverse phase column chromatography similar to the methods of Raetz et al. (*122*). The center peak fractions from the last chromatography run were combined and ultracentrifuged for 15 minutes at 256,000g. The final Kdo_2-Lipid A product was >90% purity as assessed by thin layer chromatography and matrix-assisted laser desorption/ionization time-of-flight (MALDI-TOF) mass spectroscopy. Dephosphorylated Kdo_2-Lipid A was prepared from Kdo_2-Lipid A by hydrolysis with 48% aqueous hydrofluoric acid for 42 hours at 4 ºC and subsequently purified using published procedures (*150*). The loss of the phosphate groups was confirmed by MALDI-TOF mass spectroscopy analysis.

Induction of NF-κB cytokines in THP1-Blue cells (Invivogen) was performed to test the biological activity of purified Kdo_2-Lipid A and dephosphorylated Kdo_2–lipid A as described previously (*151*) and compared to that of ultrapure LPS from *Salmonella*

Minnesota strain Re 959 (ReLPS) (List Biological Laboratories), which is structurally analogous to Kdo_2-Lipid A. The baseline activation of the cells by the ligands alone was used as a control experiment.

4.2.2 NMR MEASUREMENTS ON Kdo_2 –LIPID A COMPLEXED WITH SOLUBLE CD14

Standard two-dimensional (2D) ^1H COSY and NOESY spectra were recorded to obtain proton assignments using a 1 mg/ml sample of unlabeled Kdo_2-Lipid A in the deuterated mixed solvent system $CDCl_3$:CD_3OD:D_2O (2:3:1, v/v) at 17 ºC. Sensitivity-enhanced ^1H–^{13}C and ^1H–^{15}N HSQC experiments were also recorded on a ^{13}C, ^{15}N isotopically labeled sample (1 mg/ml) in the same mixed solvent system to obtain ^1H–^{13}C and ^1H–^{15}N correlations, except the D_2O in the solvent mixture was replaced with H_2O to keep the amides protonated in the ^1H–^{15}N experiments (*143*). Chemical shifts were referenced relative to DSS. Unlabeled samples of a truncated version of full-length human sCD14 consisting of 152 residues (amino acids 20–171) after the signal peptide sequence were prepared in *Pichia pastoris* as described in Chapter 2. The sCD14 samples used for the NMR experiments were prepared in PBS buffer with a typical concentrations of ~0.2 mM. Stock solutions of ^{13}C, ^{15}N labeled Kdo_2-Lipid A, and dephosphorylated Kdo_2-Lipid A were prepared at 5 mg/mL concentration and extensively sonicated to form a uniform suspension of the ligands. The ligands were then added to the protein to produce protein:ligand NMR samples in a molar ratio of 1:1. Recombinant human LBP (R&D systems) was also present in all samples at a concentration of 2 μM. The protein:ligand samples were incubated for 30 minutes at 37 ºC to ensure complete

binding of ligand. $^{1}H–^{13}C$ and $^{1}H–^{15}N$ HSQC spectra were recorded at 17 ºC for each protein sample with and without the ligand. $^{1}H–^{13}C$ and $^{1}H–^{15}N$ HSQC spectra for the ligands alone were also acquired in PBS buffer. All NMR experiments were carried out on a Varian VNMRS 600MHz spectrometer at 17 ºC equipped with a cold probe. Acquired NMR data was processed and analyzed using the Felix software package (Molecular Simulations).

4.3 RESULTS AND DISCUSSION

4.3.1 PREPARATION AND ISOTOPIC LABELING OF Kdo_2-LIPID A IN HEPTOSETRANSFERASE–DEFICIENT *Escherichia coli* STRAIN

LPS from gram-negative bacteria, whose molecular patterns are recognized by CD14, represents one of the strongest endotoxin activators in mammals. High-resolution structural information on specific regions relevant to interactions between LPS and CD14 is highly desirable. However, the presence of multiple highly flexible acyl chains on lipid A, as well as the micro-heterogeneity of LPS especially in the variable polysaccharide region, poses considerable difficulties to both crystallization and solution NMR studies of LPS-receptor complexes. As part of this work, we have developed an efficient protocol to isotopically label Kdo_2-Lipid A from the heptosyltransferase-deficient E. coli K-12 mutant WBB06, producing a viable alternative to native LPS because of its similar biological activity. This has not only permitted us to the probe structural interactions of Kdo_2-Lipid A with sCD14 for the first time by solution NMR spectroscopy, it has also opened up new avenues for NMR structural studies of other endotoxin–receptor

complexes in the future.

Isotopic labeling of Kdo_2-Lipid A was accomplished by culturing WBB06 cells in minimal medium supplemented with ^{13}C labeled carbon and ^{15}N labeled nitrogen sources. WBB06 showed good growth characteristics in the minimal medium under the labeling conditions we employed. This made isotopically labeled Kdo_2-Lipid A amenable to direct extraction from the cells, a process more efficient and more economical than chemical synthesis. Additionally, preparation of Kdo_2-Lipid A, unlike lipid A, does not require reaction with mild acids which can result in loss of a phosphate group or an acyl chain (*122*). Use of a multistep purification scheme enabled efficient removal of contaminating membrane phospholipids as well as minor hepta-, penta-, and tetra-acylated lipid A species, while yielding milligram quantities of highly pure and labeled Kdo_2-Lipid A for NMR structural studies. The purified Kdo_2-Lipid A exhibited bioactivity on par with the *Salmonella minnesota* Re 595 rough-type LPS (ReLPS), a structural homolog to Kdo_2-Lipid A, in cell-based assays (**Figure 4.1**).

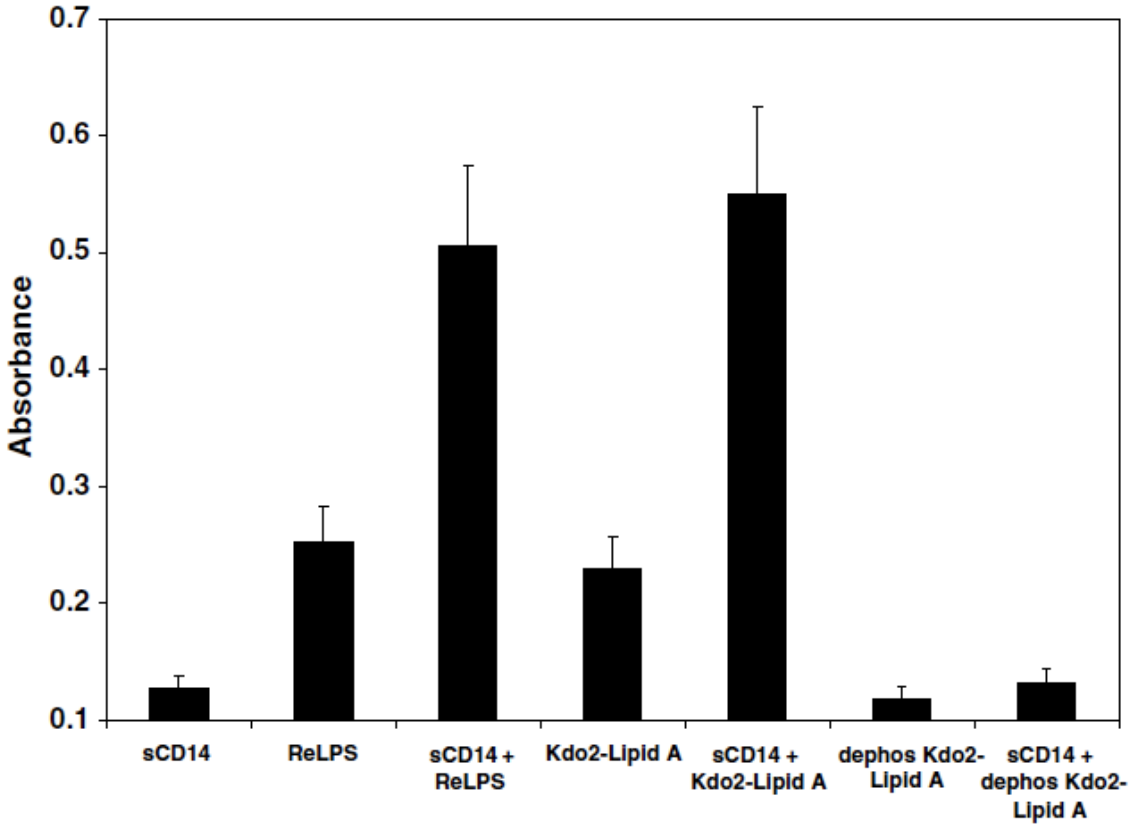


Figure 4.1: Biological activity assay of endotoxin ligands with soluble CD14.
Responses of THP1-Blue cells mediated by purified sCD14 (200 ng/mL) upon stimulation with three endotoxins, Kdo_2–Lipid A (1 μg/mL), ReLPS (1 μg/mL), and dephosphorylated Kdo_2–Lipid A (1 lg/mL) are shown. Endotoxin stimulation was assessed by measuring the levels of NF-κB inducible reporter, secreted embryonic alkaline phosphatase (SEAP), using a SEAP detection medium with absorbance values at 630 nm. Control experiments were the responses to ReLPS, Kdo_2–Lipid A, dephosphorylated Kdo_2–Lipid A, and sCD14 alone.

Successful incorporation of ^{13}C and ^{15}N labels into Kdo_2-Lipid A was confirmed by acquisition of $^{1}H–^{13}C$ and $^{1}H–^{15}N$ HSQC spectra for the ^{13}C, ^{15}N labeled compound in a mixed solvent system, which permitted chemical shift assignment of most proton and carbon resonances in the sugar headgroup and acyl chains (**Figure 4.2**). Assignment of the ^{1}H and ^{13}C chemical shifts for Kdo_2-Lipid A were carried out using standard COSY (correlation spectroscopy), NOESY (nuclear Overhauser effect spectroscopy), and ^{1}H-^{13}C HSQC (heteronuclear single quantum coherence) experiments. Assignment of ^{1}H chemical shifts was performed using ^{1}H COSY experiments, which show the correlation of protons within 2-3 bonds of each other. The sequential assignment of the COSY spectra was facilitated through the use of a predicted 1D ^{1}H-NMR spectra of Kdo_2-Lipid A as an initial reference. The 1D spectra was generated using ChemBioDraw (CambridgeSoft). Ambiguities in the identity of the proton assignments were clarified using NOESY experiments, which show though-space proton-proton connectivities for nearby protons. The proton assignments were then used to assign their correlated ^{13}C chemical shift in a ^{1}H-^{13}C HSQC spectrum. A table of the ^{1}H and ^{13}C assignments for Kdo_2-Lipid A can be found in **Table A1,** located in the Appendix.

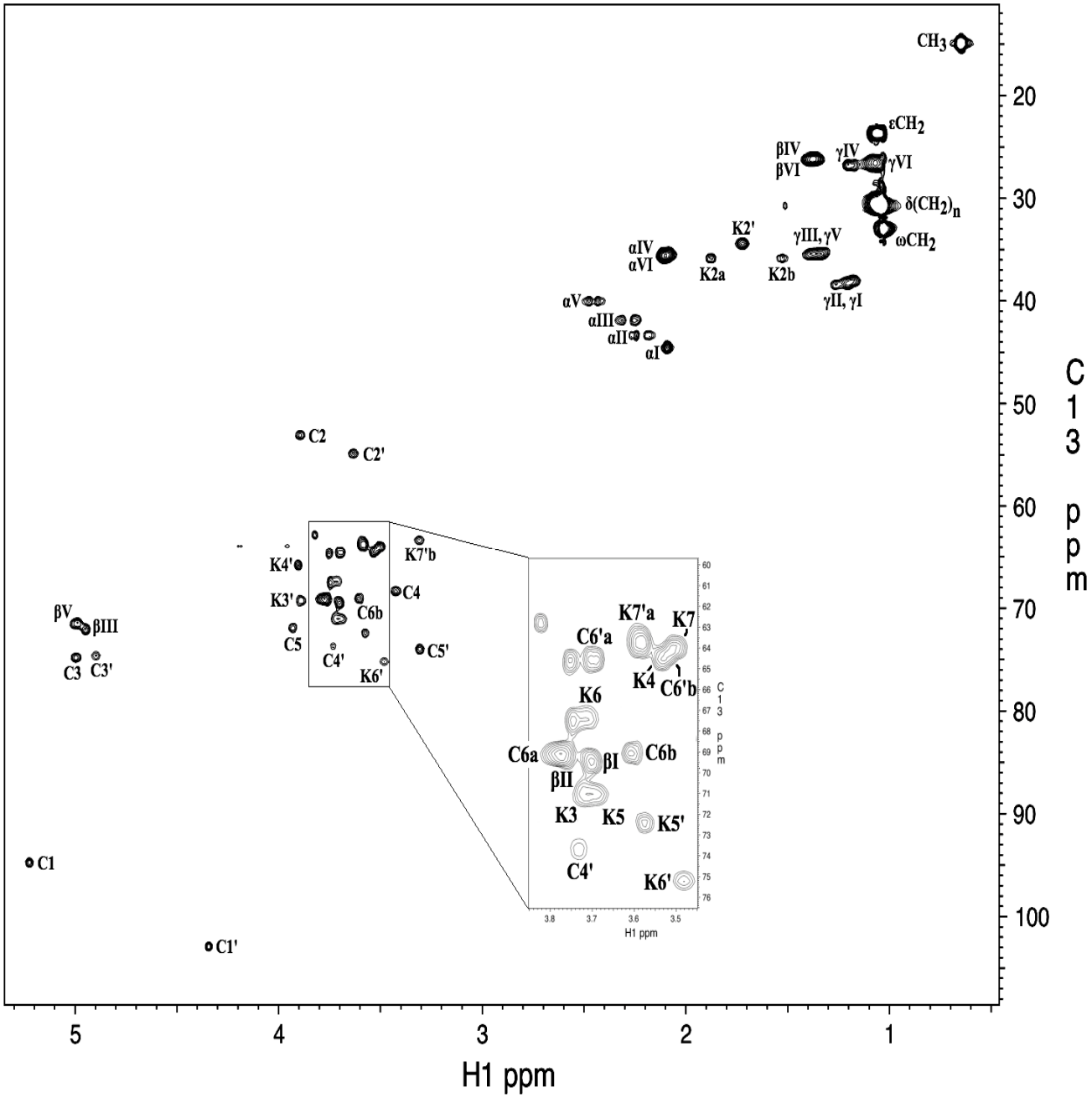


Figure 4.2: The ^{1}H-^{13}C HSQC spectrum of ^{13}C isotopically labeled Kdo_2-Lipid A.
Spectrum of ^{13}C isotopically labeled Kdo_2-Lipid A in $CDCl_3$:CD_3OD:D_2O mixed solvent system (2:3:1, v/v) showing correlations within the sugar headgroup and acyl chain regions. The inset spectra is a magnified view of a portion of the sugar headgroup region. Chemical shift assignments for the individual resonances are listed in the Appendix.

4.3.2 NMR ANALYSIS OF THE Kdo_2-LIPID A COMPLEXED WITH CD14

To delineate the structural regions of Kdo_2-Lipid A affected upon binding to CD14 spectral characteristics in the $^{1}H–^{13}C$ and $^{1}H–^{15}N$ HSQC spectra of ^{13}C, ^{15}N isotopically labeled Kdo_2-Lipid A bound to sCD14 were monitored. In aqueous solution Kdo_2-Lipid A forms large aggregates (apparent MW >1 MDa). This causes resonances in the proton NMR spectrum of Kdo_2-Lipid A to broaden beyond detection (*122, 152*). Kdo_2-Lipid A, however, binds to CD14 with high affinity (K_d ~40nM) as a monomeric complex in the presence of a catalytic amount of LBP (*142*). The binding of Kdo_2-Lipid A to CD14 as a monomer results in the appearance of well-dispersed signals with the observed chemical shifts quite similar to those for Kdo_2-Lipid A in the mixed solvent system. This allowed the chemical shift assignments of Kdo_2-Lipid A in the mixed solvent system to be transferred without ambiguity to the bound complex for analysis of spectral characteristics.

Analysis of the acyl chain resonances in the $^{1}H–^{13}C$ HSQC spectrum of sCD14 complexed Kdo_2-Lipid A shows that the resonances for the terminal methyl and methylene groups, referred to as δ and colored light gray in **Figure 4.3**, are clearly visible, although with the increased linewidths expected from binding to a 32 kDa protein (**Figure 4.4**).

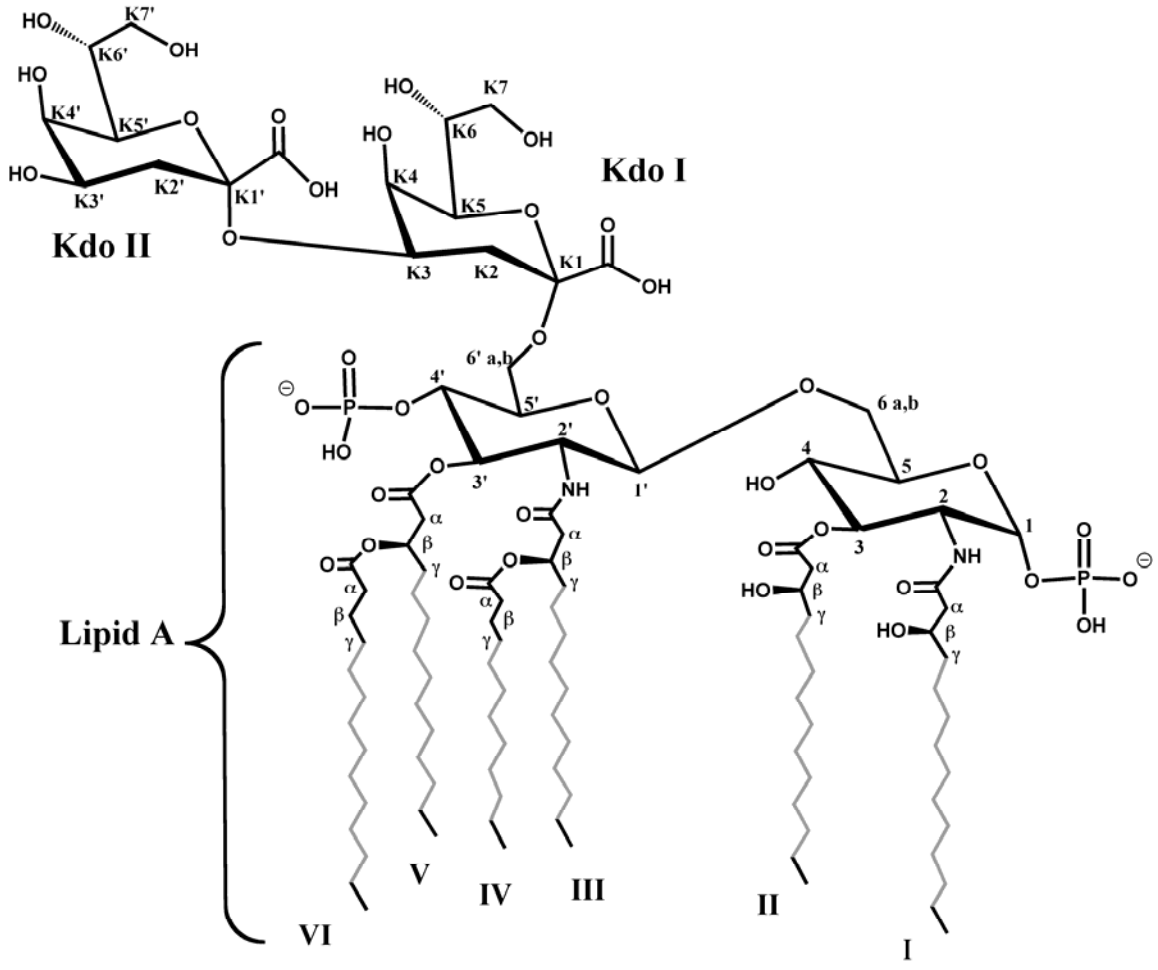


Figure 4.3: Chemical schematic of Kdo_2-Lipid A structure.
Schematic showing numbering scheme for sugar headgroup and acyl chain carbons of Kdo_2-Lipid A.

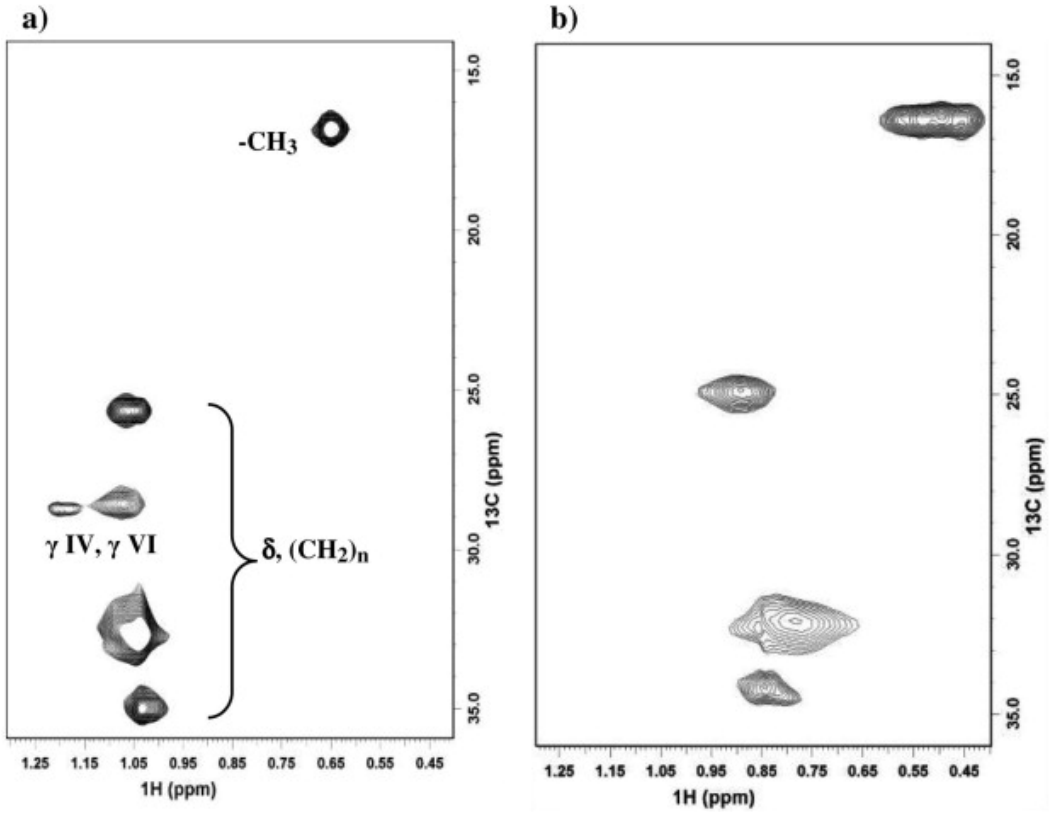


Figure 4.4: Comparison of spectral characteristics in the $^{1}H–^{13}C$ HSQC spectra of ^{13}C labeled Kdo_2–Lipid A corresponding to the lower half of the acyl chain region.

(a) Kdo_2–Lipid A only in $CDCl_3$:CD_3OD:D_2O (2:3:1, v/v) mixed solvent system and (b) Kdo_2–Lipid A complexed to sCD14 in PBS buffer solution. Differences in linewidths and chemical shifts between (a) and (b) for terminal methyl and various methylene groups are shown. The resonances for γ IV and γ VI in Kdo_2–Lipid A bound to sCD14 are less intense compared to the methylene resonances in acyl chains and are therefore not visible at contour levels used in this figure (they are clearly visible in the spectrum at lower contour levels and not shown for clarity).

It has been proposed that the mode of lipid A binding involves insertion of its acyl chains into the large hydrophobic pocket of sCD14, which is lined with the hydrophobic side-chains from the many leucine residues of the leucine-rich repeats. Based on the locations of leucine residues in the mouse sCD14 crystal structure (*75*), and the length of the Kdo_2-Lipid A acyl chains, it is likely that the methylene groups are in close proximity to these residues. Additionally, when compared to the other parts of the acyl chain (see below), the δ methylene and terminal methyl groups exhibit higher intensity signals and do not show broadening characteristic of dynamic exchange. This suggests that the lower half of the acyl chains retain some minor level of movement within the hydrophobic pocket, and are not, in effect, restricted to a single conformation. Because of this residual flexibility, the likelihood is that the lower portion of the acyl chains only makes non-specific van der Waals contacts with the leucine side-chains. Based on the observed spectral characteristics, we estimate that the lower half of acyl chains in complexed Kdo_2-Lipid A exhibiting non-polar interactions possess a length of about 10–12 Å. This corresponds to the right length for insertion into the hydrophobic portion of the binding pocket in truncated sCD14.

In contrast to the δ methylene resonances, the α, β, and γ methylene resonances in the upper portions of the acyl chains are more drastically and differentially affected, depending on the acyl chain to which they belong. As seen in **Figure 4.5 A**, the α methylenes form a group of resonances that resonate downfield between 2.1 and 2.5 ppm. In the presence of sCD14, the α methylene protons in chains III and V show severe exchange-broadening effects. The α methylene protons from chain III disappear abruptly,

while those from chain V exhibit significant resonance splitting and are now only barely visible (**Figure 4.5 B**). Furthermore, several closely spaced peaks are observed for the α protons from chain V indicating presence of multiple conformations in slow exchange relative to the NMR timescale.

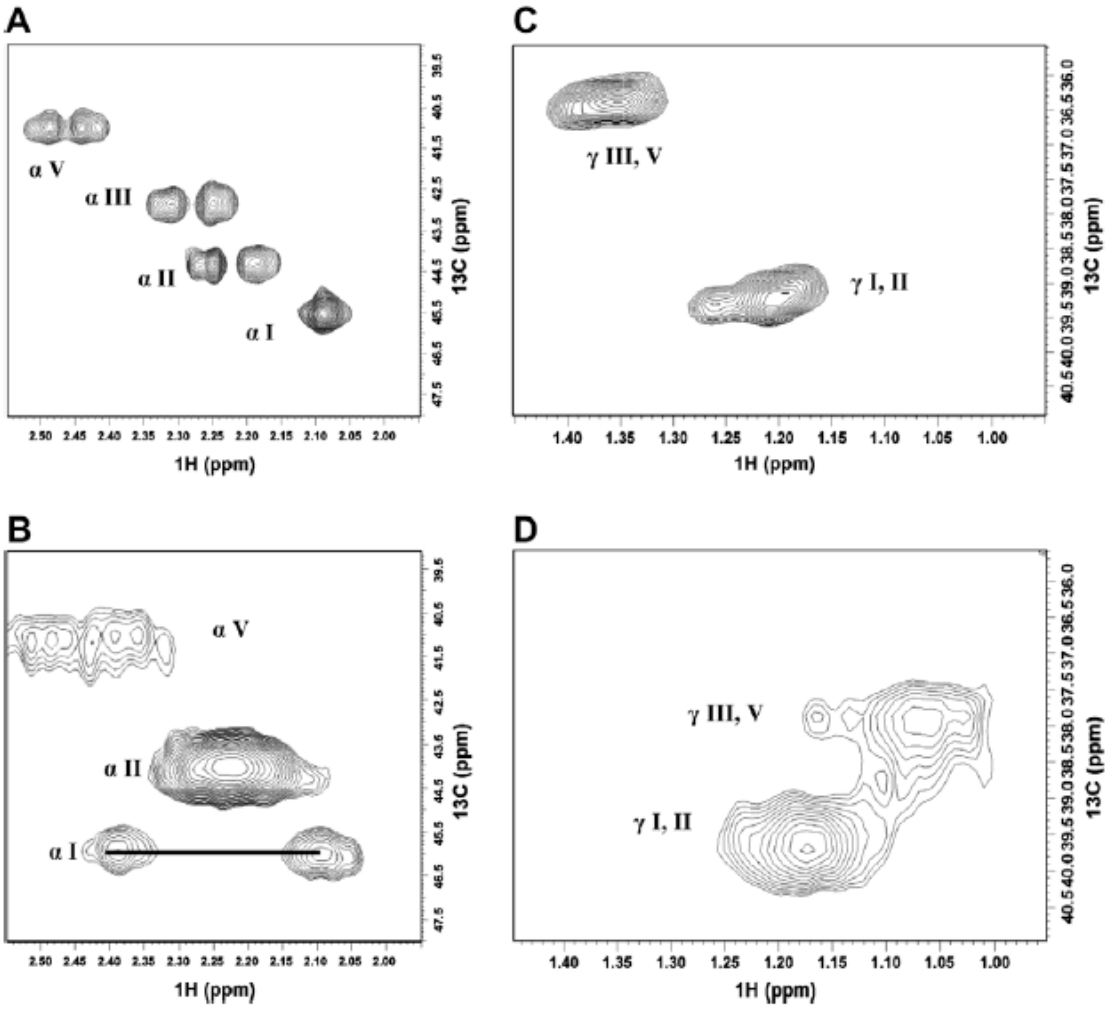


Figure 4.5: Comparison of spectral changes in the upper acyl chain resonances of Kdo_2-Lipid A upon interaction with soluble CD14.

Comparison of spectral characteristics in the $^{1}H–^{13}C$ HSQC spectra for ^{13}C labeled Kdo_2–Lipid A corresponding to upper half of acyl chain region proximal to Lipid A headgroup. (A,C) Kdo_2–Lipid A by itself in $CDCl_3$:CD_3OD:D_2O (2:3:1, v/v) mixed solvent system and (B,D) Kdo_2–Lipid A complexed to sCD14 in PBS buffer solution. A representative set of α methylene resonances and γ methylene resonances are shown.

On the other hand, the α methylene groups from the remaining chains, IV and VI, are affected to a lesser extent with no apparent exchange-broadening (data not shown).

The β and γ methylene groups exhibit a similar pattern as the α methylene groups, with resonances from chains III and V affected the most, followed by chains I and II, with the resonances from chains IV and VI affected the least. The γ methylenes from chains III and V again show the presence of multiple peaks, similar to those seen in the α resonances of these chains (**Figure 4.5 A-B**), indicating a slowing down of motion upon interaction with sCD14 (**Figure 4.5 C-D**). The α, β and γ groups of acyl chains III and V show the greatest affects of interaction and compose a region in Kdo_2-Lipid A containing several polar groups, such as the β-hydroxy and ester linkages, which could contribute significantly to polar interactions with the hydrophilic rim of sCD14. Additionally, the ^{1}HN resonances from acyl chains I and III mimic the effects of severe line broadening on chains III and V, completely broadening out in the presence of sCD14 (**Figure 4.6**). We interpret this as involvement in hydrogen bonding interactions for the amine groups, possibly with polar groups on the hydrophilic rim of sCD14.

The resonances of the sugar headgroup region of Kdo_2-Lipid A, which consist of the 1, 4'-bisphosphorylated D-glucosamine disaccharide sugar headgroup of lipid A plus the two Kdo sugar units (**Figure 4.3**), also experience differential spectral changes and exchange-broadening upon binding to sCD14. In the lipid A sugar headgroup, the resonances for the entire sugar headgroup broadened out completely when bound to sCD14, except for the resonances for H5, H5', $H6_{ab}$, and $H6'_{ab}$ which show broadening but, unlike the others, remain visible (**Figure 4.6**). The effect of CD14 binding on the Kdo sugar resonances is considerably less. In general, they exhibit higher intensity and narrower linewidths compared to the resonances of the lipid A headgroup. The only exceptions to this are H2' and H3' of the second Kdo unit, which experience significant broadening (**Figure 4.6 F**). These protons are located in close proximity to the 4'-phosphate group, which is quite important for endotoxic activity and binding interactions with CD14 (*150, 153*). It is probable that the movement of the Kdo carboxylic group located next to the H2' and H3' protons towards the 4'-phosphate group could stabilize any possible interactions of the carboxylic group with positively charged residues on the amphipathic helices and loops located in the hydrophilic rim of sCD14, or help indirectly by stabilizing the structure in its immediate vicinity. Movement of the carboxylic group towards the 4'-phosphate, with a bridging calcium atom, has been noticed previously in molecular dynamics simulation studies on Kdo_2-Lipid A (*154*) lending credence to this possibility.

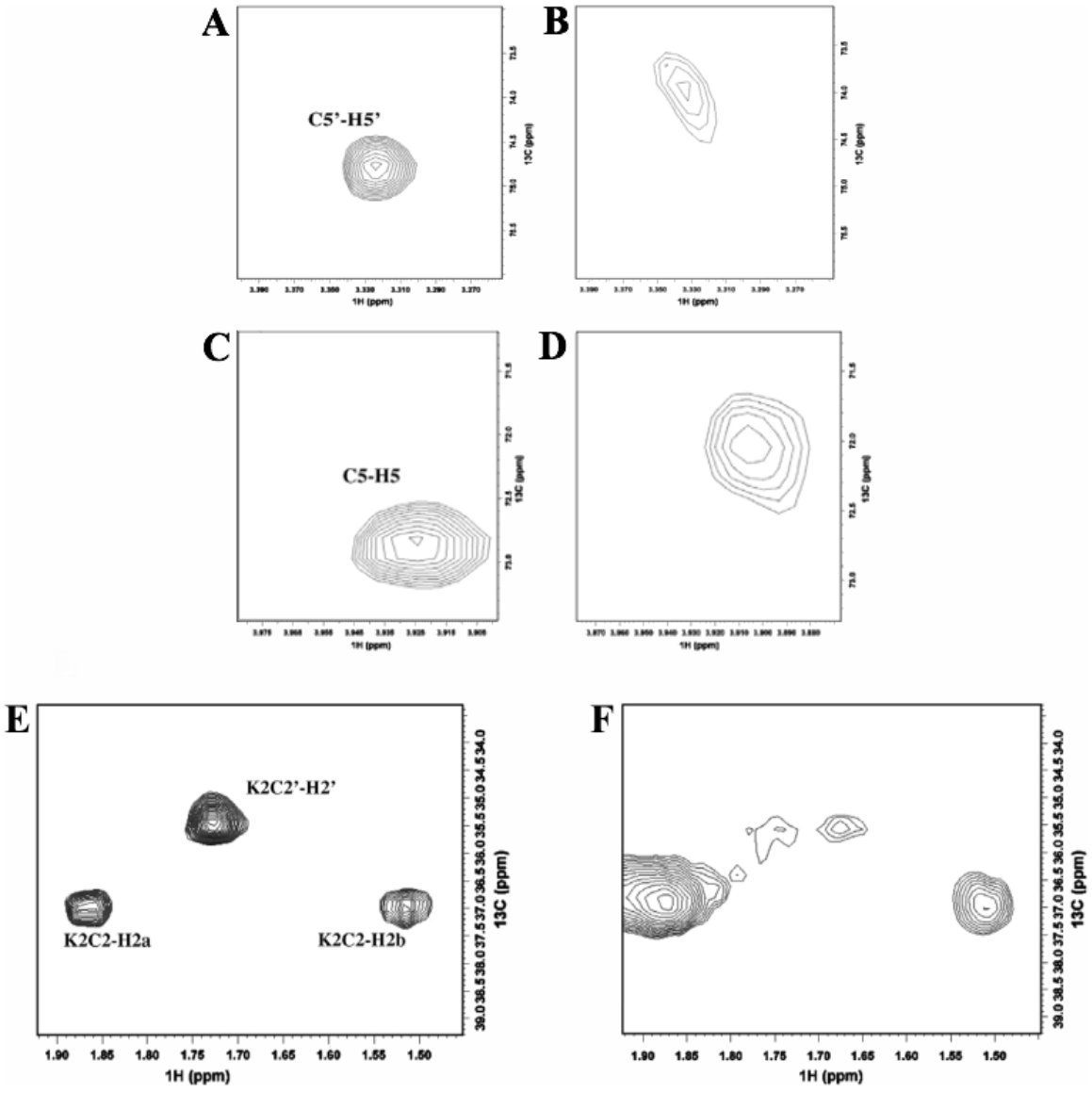


Figure 4.6: Comparison of spectral changes in the sugar headgroup and Kdo units of Kdo_2-Lipid A upon soluble CD14 binding.

Comparison of spectral characteristics in the ^{1}H–^{13}C HSQC spectra for ^{13}C labeled Kdo_2–Lipid A corresponding to the sugar headgroup region. (A, C, and E) Kdo_2–Lipid A by itself in $CDCl_3$:CD_3OD:D_2O (2:3:1, v/v) mixed solvent system and (B, D, and F) Kdo_2–Lipid A complexed to sCD14 in PBS buffer solution. A representative set of lipid A sugar resonances (H5 and H5') and Kdo unit resonances (H2 and H2') are shown.

The essential role of the phosphate groups in Kdo_2-Lipid A binding interactions with sCD14 is also confirmed by our NMR binding experiments utilizing fully dephosphorylated Kdo_2-Lipid A. No binding of the dephosphorylated Kdo_2-Lipid A to sCD14 was apparent even in the presence of LBP, reinforcing the results from cell-based activity studies (**Figure 4.1**).

Observation of strong effects for regions around the phosphates, which includes the lipid A headgroup, is significant. A sugar headgroup is a common molecular pattern shared by several endotoxin ligands that interact with sCD14 (*138, 139*), and is believed to be important in pattern recognition (*17*). The lower half of this headgroup is in close proximity to the polar substituents, the amide and ester linkages, which contain a number of electronegative oxygen and nitrogen atoms, on acyl chains I, III, and V (**Figure 4.7**).

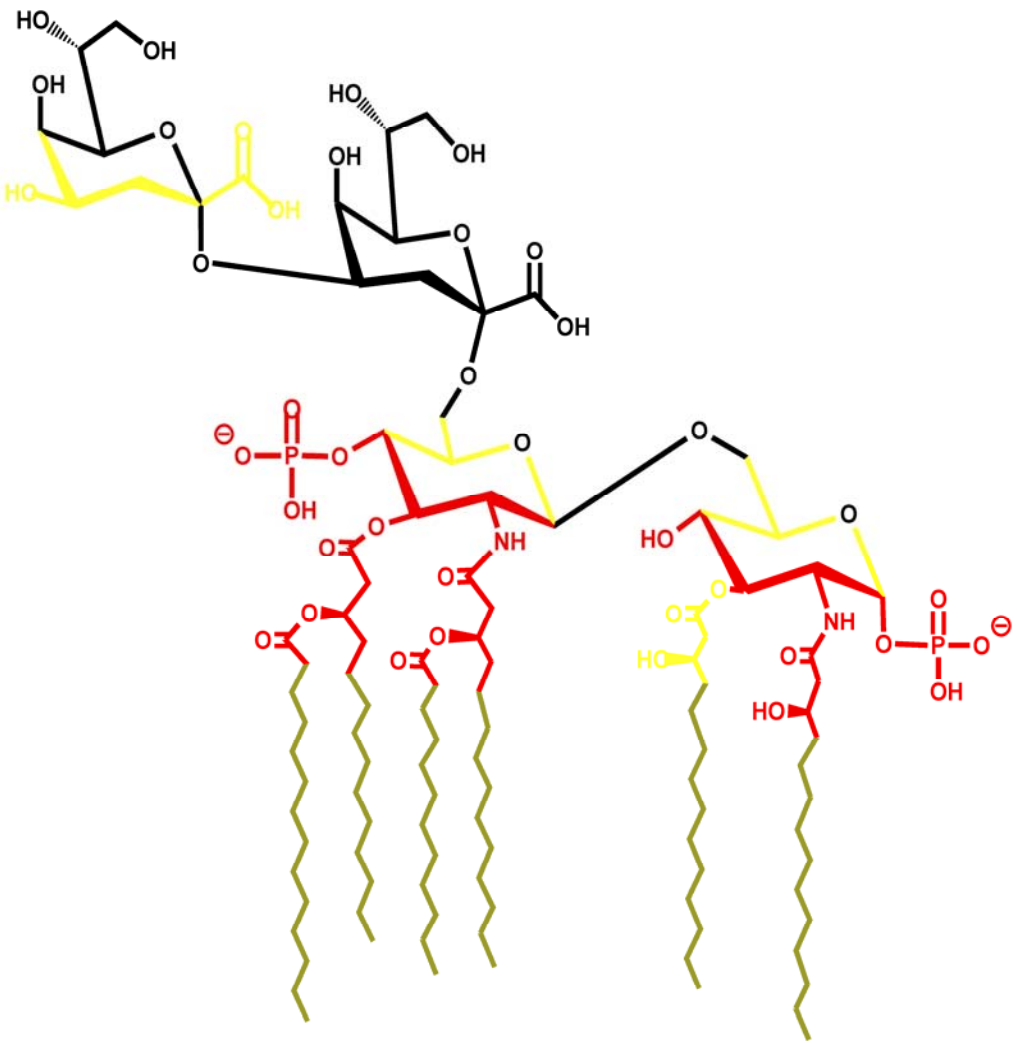


Figure 4.7: Summary of Kdo_2-Lipid A features affected upon interaction with soluble CD14.

Review of structural regions in Kdo_2–Lipid A affected upon interaction with sCD14. Regions are color coded to show the severity of interaction effects with the most severely affected regions shown in red, the moderately affected regions in yellow and unaffected regions in black. Acyl chain portions with upfield shifts in presence of sCD14 are shown in brown.

Due to the high polar composition of this region, it is conceivable that, together with the phosphate groups, they form a molecular pattern that could influence the interactions with the charged/polar residues on the hydrophilic rim of sCD14. There is some underlying evidence to support this notion. Mutagenesis studies have shown that sCD14 employs hydrophilic regions, largely containing polar and charged residues, to interact with molecular patterns on LPS (*93*). These studies demonstrated that certain charge-reversal mutations or non-polar residue substitutions greatly diminished CD14's interaction with *E. coli* LPS. The studies also indicated that the hydrophilic regions, containing polar and charged residues, functioned in determining the efficacy of pattern recognition of certain LPS species by sCD14. Since the NMR experiments performed in this study cannot distinguish between direct binding effects and secondary interaction effects, which result from conformational changes in regions affected by but not directly involved in binding, we cannot currently ascertain if these regions in Kdo_2–lipid A are in direct contact with CD14's rim. The presences of such direct interactions, however, may not be uncommon. A recent crystal structure of MD-2 with a known antagonist, tetraacyltaed Lipid IVa, revealed the presence of a large hydrophobic cavity (*155*). Lipid IVa was bound in MD-2's hydrophobic cavity with the polar moieties of Lipid IVa's sugar headgroup tethered via hydrogen-bonds to the polar MD-2 residues at the entrance of the cavity. The acyl chains of Lipid IVa were inserted deep into the cavity, and surrounded by hydrophobic MD-2 side-chains. This gives rise to the distinct possibility that similar types of interactions may well exist, to a certain extent, between lipid A and sCD14.

Another interesting finding from the NMR spectral studies of complexed Kdo_2–lipid A is the occurrence of intermediate or slow exchange, on the NMR chemical shift time scale, for many of the affected resonances. In addition, the level of exchange-broadening differs from region to region in Kdo_2-Lipid A. Given the high affinity of Kdo_2-Lipid A and CD14 for each other, this differential dynamic behavior is surprising. This dynamic behavior suggests that, rather than becoming essentially locked in one conformation, even in its bound state the ligand still possesses considerable flexibility. The existence of multiple bound configurations is consistent with the large K_{off} rate measured for this complex (*28*). This differential behavior, along with the presence of multiple resonance splittings, was also observed in the ^{1}H–^{15}N HSQC spectra of ^{15}N labeled sCD14 bound to ReLPS (*151*). While the reasons for this differential behavior are not entirely clear at this point, a ligand-induced increase in disorder upon the binding of a hydrophobic ligand has previously been correlated with specificity in ligand recognition (*156*). Increased specificity comes as a result of the number of accessible conformations available to facilitate low-energy contacts between the molecules, thereby providing a way to fine-tune the binding interactions. In addition, the ability to utilize multiple individual lower-affinity, lower-energy interactions results in the interaction as a whole having higher affinity. This is an intriguing possibility to consider for the role of dynamics in the sCD14:Kdo_2–lipid A complex, and could have implications for lipid A pattern recognition. As a result, this dynamic behavior is deserving of greater experimental scrutiny.

CHAPTER 5. NMR SPECTRAL MAPPING OF LIPOTEICHOIC ACID MOLECULAR PATTERNS INTERACTING WITH THE ENDOTOXIN RECEPTOR CD14

5.1 INTRODUCTION

For many years, gram-negative bacterial infections were the primary cause of sepsis, but since the end of the 1980's, gram-positive bacteria have surpassed gram-negative bacteria as the primary cause of sepsis in the US (*3*). Traditionally, more attention has been given to sepsis caused by LPS, and by virtue of the fact that LPS is only found in gram-negative bacteria, this has meant less attention to gram-positive bacterial sepsis. This preoccupation with gram-negative bacteria and LPS is based on the long-established viewpoint that gram-negative bacteria are the most common cause of sepsis (*157*). This LPS-centered viewpoint was based on an accurate representation of the cause of sepsis for many decades, but as the use of antimicrobials became increasingly prevalent in the landscape of sepsis, focus shifted toward gram-positive bacteria as they began to cause an increasing percentage of all sepsis case (*157*).

Because gram-positive bacteria do not possess LPS, their source of immunogenicity has, over the previous years, been a subject of heated debate. However, it has now become clear that the initial front-runner for the role of gram-positive endotoxin, peptidoglycan (PGN), is not a ligand recognized by a TLR (*51*). While it

should be noted that PGN is recognized via the intracellular immune receptors NOD1 and NOD2, our interest is in the endotoxin recognized at the first line of defense, the cell surface (*145, 158, 159*). The gram-positive cell wall component, now generally recognized as representing its endotoxin, is lipoteichoic acid (*51*). LTA has been shown to be recognized by a signaling complex composed of a heterodimer consisting of TLR2 and TLR6 (*27, 30*). The activation of the TLR signaling complex for LTA was discovered to be CD14-dependent, and makes use of LBP to present LTA to CD14 (*25*). For this reason, we selected LTA for use to investigate the differential recognition of a gram-positive endotoxin by CD14.

In an effort to determine the potential contributions of various structural elements of LTA in its recognition by CD14, we have performed detailed NMR spectral mapping of isotopically labeled LTA bound to sCD14. This study represents the first structural characterization of the identity of structural regions in a gram-positive agonist ligand affected by complex formation with sCD14. This study also provides the first structural observations of a gram-positive ligand with a host cell receptor in solution, and provides valuable insights into the mechanism of LTA pattern recognition by sCD14. In addition, comparison of the results of this study with our previous detailed investigation of Kdo_2-Lipid A's interaction with CD14 facilitates the further elucidation of pathogen-associated molecular patterns.

5.2 MATERIALS AND METHODS

5.2.1 GROWTH, EXTRACTION, AND PURIFICATION OF LIPOTEICHOIC ACID FROM *Bacillus subtilis* ATCC 6633™

Bacillus subtilis ATCC 6633™ was grown in M9 media supplemented with 0.1% casamino acids at 30 °C with agitation (*160*). Isotopic labeling was accomplished with the supplementation of $^{13}C_6$ D-glucose into the medium. After ~22-24 hours, the cells were harvested by centrifugation at 7,000 rpm for 15 minutes. The cell pellet was then stored at -80 ºC.

Upon thawing of the frozen cell pellet, an equal volume of *n*-butanol was added. This mixture was then vortexed followed by brief sonication for ~20 seconds until a fine solution was generated. The cell pellet–*n*-butanol mixture was then left stirring at room temperature. After 30 minutes of stirring, the mixture was centrifuged for 20 minutes at 10,400 rpm to yield a two-phase solution; the aqueous phase was pulled off and lyophilized. The lyophilisate was resuspended in 15% *n*-propanol in 0.1 M ammonium acetate, pH 4.7, buffer and centrifuged at 20,000 rpm for 15 minutes. The supernatant was subjected to hydrophobic interaction chromatography (HIC) on octyl-Sepharose (*49, 50*). Individual fractions were checked directly for LTA content using 1D ^{1}H-^{13}C HSQC NMR experiments. Fractions containing LTA were then pooled and warmed at 40 °C to evaporate the *n*-butanol, before being subjected to lyophilization. The lyophilisate was then resuspended in endotoxin-free water, and dialyzed against endotoxin free water to remove the ammonium acetate. The final pure samples then had their identity and purity

re-confirmed using 1D and 2D ^{1}H-^{13}C HSQC experiments. Final purity was >90% as estimated by NMR.

LTA lipid anchor was produced by hydrolyzing 40 mg of LTA with 0.9 ml of 48 % hydrofluoric acid (HF) for 40-48 hours at 4 ºC. This was followed by neutralization of the HF with saturated sodium bicarbonate solution and lyophilization. The lyophilisate was resuspended in 15 ml $H_2O/CH_2Cl_2/CH_3OH$ (3:3:1) and centrifuged at 3,200 rpm for 7 minutes. The pellet was washed with CH_2Cl_2 and the water layer with CH_2Cl_2/CH_3OH (3:1); the organic phases were then combined and evaporated (*56*). After evaporation, the remaining precipitate was loaded on an octyl-sepharose HIC column in 15 % *n*-propanol, 50 mM ammonium acetate, pH 4.7 buffer and the acylated LTA lipid anchor was eluted from the column using a linear gradient of *n*-propanol (*161*). LTA lipid anchor samples were dialyzed to eliminate any residual ammonium acetate buffer left from HIC. Cleavage of the polyglycerophosphate chain was confirmed by the disappearance of the ^{1}H-NMR signals associated with the N-acetylglucosamine and D-alanine substituents of the polyglycerophosphate chain. Purity of the LTA lipid anchor was also assessed by comparison to published 1D ^{1}H-NMR spectra (53, 55), and to the predicted ^{1}H-NMR spectra generated using ChemBioDraw (CambridgeSoft, Cambridge, MA).

5.2.2 NMR MEASUREMENTS ON LTA LIPID ANCHOR BOUND TO SOLUBLE CD14

Sensitivity-enhanced ^{1}H–^{13}C and ^{1}H–^{15}N HSQC experiments were recorded on a ~1 mg/ml sample of ^{13}C, ^{15}N isotopically labeled LTA lipid anchor (*143*). This sample was prepared using the mixed solvent system $CDCl_3$:CD_3OD:D_2O (2:3:1, v/v), and the

experiment performed at 17 ºC. An unlabeled sample of full-length human sCD14 truncated at residue 152, amino acids 20–171 following the signal peptide sequence, was prepared in *Pichia pastoris* as described earlier in Chapter 2. The sCD14 sample used for the NMR experiments was prepared in PBS buffer with a typical concentration of ~0.2 mM. A stock solution of ^{13}C, ^{15}N labeled LTA lipid anchor was prepared at 5 mg/ml concentration and vortexed vigorously to produce a uniform suspension. The ligand was then added to the sCD14 to prepare a sCD14:LTA lipid anchor NMR sample in a molar ratio of 1:1. The sCD14:LTA lipid anchor sample was incubated for 30 minutes at 37 ºC to ensure complete binding of LTA lipid anchor by sCD14. $^{1}H–^{13}C$ HSQC spectra were recorded at 17 ºC for sCD14 in the absence and presence of LTA lipid anchor. All NMR experiments were carried out on a cold probe equipped Varian VNMRS 600 MHz spectrometer at 17 ºC. Acquired NMR data was processed and analyzed using the Felix software package (Molecular Simulations) and/or NMRPipe (*162*).

5.3 RESULTS AND DISCUSSION

5.3.1 PREPARATION AND ISOTOPIC LABELING OF LIPOTEICHOIC ACID IN *Bacillus subtillis* ATCC 6633™

CD14 is capable of recognizing and interacting with cell wall components from gram-positive bacteria including LTA, which is a strong immune activator in mammals. Obtaining structural information on the specific regions pertinent to the interactions between LTA and CD14 would be very beneficial for the elucidation of CD14's role in the activation of the immune response. In the course of this work, we have successfully

developed a protocol for the efficient isotopic labeling of LTA in *B. subtilis*. In order to obtain higher cell densities as well facilitate isotope labeling, the *B. subtilis* growths were performed in M9 minimal media with additional supplementation with 0.1% casamino acids. Isotopic labeling was accomplished by simple substitution of $^{13}C_6$-glucose and ^{15}N ammonium chloride into the growth medium. LTA was extracted using the recently developed *n*-butanol method in order to prevent structural decomposition associated with traditional means of LTA extraction (*50*). Final purification of extracted LTA was performed using octyl-sepharose HIC chromatography. Together, these methods produce milligram quantities of highly purified ^{13}C and ^{15}N labeled full-length LTA, as well as labeled LTA lipid anchor. This has not only permitted us to probe the structural interactions of LTA with sCD14 for the first time by solution NMR spectroscopy, it also poses the possibility for NMR structural studies of other LTA complexes in future.

5.3.2 NMR ANALYSIS OF LIPOTEICHOIC ACID IN COMPLEX WITH SOLUBLE CD14

A detailed structural investigation of the LTA lipid anchor's interactions with CD14 was carried out using multidimensional solution NMR spectroscopy. The results of the NMR studies with full-length LTA and LTA lipid anchor indicate that the lipid anchor is sufficient to interact with CD14. The binding of LTA lipid anchor by CD14 has both similarities and differences from the binding of Kdo_2-Lipid A. In the ^{1}H-^{13}C HSQC spectra of CD14-bound LTA lipid anchor, the gentiobiose sugar headgroup resonances (structural schematic shown in **Figure 5.1**) broaden out to the point of being undetectable. This complete broadening of the sugarhead group resonances indicates that

the interactions are on the intermediate exchange timescale of NMR. This likely indicates strong interactions with the hydrophilic rim of sCD14. This strong interaction probably consists of several weaker interactions that together add up to a strong interaction. The use of multiple weaker interactions by a protein to strongly bind a substrate has been suggested to contribute to increased binding specificity, and stability by allowing greater versatility through the ability to selectively form, alter, and break multiple interactions as needed (*163*). This could be a mechanism utilized by CD14 in its differential ligand recognition and binding, as evidenced by the change in exchange rates seen in a number of resonances.

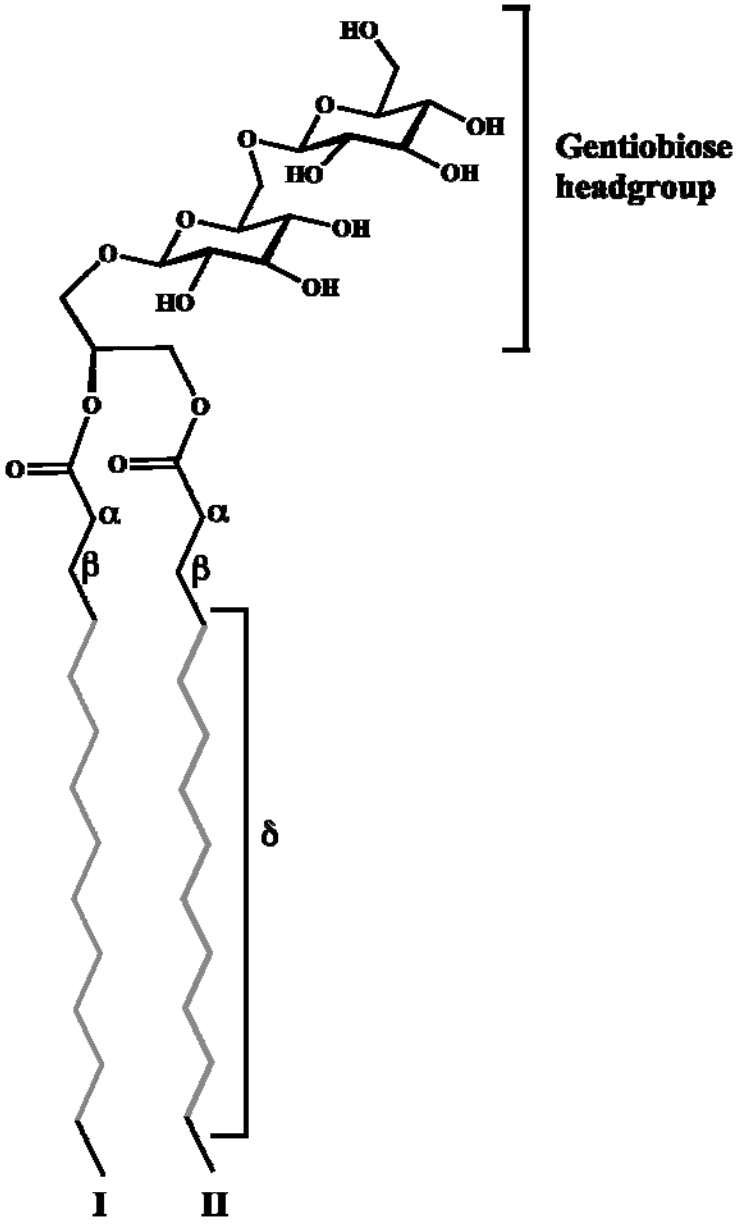


Figure 5.1: Structural schematic of LTA lipid anchor.
The numbering scheme for the acyl chains of the LTA lipid anchor are shown. The spanning δ methylenes are also indicated in gray.

The lipid anchor's two acyl chains likely undergo non-specific Van der waals interactions with the hydrophobic interior of sCD14 that result in the broadening of the methylene resonances. The interactions of LTA lipid anchor with CD14 seems to affect a greater number of resonances than in the case of Kdo_2-Lipid A. We hypothesize that this may be because the gentiobiose headgroup of the LTA lipid anchor is smaller than the lipid A sugar head group and Kdo units. This smaller size may result in a greater number of interactions between CD14's hydrophilic rim being spread over fewer ligand features. In addition, because the acyl chains of LTA and its lipid anchor are attached to the headgroup by a glycerol linker, and because of the obvious flexibility in the polyglycerophosphate chain on full-length LTA, the headgroup likely has a greater potential range of movement. This enables it to fit more extensively along the hydrophilic rim, and leads to an increase in the broadening and conformational exchange effects for a majority of the gentiobiose headgroup's resonances.

An interesting observation was that the α, β, and δ methylene residues of the LTA lipid anchor show changes in their rates of exchange between conformational states, much like those seen in Kdo_2-Lipid A (**Figure 5.2**). The two α methylenes of the acyl chain are initially seen as a broad single peak, but upon binding, the single peak experiences an upfield shift and splits into two resonance peaks, one for each acyl chain's α methylene group (**Figure 5.2 B**). The individual α methylene peaks in the CD14 bound spectra also show signs of intermediate exchange, as both peaks are broad overlapping multiplets. The upfield shift, as well as the splitting of the initial α methylene resonance into individual signals, is indicative of strong interaction with CD14.

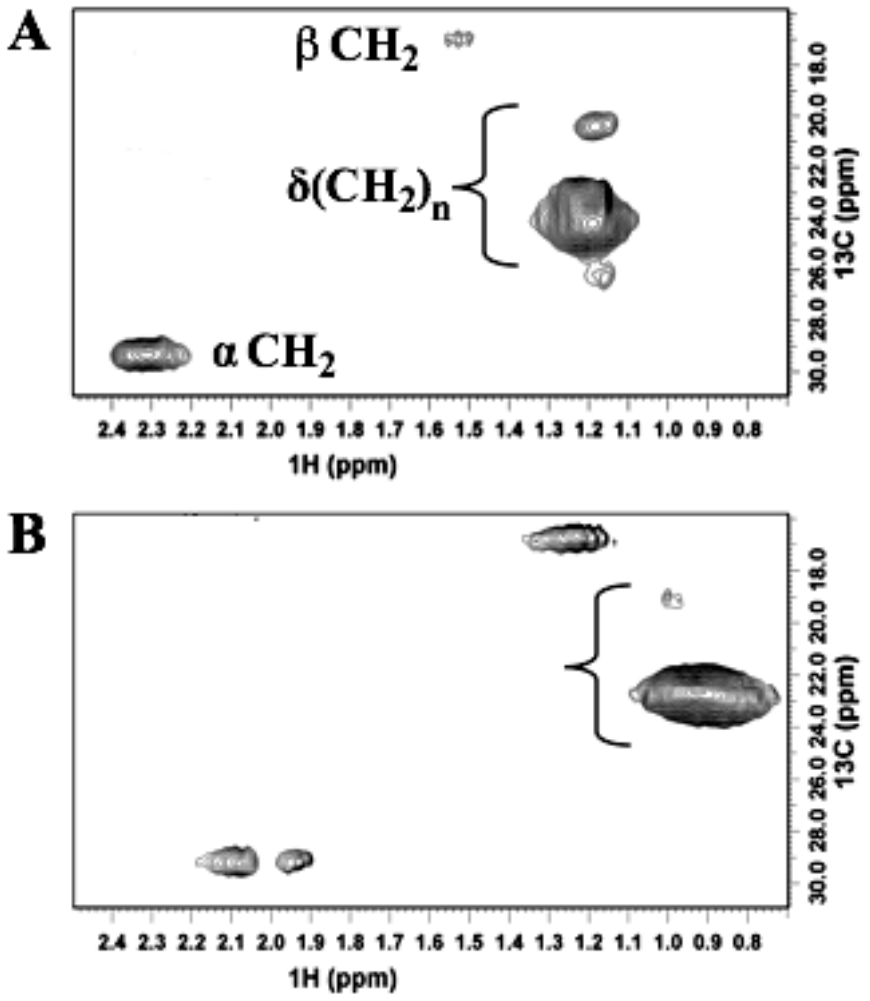


Figure 5.2: Comparison of ^{1}H-^{13}C HSQC spectra of the acyl chain region of LTA's lipid anchor upon interaction with soluble CD14.

Comparison of the acyl chain region of ^{13}C isotopically labeled LTA lipid anchor alone (A) in the mixed solvent system $CDCl_3$:CD_3OD:D_2O (2:3:1, v/v), and LTA lipid anchor complexed with sCD14 (B) in PBS buffer.

The low intensity multiplet observed for the unbound β methylenes of the LTA lipid anchor indicate they are undergoing intermediate exchange on the NMR timescale. Upon binding, the β methylene multiplet's exchange rate quickens, as indicated by the improved visibility of higher intensity of the bound peak (**Figure 5.2 B**). However, the β methylenes are still undergoing conformational exchange at intermediate rates of exchange, as shown by the retention of a broad overlapping multiplet. When compared to the other resonances of the acyl chain, the δ methylene groups, which compose the bulk of the acyl chain's methylenes (shown in gray in **Figure 5.1**), have a higher intensity signal and exhibit fewer signs of exchange broadening. This suggests that the δ methylenes are not actually restricted to a single conformation, but maintain some flexibility even when bound within the hydrophobic pocket of CD14. This also implies that the spanning δ methylenes in the acyl chains likely make only non-specific van der Waals contacts with the leucine side-chains of the hydrophobic pocket. Furthermore, the spectral changes observed for the LTA lipid anchor's δ methylenes appear analogous to the spectral changes observed in the lower half of Kdo_2-Lipid A's acyl chains upon CD14 binding.

The changes in exchange rates observed in the CD14 bound LTA lipid anchor once again illustrate that dynamics are a significant part of CD14's interactions with an endotoxin ligand. These interactions may be conserved across different ligands as a mode of recognition. Furthermore, the changes seen in the LTA lipid anchor acyl chains have a great deal of similarity to those seen in Kdo_2-Lipid A's acyl chains. The upper acyl chain carbons nearest to the headgroup show more significant modulations of their

dynamics. However, the portions of the acyl chains more distal from the sugar headgroup, the δ methylenes, show only a minor upfield shift and slight broadening effects. These changes are to be expected, due to binding to CD14. Together, this evidence supports the popularly held view that saccharides with charged moieties as well as acyl chains is a pathogen-associated molecular pattern. This is suggested by the features of LTA and Kdo_2-Lipid A affected most strongly during interaction with CD14, such as the sugarhead group, phosphares, and upper portion of the acyl chains. The role of charged saccharide groups as molecular moieties common to many PAMPs is further validated by FLS2 in plants. The features of flagellin seen to interact with the LRRs of FLS2 are the charged amino acids and hydrophobic amino acid side chains present in each flagellin monomer. This is demonstrated by the result of investigations of FLS2 that showed disruption of electrostatic interactions by salt or pH changes, as well as by mutagenesis experiments significantly reduce flagellin binding. Alanine scanning mutagenesis studies showed that a loss of hydrophobic regions in the LRRs impacted FLS2's ability to interact with flagellin (*164*). Though there are no acyl chains on flagellin, the utilization of hydrophobic interactions by FLS2 provides weight to the proposal that hydrophobic features, primarily in the form of acyl chains or alternatively amino acid side chains, are another important component in PAMP structural recognition.

CHAPTER 6. THE ROLE OF DYNAMICS IN THE INTERACTION OF CD14 WITH ENDOTOXINS

6.1 INTRODUCTION

NMR spectroscopy is well suited to probe the dynamics of a system over a wide range of time scales from picoseconds to hours. With NMR, it is possible to observe dynamically active regions in a molecule or macromolecular complex, and to analyze the dynamics of a specific region or residue at different time-scales. This is accomplished by measuring the change in certain NMR experimental parameters, such as linewidth, peak intensity, or chemical shifts, by direct observation of these changes in the NMR spectrum (*165*). Both the analysis of the impact of different endotoxin ligands on CD14 and the analysis of the effects of CD14 on lipid A showed a number of residues which showed differential line broadening, as seen earlier in **Figure 4.5 A-D**. Changes in line broadening could be indicative of a transition from fast rates of exchange between conformational states to intermediate or slow rates of exchange. A residue that is in fast exchange between two different environmental states is seen as a single peak. The peak's exact position is dependent on the percentage of each state the residue is currently occupying. If the populations are perfectly split between the two environments, then a single peak would be seen precisely between where the two possible conformations' individual peaks would have been seen. If the rate of exchange between two

conformational states is slow, then two separate peaks would appear corresponding to the two distinct states. When the rate of exchange is intermediate between fast and slow exchange rates, the peak broadens significantly as its position is now being averaged over two or more possible positions. This is sometimes seen as a broad, overlapping multiplet or the peaks may coalesce and disappear entirely (*163*).

This study constituted the first direct structural observation of specific residue combinations in CD14, or any endotoxin binding protein which differentially affect endotoxin binding. We hypothesize that conformational dynamics in CD14 might provide specificity to ligand recognition by allowing CD14 to choose conformations that facilitate low-energy contacts between the molecules and allow fine-tuning of the interactions for different ligands. This is evidenced by the differential line-broadening detected for several groups in and around the sugar headgroup of Kdo_2-Lipid A along with the existence of multiple conformations, indicating the mode of binding is dynamically-modulated. This differential broadening, as well as the presence of multiple conformations is also observed in the ^{1}H-^{15}N HSQC spectra of sCD14 (**Figure 3.4**) (*151*). Interestingly, upon formation of the CD14-endotoxin complex, there are no indications either in the ^{1}H-^{15}N HSQC spectra or in circular dichroism spectra that reveal any significant conformational changes in CD14. The lack of global conformation changes in CD14's structure upon binding in conjunction with the dynamics revealed by differential line broadening strongly implies that dynamics must play a key role in the recognition and binding of the structurally diverse endotoxin ligands of CD14. To analyze whether changes in temperature and pH can modulate CD14's dynamics in a manner similar to

those seen upon binding of different endotoxin ligands, we have performed a series of pH and temperature dependence studies.

6.2 MATERIALS AND METHODS

6.2.1 EXPRESSION AND PURIFICATION OF ISOTOPICALLY LABELED SOLUBLE CD14

Isotopically labeled samples of a truncated version of full-length human sCD14 sequence consisting of the 152 N-terminal residues (amino acids 20–171), after the signal peptide sequence, were prepared in *Pichia pastoris*. Isotopic labeling was accomplished by supplementing the expression medium with ^{15}N ammonium sulfate. The expression conditions and purification procedures are the same as described earlier in Chapter 2.

6.2.2 NMR STUDIES ON THE TEMPERATURE AND pH DEPENDENCE OF SOLUBLE CD14

The ^{15}N labeled sCD14 sample used for the temperature dependent NMR experiment series was prepared in PBS, pH 8.9 buffer containing 0.5M D_5-Glycine with a sCD14 concentration of ~0.2 mM. ^{1}H-^{15}N HSQC spectra were collected on this sample at 17, 27, and 37 ºC. Prior to the start of each NMR experiment, the sCD14 sample was allowed to equilibrate, in the spectrometer, at each new temperature increment for 15 minutes.

The ^{15}N-labeled sCD14 sample utilized for the pH dependent experiment series was prepared in PBS pH 7 buffer containing 0.5 M D_5-glycine. For each pH investigated, a 5 ml volume of PBS pH 7.0 containing 0.5 M D_5-glycine was adjusted to pH 8.0, and 9.0 by the dropwise addition of 6 M potassium hydroxide. Adjustment of the PBS's pH was monitored using an automatic temperature correction pH probe (Denver

Instruments). The sCD14 sample's pH was raised incrementally to each new pH level by performing buffer exchange using an Amicon Ultra-4 centrifugal filter unit (Millipore, Billerica, MA). All of the pH dependent NMR experiments were carried out at 37 ºC.

Sensitivity-enhanced ^{1}H-^{15}N HSQC spectra were recorded at each temperature and pH for the protein samples (*143*). Data was collected with 1024 complex points in the direct dimension and 64 complex points in the indirect dimension for the HSQC experiments. All NMR experiments were carried out on a Varian VNMRS 600 MHz spectrometer equipped with a cold probe. Acquired NMR data was processed and analyzed using NMRPipe (*162*) or the Felix software package (Molecular Simulations).

6.3 RESULTS AND DISCUSSION

6.3.1 ENHANCEMENT OF SOLUBLE CD14 SOLUTION STABILITY

The need for a sCD14 sample with good stability over an extended timespan was an important factor in being able to perform lengthy experiment series. Previously, we had seen that ligand-free sCD14 at high concentration had a limited lifespan, especially at higher temperature, and would begin to unfold and aggregate after ~6 hours. This reduced stability was compensated for in our earliest studies by running NMR experiments at low temperature, 17 ºC (*151*). However, with the addition of osmolytes, a protein's stability can often be increased, and therefore its lifespan in its folded form can be extended. The manner by which osmolytes extend the useful life of a protein is not fully understood, but is thought to work by helping maintain the protein's folded structure through preferential hydration of the protein, which is entropically favorable for the

folded state (*166, 167*) However, the use of high concentrations of osmolyte in an NMR sample would result in the introduction of new and overwhelmingly large signals into the NMR spectra. This requires that osmolytes used in NMR be perdeuterated and, given its small size and low-cost, perdeuterated glycine is an excellent choice (*167*). 0.5 M D_5-glycine was determined to be an optimum concentration for maintaining CD14 stability, and was added to the PBS buffers used in the sCD14 pH and temperature dependent studies. This extended the lifetime of the sCD14 samples used from hours to days.

6.3.2 TEMPERATURE AND pH DEPENDENT CHANGES IN THE NMR SPECTRA OF CD14

In recent years, the importance of dynamics in a protein's ability to function has been shown to be absolutely critical. Without the dynamics present in regions of many proteins' structures, they would no longer be capable of functioning effectively if they functioned at all (*168*). The results of our NMR structural studies have demonstrated that CD14 has a significant amount of dynamic motion present in its structure. CD14 was observed to sample multiple conformational states as evidenced by the splitting of single resonances into multiple resonances. In our previous analysis of ligand recognition by CD14, we proposed that dynamics plays a role in modulating the specificity of CD14's interactions with its endotoxin ligands. This is in line with studies that have shown an increase in the overall protein backbone conformational entropy upon binding of a hydrophobic ligand. This was correlated with increased stabilization of the protein-ligand complex, as well as greater ligand specificity (*156*). By carrying out NMR studies of isotopically labeled sCD14 under varying temperature and pH conditions, the range of

possible dynamic behavior in CD14 could be investigated, and compared to the endotoxin binding induced changes in dynamics. A number of the dynamic CD14 resonances exhibited multiple broad, overlapping peaks characteristic of intermediate exchange rates. Based on the intensity of the individual peaks composing the multiplet, it can be discerned that the different populations represented in the multiplet are actually differing conformational states. By collecting ^{1}H-^{15}N HSQC spectra of CD14 over a series of incremental temperature increases, we observed temperature-dependent modulations of the range of conformational states that some resonances were able to sample. This was evidenced by changes in the intensities of specific peaks within the splitting indicated by the bracket in **Figure 6.1**.

An increase in temperature generally has more effect on the flexible regions of a protein's structure. Higher temperatures cause the exchange rates to shift toward faster exchange regimes. Changes in temperature can also effect the formation and dissociation of hydrogen bonds, as well as changing the entropy of the system, which will favor protein unfolding (*169*). At low temperature, the conformational states being sampled by the indicated CD14 resonance are quite varied in terms of their populations as seen by the multiple peaks (**Figure 6.1**). However, as the temperature is raised, the populations in each conformations being sampled shift, as indicated by the shift of intensity from the upper peak of the multiplet to the lower peak at 27 ºC. As the temperature is increased further, the intensity shifts from the lower peaks of the multiplet back to the upper peak at 37 ºC. These shifts likely indicate that those specific conformations are not as highly, or possibly not as easily, populated at low temperatures, but as the temperature is raised,

these conformational states become progressively more favorable for occupancy. This is illustrated by the shift of intensity to different positions within the multiplet at 27 ºC and 37 ºC. The conformation favored at 27 ºC is not the same conformation favored at 37 ºC.

In addition, as the temperature changes this results in changes in the local environments experienced by a residue, this change in environment also causes change in the chemical shift of the residue this is illustrated in **Figure 6.1**, by the shift of intensity in the multiplet down and toward the left at 27 ºC and the up and toward the right at 37 ºC.

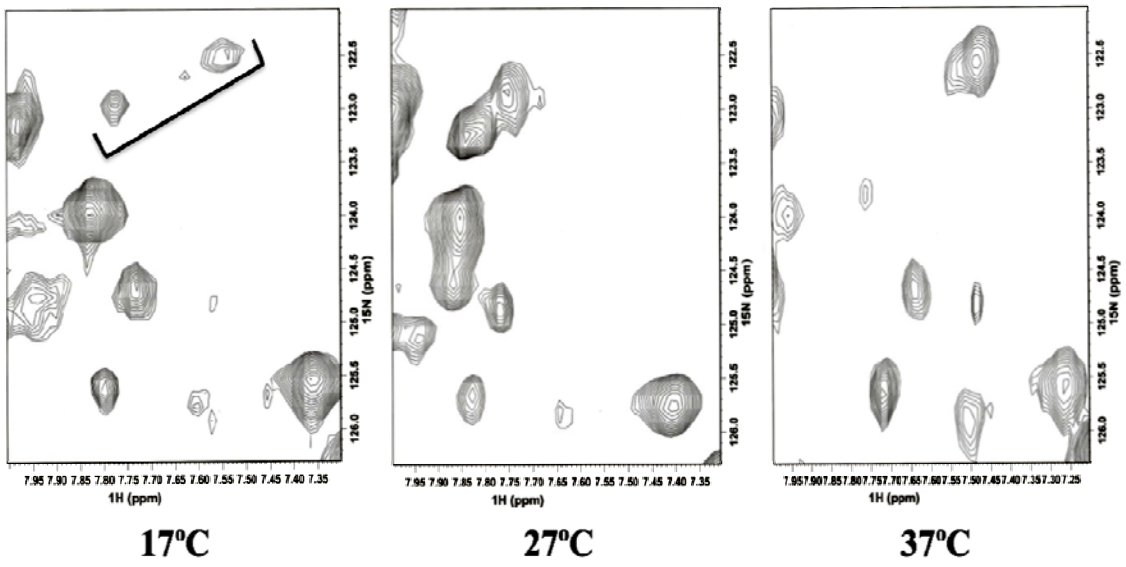


Figure 6.1: Temperature-dependent changes in ^{1}H-^{13}C HSQC spectrum of CD14. The bracket indicates the multiplet showing representative temperature-dependent changes over the tested temperature range. Also, visible in the lower portion of the spectra, are the temperature-dependent appearance and disappearance of several additional resonances.

In addition, by adjusting the pH of the sample, the transitions between various conformational states for some resonances could also be modulated (**Figure 6.2**). Changes in pH can affect the charge and electrostatic interactions in a protein by causing the protonation or deprotonation of side chains; this in turn can directly affect the stabilization of different conformational states (*170*). By incrementally increasing the pH of the sCD14 sample, we observed the sampling of a series of conformational states evidenced by the shift of peak intensity among the peaks composing the multiplet. This is most clearly illustrated by the multiplet indicated in **Figure 6.2** by the bracket. As the pH is changed, the more intense peaks of the multiplet at pH 7.0 lose intensity while the less intense peaks gain intensity, as seen at pH 8.0. At pH 9.0 the distribution of intensity between the peaks of the multiplet has reversed, with the originally less intense peaks at pH 7.0 now being the most intense at pH 9.0, and the initially intense peaks seen at pH 7.0 completely disappearing at pH 9.0. In addition, the number of peaks observed in the multiplet decreases, suggesting that fewer distinct conformational states are now accessible. At pH 9.0, only two conformations appear to be favored, and the dynamic exchange between other possible conformations is no longer discernable. Once again we see that CD14 is sampling multiple different conformational states, and that through incremental pH adjustments we are able to influence what conformations are favored.

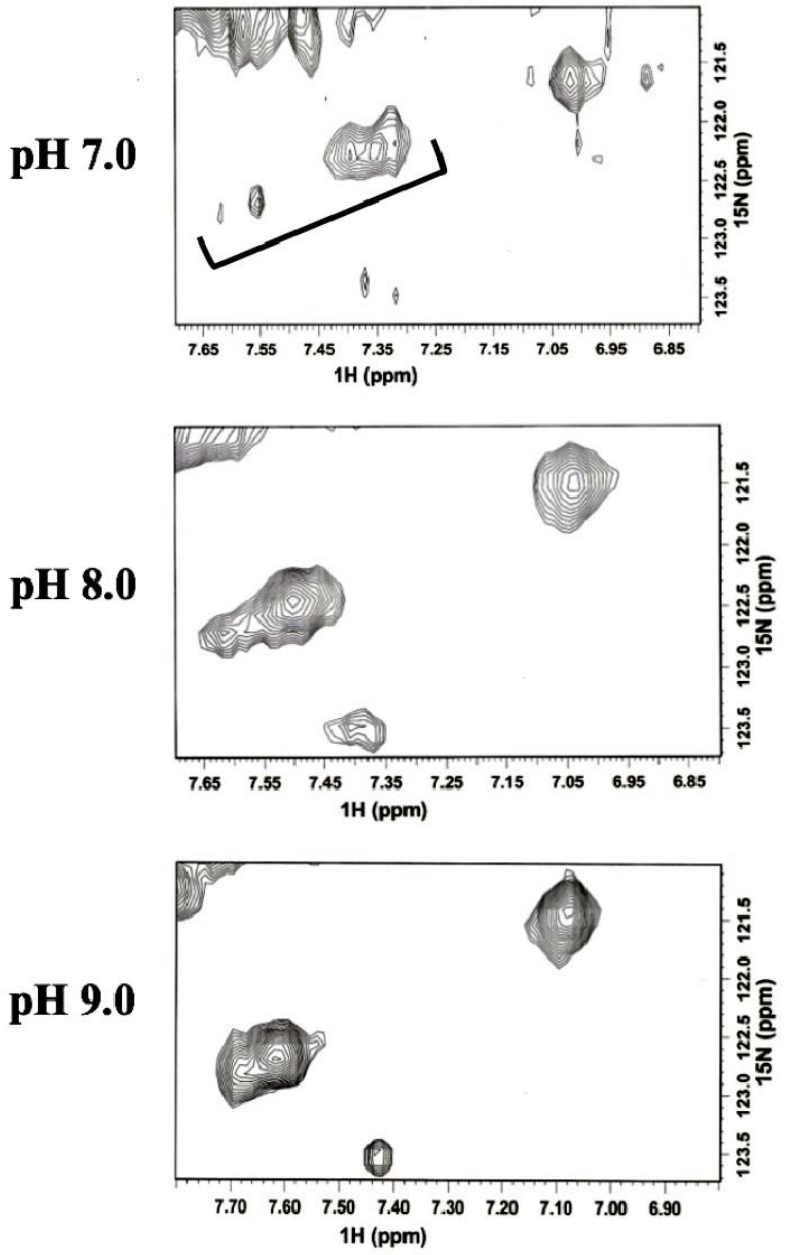


Figure 6.2: pH-dependent changes in ^{1}H-^{13}C HSQC spectrum of soluble CD14.
The bracket indicates the resonance showing the greatest pH-dependent changes, over the examined pH range.

Our ability to influence what conformational states a resonance is able to sample provides further corroboration that CD14 is indeed undergoing dynamic conformational sampling. This correlates with our previous studies, which indicated that the interaction of CD14 with its ligands had a dynamic component. While the identity of the residues showing dynamic behavior is not known at this point due to a lack of CD14 resonance assignments, the significance of the observed modulations still carries substantial implications for how CD14 interacts with such a diverse array of ligands. The presence of structurally dynamic regions and residues might help in explaining how CD14 is able to differentially recognize endotoxin ligands. The contribution of conformational dynamics to protein function and ligand binding specificity has been highlighted by a number of recent studies. These studies have shown that the internal dynamics of a protein varied depending on what ligand was bound, and this contributed substantially to ligand specificity as well as to the formation of high-affinity protein-ligand interactions (*171-173*). The multiple conformations populated by CD14 suggest that CD14 may use different conformational states to either aid in binding specific ligands, or that these states may represent distinct states induced in CD14 by ligand binding.

CHAPTER 7. USE OF A SPIN-LABELED LIPID A TO MEASURE DISTANCE RESTRAINTS FOR LIPID A IN COMPLEX WITH CD14

7.1 INTRODUCTION

For many years now, the popularity of utilizing spin-labels in solution NMR to collect long distance restraints, and map the binding interactions of protein-ligand complexes has been growing. The application of spin-labels to use in protein-ligand interactions allows for observations of residue-specific binding in large macromolecule complex, as well as detailed distance information to be collected. The principle that allows a spin-label to be used for this is paramagnetic relaxation enhancement (PRE) (*174-176*). In general terms, the spin-label's free radical, a paramagnetic center, has the ability to interact with any neighboring proton within 15-25 Å. This dipolar interaction of the free electron with surrounding protons causes the resonance signal for the affected protons to relax more rapidly than in normal conditions. In NMR, the faster the relaxation of a given nuclear spin, the broader /weaker its signal appears, and the closer to the spin-label a spin is, the greater the broadening. Because the magnitude of the paramagnetic relaxation enhancement is directly related to distance from the free radical, it is possible to calculate physical distances between a given interacting proton resonance and the spin-label (*174, 177*). The calculation of the distances is accomplished by measuring the change in peak intensity in the presence and absence of the spin label. This technique is

convenient in that it does not require multiple, perfectly matched samples in a spin-labeled and non-spin-labeled versions. First, a spectrum is collected on the spin-labeled complex in its oxidized, paramagnetic state followed by addition of a reducing agent to the sample, and collection of a spectrum of the complex with the spin-label in a reduced, diamagnetic state (*178*).

Though a high-resolution crystal structure of mouse CD14 has been solved, revealing a great deal of new data about CD14 and its structure, the lack of a bound endotoxin ligand ultimately limits the overall usefulness of the structure (*75*). This limitation is further compounded by the significance of endotoxin binding in CD14's function. CD14's binding abilities form the foundation of its critical differential recognition of endotoxin, and thus its ability to activate different TLR's. Therefore, a ligand bound CD14 structure is of vital interest. Our recent investigations have greatly expanded the scope of structural information regarding CD14's ability to differentially recognize endotoxin-associated patterns and provided detailed insights into the specific structural elements recognized in an agonist ligand (*151, 179*). However, the lack of a structure for a CD14-ligand complex is a conspicuous gap in the field of knowledge for CD14. A high-resolution structural model of CD14 with an agonist would provide information that would greatly strengthen the understanding of how CD14 functions, and provide clues into how the transfer of an endotoxin from CD14 to its requisite TLR might take place. At this time, NMR assignments for CD14 are not available, but NMR assignments are available for ^{13}C ^{15}N isotopically labeled Kdo_2-Lipid A and they transfer directly to lipid A. Our ability to produce isotopically labeled lipid A in large amounts

with high purity afforded us the opportunity to produce a spin-labeled and isotopically labeled version of lipid A. Spin-labeled, ^{13}C ^{15}N lipid A provides a way to collect paramagnetic relaxation enhancement-based distance restraints, which offer a means to solving the structure of lipid A's bound conformation. Determination of lipid A's bound conformation would allow a high-resolution CD14-lipid A structure to be modeled. In an effort to achieve this goal, we have undertaken the preparation and characterization of spin-labeled, ^{13}C labeled lipid A, and collected reduced and oxidized ^{1}H-^{13}C HSQC experiments on spin-labeled lipid A-CD14 complex in reduced and oxidized forms. These experiments have been used to calculate a partial set of intermolecular distances for bound lipid A.

7.2 MATERIALS AND METHODS

7.2.1 PREPARATION, SPIN-LABELING, AND PURIFICATION OF ^{13}C LIPID A

^{13}C ^{15}N isotopically labeled Kdo_2-Lipid A was produced using the *E. coli* mutant WBB06 as described previously (*179*). Preparation of lipid A from ^{13}C isotopically labeled Kdo_2-Lipid A was prepared as described in Chapter 2.

Spin labeling of lipid A was performed following the protocol outlined by Bretscher et al. (*180*). In order to attach the nitroxide spin-label 3-carboxy proxyl (Sigma Aldrich, St. Louis, MO) to lipid A it was converted to an acid chloride form. This was performed by dissolving 12.5 mg of 3-carboxy proxyl in 750 μl benzene in an amber vial with a Teflon septa. Also added to the solution was 0.27 mmol pyridine and 0.37 mmol

thionyl chloride. This mixture was stirred for 1 hour at room temperature, open to the air via a needle inserted in the septa. All solvents were evaporated under a stream of nitrogen gas then resuspended in 250 µl chloroform. In a fresh vial, 1 mg of ^{13}C ^{15}N lipid A, determined by weighing of the sample on a Sartorius MC1 scale accurate to 0.1mg in a pre-weighed tube, was resuspended in 1 ml chloroform, and 3.2 µl 3-carboxy chloride acid solution, and 0.2 µl triethylamine. This reaction solution was sealed and incubated with stirring for 20 hours at 4 ºC. After incubation, the sample was dried under a stream of nitrogen gas and resuspended in endotoxin free water. Unreacted spin-label was removed from the resuspended sample by repeated washes, and followed by loading onto a NAP-25 column (GE Healthcare). The spin-labeled lipid A was eluted following the recommended procedure. Failure to adequately dilute and sonicate the sample prior to loading on the NAP-25 column can result in the lipid A aggregate remaining on top of the columns upper frit. After elution, the upper frit was washed with endotoxin free water, and the wash checked for spin-labeled lipid A. If the sample was to be stored for an extend time before use it was lypholized and kept at -20 ºC.

7.2.2 CHARACTERIZATION OF SPIN-LABELED ^{13}C LIPID A BY EPR AND MALDI-TOF

The presence of lipid A in the spin-labeled lipid A sample was verified by collecting one dimensional ^{1}H-^{13}C HSQC spectra of the sample in the mixed solvent system $CDCl_3$:CD_3OD:D_2O (2:3:1, v/v) at 25 ºC using a cold probe equipped Varian VNMRS 600 MHz spectrometer. The presence of lipid A was confirmed by the characteristic lipid A acyl chain peaks in the ^{1}H-^{13}C HSQC spectra.

The presence and magnetic state of the spin-label was confirmed by electron paramagnetic resonance spectroscopy. The spin-labeled sample was resuspended in a minimal volume of endotoxin free water and placed in a quartz capillary tube. All experiments were carried out at 37ºC on a Bruker EMX X-Band spectrometer equipped with a temperature control module.

MALDI-TOF mass spectrometry was used to ensure that only a single spin label was being attached to the lipid A molecule. 2,5-dihydroxybenzoic acid (DHB) was selected for use as the matrix and was prepared in methanol at a concentration of 30 mg/mL. 0.5μL of matrix was spotted onto the target plate and allowed to dry before addition of 0.5μL of spin-labeled ^{13}C ^{15}N lipid A, at ~5 mg/mL in CH_3OH:$CHCl_3$:H_2O (3:2:1 v/v). Deuterated versions of the three solvents were used in NMR samples (*181, 182*). An external calibration was performed using Bruker's peptide calibration standard II prepared per the manufacturers instructions, and applied to the target plate in the same manner as the lipid A samples. MALDI-TOF was preformed on a Bruker-Daltonics microflex system in positive detection mode. MALDI-TOF of samples was performed following confirmation of the spin-label's presence by EPR and lipid A by NMR.

Because the area under an NMR resonance peak is proportional to the number of protons represented by the resonance, the ratio of spin-label to lipid A can be determined based on comparison of the integral values for peaks known to belong to lipid A and 3-carboxy proxyl. This allowed NMR conformation of the attachment of a single 3-carboxy proxyl to lipid A by integration of the ^{1}H-NMR of a fully reduced spin-labeled lipid A sample in CH_3OH:$CHCl_3$:H_2O (3:2:1 v/v). The ^{1}H-NMR spectrum was processed and

the peaks integrated using MestReNova (Mestrelab Research). In order to minimize error in the automated intensity measurements the signal suppression function was applied to the residual water, methanol, and chloroform peaks, followed by a polynomial baseline correction. The integrals were then measured using MestReNova's automated integration method, and the integral values were normalized to the methyl proton signal of Lipid A's acyl chains.

7.2.3 NMR MEASUREMENTS OF SPIN-LABELED ^{13}C LIPID A IN COMPLEX WITH SOLUBLE CD14

Unlabeled samples of the 152-residue truncation of full-length human sCD14, amino acids numbering 20–171 without the signal peptide sequence, were prepared in *Pichia pastoris* as described in Chapter 2. The samples used for the NMR experiments were prepared in PBS buffer pH 7.4 with typical concentrations of ~0.25 mM. A stock solution of spin-labeled ^{13}C, ^{15}N lipid A was prepared at 5 mg/mL concentration in 99% D_2O and briefly sonicated to ensure uniform resuspension. Spin-labeled ^{13}C lipid A was then added to the protein in a molar ratio of 1:1.5 and incubated for 45 minutes at 37 ºC to ensure complete binding of ligand. The 1.5 ml tube containing the sample was then placed in a vacuum flask and degassed for 15 minutes under vacuum. Reduction of the spin-label was carried out by addition of sodium dithionite, $Na_2S_2O_4$, to the sample in a 12:1 molar ratio of $Na_2S_2O_4$ to spin-label. Elimination of the sample's EPR signal was monitored and taken as an indication of reduction of the spin-label's free radical, which also allowed monitoring for exhaustion of the transient sulfur dioxide anion radical seen upon addition of ice-cold $Na_2S_2O_4$ to the sample (*183*). ^{1}H–^{13}C HSQC were recorded at

37 ºC for the oxidized and reduced sample. Data was collected with 1024 complex points in the direct dimension and 72 complex points in the indirect dimension. All NMR samples were run in 4 mm D_2O matched Shigemi tubes (Shigemi, Allison Park, PA). Experiments were carried out on a Varian VNMRS 600 MHz spectrometer equipped with a cold probe. NMR data was processed and analyzed using NMRPipe (*162*) Polynomial baseline corrections was applied to minimize baseline distortions near the water peak. An exponential window function was applied to the direct dimension, and a 90º-shifted squared sinebell window function was used for the indirect dimension. Distances were calculated based on peak intensities as described in detail below.

7.3 RESULTS AND DISCUSSION

7.3.1 PREPARATION AND CHARACTERIZATION OF SPIN-LABELED ^{13}C ^{15}N LIPID A

Using the methods and protocols described earlier in this dissertation, highly purified ^{13}C ^{15}N Kdo_2-Lipid A was produced, hydrolyzed with 1% acetic acid, and re-purified yielding high purity ^{13}C ^{15}N lipid A. The choice to attach the spin-label to lipid A as opposed to Kdo_2-Lipid A provided several advantages. One advantage was that upon removal of the Kdo_2 unit, lipid A had only a single primary alcohol, located distal to the C6' position (refer to **Figure 1.3**). The labeling protocol described in Bretscher et al. takes advantage of this by using conditions that highly favor conjugation of the spin-label to a primary alcohol (*180*). In addition, the 3-carboxy proxyl spin label has a molecular weight and relative size on par with a single Kdo unit. This suggested that the attached spin-label should not interfere with binding by CD14, and should easily be

accommodated in the CD14 binding pocket. This proved true based on the observation of lipid A signals in the ^{1}H-^{13}C HSQC spectra of spin-labeled ^{13}C ^{15}N lipid A bound by sCD14. Had binding not occurred, no lipid A signals would have been seen due to spin-labeled lipid A forming a micelle in aqueous environments. These micelles have a high molecular weight >1MDa, rendering them unobservable in NMR

EPR analysis of the spin-labeled lipid A in the mixed solvent system CH_3OH:$CHCl_3$:H_2O 3:2:1 (v/v) as well as in endotoxin-free water revealed that the spin-label was present and in an oxidized state as indicated by the presence of a signal in the EPR spectrum (**Figure 7.1**). The absence of a signal would have indicated either failure of the conjugation reaction or the reduction of the spin-label at some early point. In the case of a weak EPR signal, this would could be a sign of incomplete labeling of lipid A population in the spin-labeling reaction. A weak signal could also be a result of line broadening. Analysis of spin-labeled lipid A samples in the mixed three solvent system, which dissolves lipid A micelles, as well as in endotoxin-free water, which favors micelle formation, allowed for lineshape changes due to solvent environment or micelle formation to be observed. This was then taken into account when estimating whether the observed EPR signals met the expected signal strength, based on the concentration of spin-labeled lipid A being used.

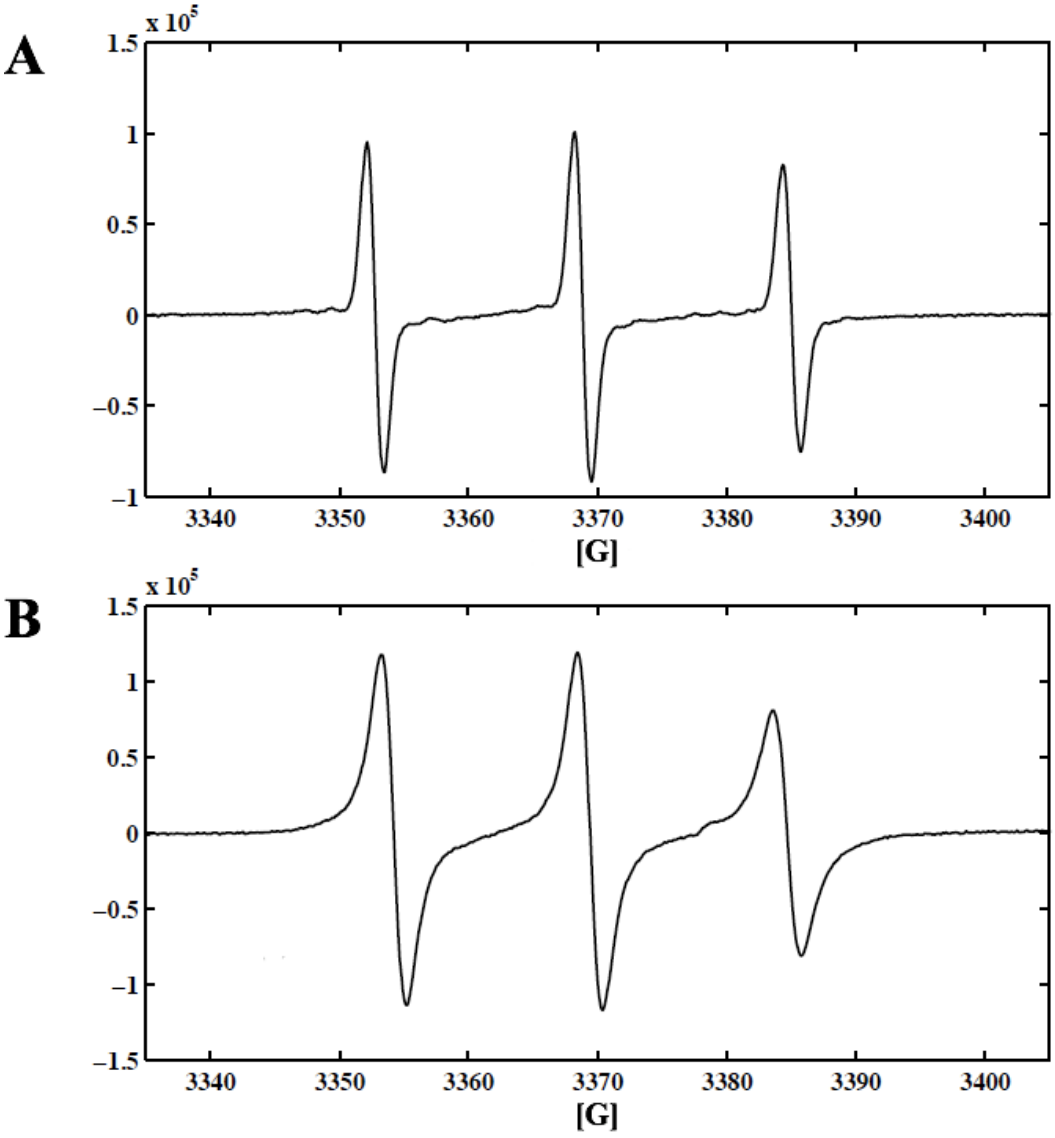


Figure 7.1: EPR spectra of Spin-Labeled Lipid A in aqueous and organic solvent.

Comparison of signal characteristics in PBS, pH 7.4, (A), and in CH_3OH:$CHCl_3$:H_2O (3:2:1 v/v) solvent mixture (B). Both spectra are indicative of fast regime rotational correlation times, but the environment occupied by the spin-labels differ, as seen by the broader lineshapes in the mixed solvents.

To check that only a single spin-label was being attached per lipid A molecule, samples were examined using MALDI-TOF mass spectrometry. The expected weight of ^{13}C ^{15}N lipid A with a single 3-carboxy proxyl spin label attached is ~2061.63 Da. The MALDI-TOF spectra showed a number of peaks corresponding to lipid A fragmentation variants common to MALDI-TOF analysis (*182*). MALDI-TOF of lipopolysaccharide and lipid A samples can be problematic due to the hydrophobic nature of the sample, which leads to poor ionization and requires the use of higher power settings. The use of higher power settings leads to greater desorption fragmentation of the lipid A molecule. The most common fragmentation variants resulting during MALDI-TOF analysis of lipid A and Kdo_2-Lipid A samples are the loss of acyl chain VI. Additionally, in the case of Kdo_2-Lipid A, MALDI-TOF analysis also leads to the loss of the Kdo_2 units (*181, 182*). Since the spin-label is attached at the primary alcohol where the Kdo_2 unit was attached, it is reasonable to presume that loss of the spin-label could occur in spin-labeled lipid A samples in much the same way as the Kdo_2 units could be lost from a Kdo_2-Lipid A sample. Taking this into consideration, the major peaks located at 1837.90 and 1854.90 m/z correspond to a single spin label attached to a lipid A that has the lost acyl chain VI (~226Da) (**Figure 7.2**). The small difference between the two is roughly equivalent to the presence or absence of a sodium ion. There were also peaks of 2062.03 and 2054.04 m/z present correlating to a fully intact spin-labeled ^{13}C ^{15}N lipid A molecule in the presence or absence of a sodium ion. The peaks at 1613.51 and 1631.50 m/z match the weight of lipid A that has lost acyl chain VI and either lacks or loses the spin-label during ionization by the laser (**Figure 7.2**).

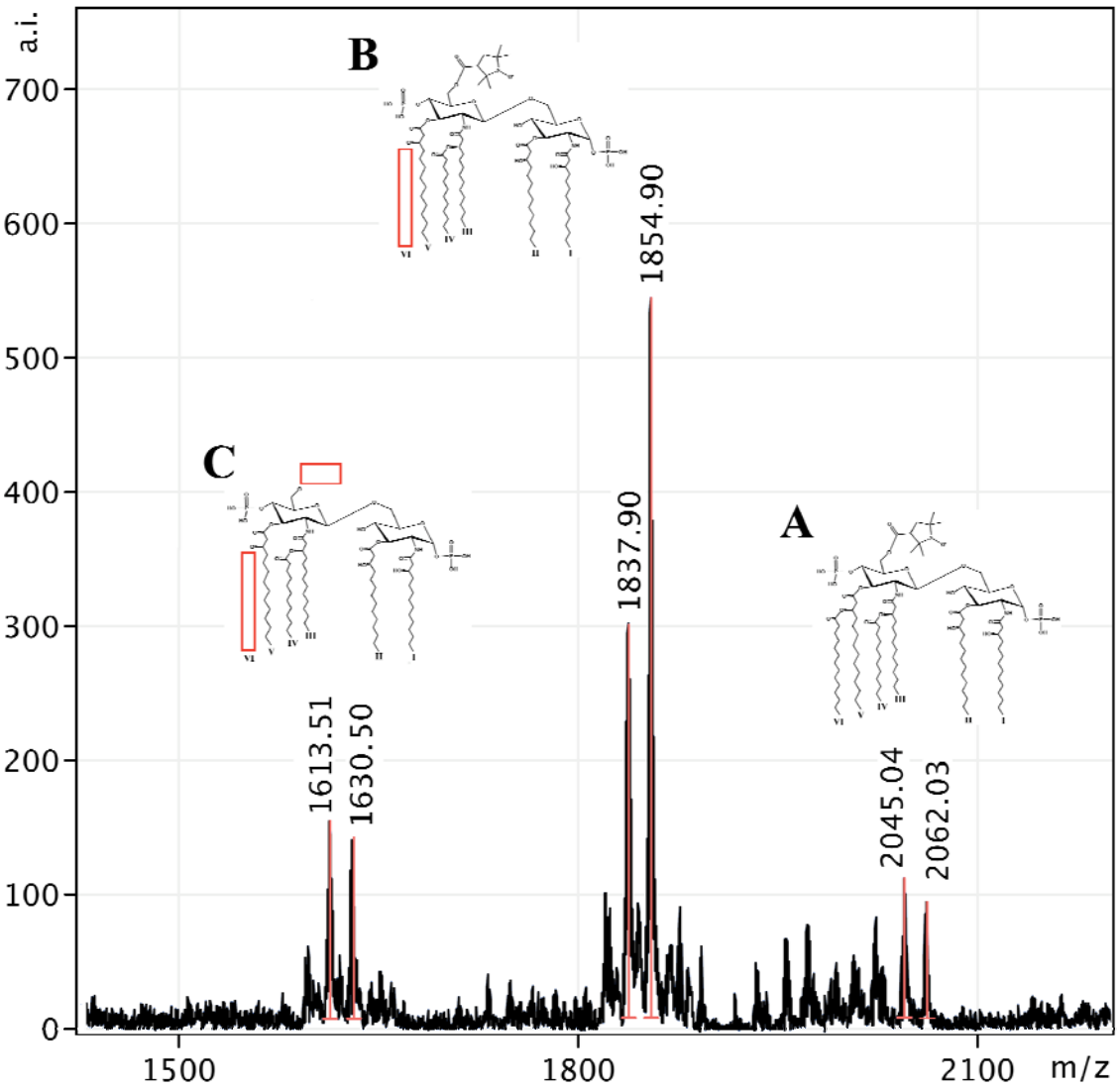


Figure 7.2: MALDI-TOF spectra of spin-labeled ^{13}C ^{15}N Lipid A.
The major peaks seen in spin-labeled ^{13}C ^{15}N lipid A. Each inset spin-labeled lipid A schematic is positioned near its representative peaks. Red boxes indicate the position of the lost spin-labeled lipid A fragment(s). Inset (A) shows the intact spin-labeled lipid A structure, (B) shows the most common fragmentation artifact, loss of acyl chain VI. Inset (C) shows the second most common desorption artifact; a lipid A which has lost the spin-label and acyl chain VI.

7.3.2 NMR ANALYSIS OF SPIN-LABELED LIPID A IN COMPLEX WITH CD14

Initial experiments on the CD14-spin-labeled lipid A complex utilized PBS, pH 8.9, containing 2 M D_5-glycine. This particular buffer provided a longer usable lifetime for sCD14 NMR samples, especially ligand-less sCD14 samples run at higher temperatures. However, over the course of the spin-labeling study, it became apparent that this buffer, for some unknown reason, impeded the complete binding of ligand. Additionally, the extensive washing steps, necessary to ensure the sample had no residual protonated glycine present because of the use of PBS, pH 8.9, 2 M glycine buffer to increase long-term storage life of sCD14 samples, were resulting in a loss of sample and stability rather than an extension.

The most problematic aspect of using basic pH conditions in conjunction with glycine was the fact that this buffer hampered complete reduction of the spin-label by $Na_2S_2O_4$ or ascorbic acid. When a free radical is fully reduced and the spin-label is in a diamagnetic state, it is no longer detectable by EPR. This complete elimination of the EPR signal was used as the standard by which the reduction of the NMR sample was considered complete.

Earlier attempts at performing the oxidized and reduced NMR experiments required an astonishingly high amount of the reducing agent ascorbic acid. Due to the large NMR signals introduced into the spectra by dehydroascorbic acid, an oxidized form of ascorbic acid, it was decided to switch to sodium dithionite, $Na_2S_2O_4$, which has no ^{1}H or ^{13}C NMR signals. However, even when using $Na_2S_2O_4$ the amount of reducing agent needed was well beyond the normal ratios typical of this type of experiment. The

use of ascorbic acid to reduce the spin-label ultimately precipitated the investigation that led to discontinuing the use of the PBS, pH 8.9, 2 M glycine buffer conditions for spin-labeled lipid A-CD14 samples. This was necessitated by an experiment in which a sCD14-spin-labeled lipid A sample used to collect an oxidized and reduced ^{1}H-^{13}C HSQC data set changed colors. Initially, the sample had the appearance of water, before and after the collection of the oxidized ^{1}H-^{13}C HSQC spectra. After the sample was reduced with ascorbic acid the reduced ^{1}H-^{13}C HSQC spectra was collected. Upon removal of the sample from the spectrometer, it had turned a bright brownish-red. Upon further investigation we discovered that ascorbic acid and glycine in basic pH conditions has been utilized in certain industrial food coloration procedures to make red, yellow, and brown color pigments (*184, 185*).

The appearance of the red color pigments in the reduced NMR sample led to an investigation to ascertain the effect of pH and glycine on the amount of reducing agent needed to fully reduce spin-labeled lipid A. A series of 50 μM spin-labeled lipid A samples were prepared for EPR in one of four different buffers. Those buffers were PBS pH 7.4, PBS pH 7.4 with 2 M glycine, PBS pH 8.9, and PBS pH 8.9 with 2 M glycine, the amount of $Na_2S_2O_4$ needed to reduce the sample was monitored under each buffer conditions. The sample in PBS buffer, pH 8.9 with 2 M glycine required a final $Na_2S_2O_4$ concentration of 34 mM to fully reduce, but in PBS pH 8.9 lacking glycine it took only 15 mM. In the identical pair of experiments performed in PBS pH 7.4 with and without 2 M glycine, the sample with 2 M glycine required 22 mM $Na_2S_2O_4$ to fully reduce the free radical whereas without glycine the same sample required only 15 mM. Additionally,

attempts to use ascorbic acid as the reducing agent required similar quantities, and its use would have still added undesirably large NMR signals into the reduced ^{1}H-^{13}C HSQC spectra. The incompatibility of the PBS, pH 8.9, 2 M glycine buffer with the reduction of the spin-label became apparent after these experiments.

During initial reduction trials, the addition of the reducing agent rapidly resulted in the loss of the typical 3-signal EPR splitting, illustrated by **Figure 7.1**, but resulted in a persistent central signal. This signal was eventually determined to be caused by the presence of sulfur dioxide anion radicals (*183, 186*). Careful degassing and the use of the minimum reducing agent possible to fully reduce the spin-label, in conjunction with short incubations open to the air, resulted in the elimination/exhaustion of the sulfur dioxide anion radical signal. It was also found that addition of chilled $Na_2S_2O_4$ to the slightly warmer CD14-spin-labeled lipid A sample increased the anion radical signal seen. Fortunately, this signal was only short lived.

By preparing spin-labeled ^{13}C ^{15}N lipid A-sCD14 NMR samples in PBS pH 7.4 buffer, better binding of spin-labeled lipid A was seen as indicated by increased signal intensity in ^{1}H-^{13}C HSQC spectra. The use of PBS pH 7.4 also led to a faster more complete reduction of the spin-label using significantly lower concentrations of $Na_2S_2O_4$.

Successful collection of an oxidized and a reduced ^{1}H-^{13}C HSQC spectra from the same sample allowed for resonance intensities to be measured for a number of peaks.

7.3.3 CALCULATION OF INTENSITY BASED DISTANCES FOR CD14 BOUND SPIN-LABELED LIPID A

Calculation of the distance between individual lipid A's protons and the unpaired electron of the spin label were based on measurement of the intensities of the lipid A resonances in the presence of the oxidized spin-label, and again after reduction of the spin-label to its diamagnetic state (*178*). Collection of ^{1}H-^{13}C HSQC spectra in the oxidized and reduced state allowed the change in peak intensities between the two states to be quantified using NMRpipe (*162*). These intensities in turn are used in the following equation, where I_{osl} and I_{rsl} are the peak intensities of resonances in the oxidized and reduced states, and t is the total time during the insensitive nuclei enhanced by polarization transfer (INEPT) period of the HSQC pulse sequence.

$$\left(\frac{1}{T_2}\right)_{osl} - \left(\frac{1}{T_2}\right)_{rsl} = \frac{1}{t}\ln\left(\frac{I_{rsl}}{I_{osl}}\right) \qquad (1)$$

The value obtained for $(1/T_2)_{osl} - (1/T_2)_{rsl}$ using equation 1 was then used in equation 2,

$$\left(\frac{1}{T_2}\right)_{osl} - \left(\frac{1}{T_2}\right)_{rsl} = \frac{K}{r^6}\left(4\tau_c + \frac{3\tau_c}{\left(1+\omega_H^2\tau_c^2\right)}\right) \qquad (2)$$

in which τ_c is the rotational correlation time for CD14, ω_H is the Larmor frequency, r is the distance of the nucleus from the unpaired electron, and K is a compilation of constants related to spin properties of the system whose value is 1.23×10^{-32} cm^6s^{-2} (*178*).

In order to use equation 2, the value of rotational correlation time (τ_c) must be known. Because we lack direct NMR measurement of the τ_c for CD14, the Stokes equation, given below, was used to determine the value of τ_c (*187*).

$$\tau_C = \frac{4\pi\eta_w r_H^3}{(3k_B T)} \qquad (3)$$

Where η_w is the viscosity of the solvent, in this case the viscosity value of PBS pH 7.4 at 37 ºC was 0.713 mPa·s (*188*). *T* is the temperature, k_B is the Boltzmann constant, and r_H is the hydrodynamic radius of CD14 calculated using the equation given below (*187*).

$$r_H = \left[\frac{3\bar{V}M_r}{(4\pi N_A)}\right]^{1/3} + r_w \qquad (4)$$

The symbol $\bar{v}$ is the specific volume of the protein, assumed to be 0.73 cm^3/g, N_A is Avogadro's number, M_r is the molecular weight of the protein, and r_w is one half of the hydration shell, ~1.6Å.

The τ_C value calculated for CD14 using equation 3 is not as accurate as could be calculated for other proteins. This is because the equation is meant to be used to calculate the τ_C for proteins with spherical/ellipsoid shape, whereas CD14 does not have that shape. Calculation of τ_C using measurements of CD14's longitudinal relaxation time (T_1) would be more accurate, but the lack of CD14 assignments prevents the use of T_1 values to calculate τ_C. There is an additional source of error in the τ_C calculation that being the calculated value of r_H, though the error in this calculation is reduced due to the only unknown value being used for the hydration shell (r_w). An accurate hydrodynamic radius and even a value for τ_C could have been readily measured using a dynamic light scattering instrument, without the need for isotopically labeled proteins samples, but unfortunately one was not available within the time constraints needed to complete this work.

However, the use of these four equations allowed for the calculation of distances for each identifiable lipid A resonance, seen in the oxidized and reduced ^{1}H-^{13}C HSQC spectra, of sCD14 bound spin-labeled ^{13}C lipid A. The calculated distances are shown in **Table 2**, and **Figure 7.3** shows the lipid A atoms which correspond to the measured distances. The standard error of the mean was calculated to be 0.8 Å, and the sample standard deviation was 2.7 Å. Given the plausible level of error in the τ_C and r_H values the total error values of 3.5 Å, seem, realistic given the unknown level of error in the τ_C and r_H values.

Table 2: Intermolecular distances calculated for spin-labeled lipid A

Residue	Distance from spin-label (Å) (*±3.5 Å)*
C1	**9.8**
C4	**11.9**
C5	**10.6**
C6a	**12.1**
C6b	**14.6**
C1'	**10.4**
C4'	**10.3**
α4	**9.4**
α6	**9.2**
βI	**19.7**
βII	**11.5**
γIV	**9.6**
γVI	**9.9**

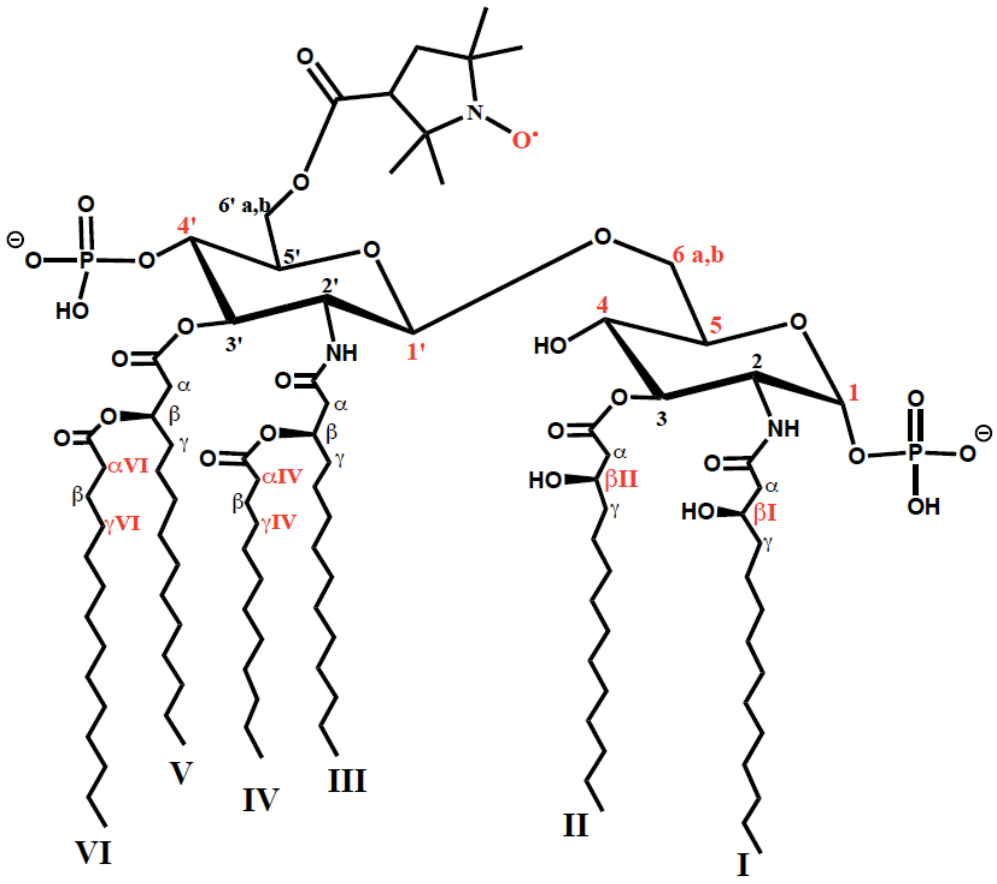


Figure 7.3: Spin-labeled lipid A schematic indicating atoms for which distances were determined.
Atoms labeled in red correlate to the atom names listed with distances from the spin-label's unpaired electron, in Table 2.

The calculated distances seem to agree with what would be expected for most of the lipid A atoms, such as the distances for C1, C4, C5, C6a, βI, and βII. However, some of the other resonances fall farther outside the anticipated distance ranges, estimated from our NOE-derived unbound lipid A structure. These particular distances could be plausible given the lack of a bound lipid A structure, using the calculated distances as restraints, as well as the inherent uncertainty in using speculated distance range estimates as the measure of feasibility. The residues whose calculated distances do not seem to fall within the estimated distance ranges are C6a, γIV, γVI', αIV, and αVI. The cause of these discrepancies is unknown at this time. While a structure of lipid A using these distances as restraints was not completed at the time of this writing, future generation of a bound lipid A structure could provide a firmer estimate of these distances. The extensive optimization and troubleshooting performed in this experiment has laid the foundation for the collection of high quality spin-labeled ligand-CD14 NMR data in a future investigation.

Application of spin-label derived distances to the production of a CD14 bound lipid A structure could allow our lab to generate a model structure of the CD14-lipid A complex. This is possible because CD14 does not undergo significant global conformational changes upon ligand binding. This allows a lipid A structure in the bound conformation to be docked into the homology model of truncated sCD14 to yield a model of the complex. Creation of a CD14-lipid A complex from the experimentally derived bound lipid A structure will give a considerably more accurate complex structure than one produced using only molecular dynamics simulation.

CHAPTER 8. CONCLUSIONS

The TLRs may be the first signaling step in the complex inflammatory signal cascade found in the innate immune system, but CD14's role in over-activating the inflammatory response has made studying its differential endotoxin recognition vitally important.

In the course of our investigations of CD14, we have demonstrated that the pattern recognition hypothesis, which stated that CD14 uses pathogen-associated molecular patterns to recognize endotoxin ligands, is well founded. This was revealed by the mapping and comparison of chemical shift changes in the HSQC spectra of ^{15}N labeled CD14 in the presence and absence of gram-negative and gram-positive endotoxin. The observation of changes to a common set of resonances with each endotoxin as well as distinct endotoxin specific changes proved that CD14's versatile differential ligand recognition abilities are based in the use of common as well as specific interactions to bind endotoxins.

The potential to produce specific antagonists that function to mitigate the inflammatory response upstream of the TLRs would be a tremendous benefit in the treatment of sepsis. By competing against the excessive amounts of endotoxin present in the host during sepsis, an antagonist acting on CD14 could slow the constant inflammatory signal being generated, dampening the inflammatory response. For this reason, a detailed NMR investigation of the structural features of Kdo_2-Lipid A's interactions with CD14 was undertaken. The result of this work was the first direct

observation and identification of the lipid A structural elements strongly affected by CD14 binding. Identification of these features lays the groundwork for the future design of an antagonist.

The complementary study of isotopically labeled LTA's interactions with CD14 provided further insight into the nature of pattern recognition by CD14. This demonstrated how the interaction of CD14 with similar/common structural features of endotoxins, such as the acyl chains, could contribute to the broad recognition of endotoxin ligands by CD14.

The ability of CD14 to bind a wide range of diverse ligands is an impressive but perplexing attribute given CD14's lone binding site. As a result of investigating CD14's recognition of LPS and LTA, and again while determining the structural features of lipid A involved in interactions with CD14, dynamic changes in CD14 were continually revealed. Through the modulation of temperature and pH, we were able to use NMR to observe the broad scope of conformational states that some CD14 residues are able to sample. The capacity of CD14 to use dynamics to modulate which residues it uses in an interaction with a ligand clearly displays a level of structural versatility that is translated into its aptitude for recognizing and interacting with numerous endotoxin ligands. Based on this, we can hypothesize that ligands recognized by CD14 interact using a combination of hydrophobically driven interactions between its hydrophobic pocket and the acyl chains found on many endotoxin cell wall components, while also using groups of charged residues in its hydrophilic rim to make specific interactions with the polar sugar head groups common to many endotoxins. It is also plausible that ligands could

interact with CD14 primarily through electrostatic interactions with the hydrophilic rim. For example, dsRNA has many exposed phosphate groups, but has all its hydrophobic features sequestered within the core of the helix.

Each of these investigations has provided new insights into the structure and function of CD14, and has generated new data that could aid in the development of novel anti-sepsis therapies. Potential therapies could make use of the structural features identified as having strong interactions with CD14, such as the acyl chains, and phosphate groups, as the basis for the directed design of a potential antagonist to use in reducing the over-activated inflammatory response in cases of severe sepsis. A reduction in the inflammatory response would provide more options and more time to treat a patient's underlying illness, without the devastating damage caused by the domino effect of the inflammatory cascade. An example of this targeted design process is the synthetic TLR4 antagonist eritoran. Eritoran is a synthetic LPS, whose structure was designed based on the weakly antagonistic lipid A of *Rhodobacter sphaeroides* (*189*). Currently in phase II trials, eritoran has been shown to block some of the effects of endotoxin in humans, illistrating the value of structural data on the binding and recognition of endotoxin by the innate immune system.

REFERENCES

1. Martin, G. S., Mannino, D. M., Eaton, S., and Moss, M. (2003) The epidemiology of sepsis in the United States from 1979 through 2000, *New England Journal of Medicine 348*, 1546-1554.
2. Angus, D. C., Linde-Zwirble, W. T., Lidicker, J., Clermont, G., Carcillo, J., and Pinsky, M. R. (2001) Epidemiology of severe sepsis in the United States: Analysis of incidence, outcome, and associated costs of care, *Critical Care Medicine 29*, 1303-1310.
3. Cohen, J. (2002) The immunopathogenesis of sepsis, *Nature 420*, 885-891.
4. Wisplinghoff, H., Bischoff, T., Tallent, S. M., Seifert, H., Wenzel, R. P., and Edmond, M. B. (2004) Nosocomial bloodstream infections in US hospitals: Analysis of 24,179 cases from a prospective nationwide surveillance study, *Clin. Infect. Dis. 39*, 309-317.
5. Levy, M. M., Dellinger, R. P., Townsend, S. R., Linde-Zwirble, W. T., Marshall, J. C., Bion, J., Schorr, C., Artigas, A., Ramsay, G., Beale, R., Parker, M. M., Gerlach, H., Reinhart, K., Silva, E., Harvey, M., Regan, S., and Angus, D. C. (2010) The Surviving Sepsis Campaign: results of an international guideline-based performance improvement program targeting severe sepsis, *Intensive Care Medicine 36*, 222-231.
6. Bernard, G. R., Vincent, J. L., Laterre, P., LaRosa, S. P., Dhainaut, J. F., Lopez-Rodriguez, A., Steingrub, J. S., Garber, G. E., Helterbrand, J. D., Ely, E. W., Fisher, C. J., and Protei, R. H. A. (2001) Efficacy and safety of recombinant human activated protein C for severe sepsis., *New England Journal of Medicine 344*, 699-709.
7. Levy, M. M., Fink, M. P., Marshall, J. C., Abraham, E., Angus, D., Cook, D., Cohen, J., Opal, S. M., Vincent, J. L., and Ramsay, G. (2003) 2001 SCCM/ESICM/ACCP/ATS/SIS International Sepsis Definitions Conference, *Crit Care Med 31*, 1250-1256.
8. Choy, E. H., and Panayi, G. S. (2001) Cytokine pathways and joint inflammation in rheumatoid arthritis, *N Engl J Med 344*, 907-916.
9. Libby, P., Ridker, P. M., and Maseri, A. (2002) Inflammation and atherosclerosis, *Circulation 105*, 1135-1143.
10. Gan, W. Q., Man, S. F., Senthilselvan, A., and Sin, D. D. (2004) Association between chronic obstructive pulmonary disease and systemic inflammation: a systematic review and a meta-analysis, *Thorax 59*, 574-580.
11. Xu, H., Barnes, G. T., Yang, Q., Tan, G., Yang, D., Chou, C. J., Sole, J., Nichols, A., Ross, J. S., Tartaglia, L. A., and Chen, H. (2003) Chronic inflammation in fat plays a crucial role in the development of obesity-related insulin resistance, *J Clin Invest 112*, 1821-1830.
12. Bas, S., Gauthier, B. R., Spenato, U., Stingelin, S., and Gabay, C. (2004) CD14 is an acute-phase protein, *J. Immunol. 172*, 4470-4479.

13. Van Amersfoort, E. S., Van Berkel, T. J., and Kuiper, J. (2003) Receptors, mediators, and mechanisms involved in bacterial sepsis and septic shock, *Clin Microbiol Rev 16*, 379-414.
14. Dellinger, R. P., Levy, M. M., Carlet, J. M., Bion, J., Parker, M. M., Jaeschke, R., Reinhart, K., Angus, D. C., Brun-Buisson, C., Beale, R., Calandra, T., Dhainaut, J. F., Gerlach, H., Harvey, M., Marini, J. J., Marshall, J., Ranieri, M., Ramsay, G., Sevransky, J., Thompson, B. T., Townsend, S., Vender, J. S., Zimmerman, J. L., Vincent, J. L., and Campai, I. S. S. (2008) Surviving Sepsis Campaign: International guidelines for management of severe sepsis and septic shock: 2008, *Critical Care Medicine 36*, 296-327.
15. Wenzel, R. P. (2002) Treating sepsis, *N Engl J Med 347*, 966-967.
16. Lopez-Bojorquez, L. N., Dehesa, A. Z., and Reyes-Teran, G. (2004) Molecular mechanisms involved in the pathogenesis of septic shock, *Arch. Med. Res. 35*, 465-479.
17. Pugin, J., Heumann, D., Tomasz, A., Kravchenko, V. V., Akamatsu, Y., Nishijima, M., Glauser, M. P., Tobias, P. S., and Ulevitch, R. J. (1994) CD14 is a pattern recognition receptor, *Immunity 1*, 509-516.
18. Schumann, R. R., Leong, S. R., Flaggs, G. W., Gray, P. W., Wright, S. D., Mathison, J. C., Tobias, P. S., and Ulevitch, R. J. (1990) Structure and function of lipopolysaccharide binding protein, *Science 249*, 1429-1431.
19. Akira, S., and Takeda, K. (2004) Toll-like receptor signalling, *Nature Reviews Immunology 4*, 499-511.
20. Brightbill, H. D., and Modlin, R. L. (2000) Toll-like receptors: molecular mechanisms of the mammalian immune response, *Immunology 101*, 1-10.
21. Hailman, E., Vasselon, T., Kelley, M., Busse, L. A., Hu, M. C. T., Lichenstein, H. S., Detmers, P. A., and Wright, S. D. (1996) Stimulation of macrophages and neutrophils by complexes of lipopolysaccharide and soluble CD14, *J. Immunol. 156*, 4384-4390.
22. Akira, S., Uematsu, S., and Takeuchi, O. (2006) Pathogen recognition and innate immunity, *Cell 124*, 783-801.
23. Takeuchi, O., Hoshino, K., Kawai, T., Sanjo, H., Takada, H., Ogawa, T., Takeda, K., and Akira, S. (1999) Differential roles of TLR2 and TLR4 in recognition of gram-negative and gram-positive bacterial cell wall components, *Immunity 11*, 443-451.
24. Beutler, B., Du, X., and Poltorak, A. (2001) Identification of Toll-like receptor 4 (Tlr4) as the sole conduit for LPS signal transduction: genetic and evolutionary studies, *J Endotoxin Res 7*, 277-280.
25. Schroder, N. W. J., Morath, S., Alexander, C., Hamann, L., Hartung, T., Zahringer, U., Gobel, U. B., Weber, J. R., and Schumann, R. R. (2003) Lipoteichoic acid (LTA) of *Streptococcus pneumoniae* and *Staphylococcus aureus* activates immune cells via toll-like receptor (TLR)-2, lipopolysaccharide-binding protein (LBP), and CD14, whereas TLR-4 and MD-2 are not involved, *J. Biol. Chem. 278*, 15587-15594.

26. Farhat, K., Riekenberg, S., Heine, H., Debarry, J., Lang, R., Mages, J., Buwitt-Beckmann, U., Roschmann, K., Jung, G., Wiesmuller, K. H., and Ulmer, A. J. (2008) Heterodimerization of TLR2 with TLR1 or TLR6 expands the ligand spectrum but does not lead to differential signaling, *J Leukoc Biol 83*, 692-701.
27. Takeuchi, O., Kawai, T., Muhlradt, P. F., Morr, M., Radolf, J. D., Zychlinsky, A., Takeda, K., and Akira, S. (2001) Discrimination of bacterial lipoproteins by Toll-like receptor 6, *Int Immunol 13*, 933-940.
28. Shin, H. J., Lee, H., Park, J. D., Hyun, H. C., Sohn, H. O., Lee, D. W., and Kim, Y. S. (2007) Kinetics of binding of LPS to recombinant CD14, TLR4, and MD-2 proteins, *Mol Cells 24*, 119-124.
29. Jin, M. S., Kim, S. E., Heo, J. Y., Lee, M. E., Kim, H. M., Paik, S. G., Lee, H., and Lee, J. O. (2007) Crystal structure of the TLR1-TLR2 heterodimer induced by binding of a tri-acylated lipopeptide, *Cell 130*, 1071-1082.
30. Ozinsky, A., Underhill, D. M., Fontenot, J. D., Hajjar, A. M., Smith, K. D., Wilson, C. B., Schroeder, L., and Aderem, A. (2000) The repertoire for pattern recognition of pathogens by the innate immune system is defined by cooperation between Toll-like receptors, *Proceedings of the National Academy of Sciences of the United States of America 97*, 13766-13771.
31. Takeda, K., and Akira, S. (2004) TLR signaling pathways, *Semin Immunol 16*, 3-9.
32. Yamamoto, M., Sato, S., Hemmi, H., Sanjo, H., Uematsu, S., Kaisho, T., Hoshino, K., Takeuchi, O., Kobayashi, M., Fujita, T., Takeda, K., and Akira, S. (2002) Essential role for TIRAP in activation of the signalling cascade shared by TLR2 and TLR4, *Nature 420*, 324-329.
33. Slack, J. L., Schooley, K., Bonnert, T. P., Mitcham, J. L., Qwarnstrom, E. E., Sims, J. E., and Dower, S. K. (2000) Identification of two major sites in the type I interleukin-1 receptor cytoplasmic region responsible for coupling to pro-inflammatory signaling pathways, *J Biol Chem 275*, 4670-4678.
34. Kenny, E. F., and O'Neill, L. A. J. (2008) Signalling adaptors used by Toll-like receptors: An update, *Cytokine 43*, 342-349.
35. Schmitz, G., and Orso, E. (2002) CD14 signalling in lipid rafts: new ligands and co-receptors, *Curr Opin Lipidol 13*, 513-521.
36. Silipo, A., and Molinaro, A. (2010) The diversity of the core oligosaccharide in lipopolysaccharides, *Subcell Biochem 53*, 69-99.
37. Wang, X., and Quinn, P. J. (2010) Endotoxins: lipopolysaccharides of gram-negative bacteria, *Subcell Biochem 53*, 3-25.
38. Holst, O., Ulmer, A. J., Brade, H., Flad, H. D., and Rietschel, E. T. (1996) Biochemistry and cell biology of bacterial endotoxins, *FEMS Immunol Med Microbiol 16*, 83-104.
39. Wang, L., Wang, Q., and Reeves, P. R. (2010) The variation of O antigens in gram-negative bacteria, *Subcell Biochem 53*, 123-152.
40. Raetz, C. R., and Whitfield, C. (2002) Lipopolysaccharide endotoxins, *Annu Rev Biochem 71*, 635-700.

41. Qureshi, N., Takayama, K., Mascagni, P., Honovich, J., Wong, R., and Cotter, R. J. (1988) Complete structural determination of lipopolysaccharide obtained from deep rough mutant of Escherichia coli. Purification by high performance liquid chromatography and direct analysis by plasma desorption mass spectrometry, *J Biol Chem 263*, 11971-11976.
42. Galanos, C., Luderitz, O., Rietschel, E. T., Westphal, O., Brade, H., Brade, L., Freudenberg, M., Schade, U., Imoto, M., Yoshimura, H., Kusumoto, S., and Shiba, T. (1985) Synthetic and natural *Escherichia coli* free lipid A express identical endotoxic activities, *European Journal of Biochemistry 148*, 1-5.
43. Raetz, C. R. (1990) Biochemistry of endotoxins, *Annu Rev Biochem 59*, 129-170.
44. Brabetz, W., Muller-Loennies, S., Holst, O., and Brade, H. (1997) Deletion of the heptosyltransferase genes rfaC and rfaF in Escherichia coli K-12 results in an Re-type lipopolysaccharide with a high degree of 2-aminoethanol phosphate substitution, *Eur J Biochem 247*, 716-724.
45. Flad, H. D., Loppnow, H., Rietschel, E. T., and Ulmer, A. J. (1993) Agonists and antagonists for lipopolysaccharide-induced cytokines, *Immunobiology 187*, 303-316.
46. Kitchens, R. L., Ulevitch, R. J., and Munford, R. S. (1992) Lipopolysaccharide (LPS) partial structures inhibit responses to LPS in a human macrophage cell line without inhibiting LPS uptake by a CD14-mediated pathway, *J Exp Med 176*, 485-494.
47. Galloway, S. M., and Raetz, C. R. (1990) A mutant of Escherichia coli defective in the first step of endotoxin biosynthesis, *J Biol Chem 265*, 6394-6402.
48. Morath, S., von Aulock, S., and Hartung, T. (2005) Structure/function relationships of lipoteichoic acids, *J Endotoxin Res 11*, 348-356.
49. Morath, S., Geyer, A., and Hartung, T. (2001) Structure-function relationship of cytokine induction by lipoteichoic acid from Staphylococcus aureus, *J. Exp. Med. 193*, 393-397.
50. Morath, S., Geyer, A., Spreitzer, I., Hermann, C., and Hartung, T. (2002) Structural decomposition and heterogeneity of commercial lipoteichoic acid preparations, *Infection and Immunity 70*, 938-944.
51. Travassos, L. H., Girardin, S. E., Philpott, D. J., Blanot, D., Nahori, M. A., Werts, C., and Boneca, I. G. (2004) Toll-like receptor 2-dependent bacterial sensing does not occur via peptidoglycan recognition, *Embo Reports 5*, 1000-1006.
52. Schwandner, R., Dziarski, R., Wesche, H., Rothe, M., and Kirschning, C. J. (1999) Peptidoglycan- and lipoteichoic acid-induced cell activation is mediated by toll-like receptor 2, *J. Biol. Chem. 274*, 17406-17409.
53. Kimbrell, M. R., Warshakoon, H., Cromer, J. R., Malladi, S., Hood, J. D., Balakrishna, R., Scholdberg, T. A., and David, S. A. (2008) Comparison of the immunostimulatory and proinflammatory activities of candidate Gram-positive endotoxins, lipoteichoic acid, peptidoglycan, and lipopeptides, in murine and human cells, *Immunol Lett 118*, 132-141.
54. Inamura, S., Fujimoto, Y., Kawasaki, A., Shiokawa, Z., Woelk, E., Heine, H., Lindner, B., Inohara, N., Kusumoto, S., and Fukase, K. (2006) Synthesis of

peptidoglycan fragments and evaluation of their biological activity, *Org Biomol Chem 4*, 232-242.
55. Deininger, S., Stadelmaier, A., von Aulock, S., Morath, S., Schmidt, R. R., and Hartung, T. (2003) Definition of structural prerequisites for lipoteichoic acid-inducible cytokine induction by synthetic derivatives, *J Immunol 170*, 4134-4138.
56. Morath, S., Stadelmaier, A., Geyer, A., Schmidt, R. R., and Hartung, T. (2002) Synthetic lipoteichoic acid from Staphylococcus aureus is a potent stimulus of cytokine release, *J. Exp. Med. 195*, 1635-1640.
57. Wright, S. D., Ramos, R. A., Tobias, P. S., Ulevitch, R. J., and Mathison, J. C. (1990) CD14, a receptor for complexes of lipopolysaccharide (LPS) and LPS binding protein, *Science 249*, 1431-1433.
58. Seydel, U., Schromm, A. B., Blunck, R., and Brandenburg, K. (2000) Chemical structure, molecular conformation, and bioactivity of endotoxins, *Cd14 in the Inflammatory Response 74*, 5-24.
59. Haziot, A., Ferrero, E., Kontgen, F., Hijiya, N., Yamamoto, S., Silver, J., Stewart, C. L., and Goyert, S. M. (1996) Resistance to endotoxin shock and reduced dissemination of gram-negative bacteria in CD14-deficient mice, *Immunity 4*, 407-414.
60. Haziot, A., Chen, S., Ferrero, E., Low, M. G., Silber, R., and Goyert, S. M. (1988) The Monocyte Differentiation Antigen, Cd14, Is Anchored to the Cell-Membrane by a Phosphatidylinositol Linkage, *J. Immunol. 141*, 547-552.
61. Bazil, V., Baudys, M., Hilgert, I., Stefanova, I., Low, M. G., Zbrozek, J., and Horejsi, V. (1989) Structural relationship between the soluble and membrane-bound forms of human monocyte surface glycoprotein CD14, *Mol Immunol 26*, 657-662.
62. Bazil, V., and Strominger, J. L. (1991) SHEDDING AS A MECHANISM OF DOWN-MODULATION OF CD14 ON STIMULATED HUMAN MONOCYTES, *J. Immunol. 147*, 1567-1574.
63. Frey, E. A., Miller, D. S., Jahr, T. G., Sundan, A., Bazil, V., Espevik, T., Finlay, B. B., and Wright, S. D. (1992) Soluble CD14 participates in the response of cells to lipopolysaccharide, *J. Exp. Med. 176*, 1665-1671.
64. Burgmann, H., Winkler, S., Locker, G. J., Presterl, E., Laczika, K., Staudinger, T., Knapp, S., Thalhammer, F., Wenisch, C., ZedwitzLiebenstein, K., Frass, M., and Graninger, W. (1996) Increased serum concentration of soluble CD14 is a prognostic marker in gram-positive sepsis, *Clin. Immunol. Immunopathol. 80*, 307-310.
65. Pugin, J., Kravchenko, V. V., Lee, J. D., Kline, L., Ulevitch, R. J., and Tobias, P. S. (1998) Cell activation mediated by glycosylphosphatidylinositol-anchored or transmembrane forms of CD14, *Infect Immun 66*, 1174-1180.
66. Triantafilou, M., Manukyan, M., Mackie, A., Morath, S., Hartung, T., Heine, H., and Triantafilou, K. (2004) Lipoteichoic acid and Toll-like receptor 2 internalization and targeting to the Golgi are lipid raft-dependent, *J. Biol. Chem. 279*, 40882-40889.

67. Pugin, J., Schurer-Maly, C. C., Leturcq, D., Moriarty, A., Ulevitch, R. J., and Tobias, P. S. (1993) Lipopolysaccharide activation of human endothelial and epithelial cells is mediated by lipopolysaccharide-binding protein and soluble CD14, *Proc Natl Acad Sci U S A 90*, 2744-2748.
68. Verbon, A. (2002) Role of CD14 in host response to infection, *Curr. Med. Chem.: Anti-Inflammatory Anti-Allergy Agents 1*, 205-210.
69. Lloyd-Jones, K. L., Kelly, M. M., and Kubes, P. (2008) Varying importance of soluble and membrane CD14 in endothelial detection of lipopolysaccharide, *J Immunol 181*, 1446-1453.
70. Juan, T. S. C., Kelley, M. J., Johnson, D. A., Busse, L. A., Hailman, E., Wright, S. D., and Lichenstein, H. S. (1995) Soluble CD14 Truncated at Amino Acid 152 Binds Lipopolysaccharide (LPS) and Enables Cellular Response to LPS, *J. Biol. Chem. 270*, 1382-1387.
71. Bell, J. K., Mullen, G. E., Leifer, C. A., Mazzoni, A., Davies, D. R., and Segal, D. M. (2003) Leucine-rich repeats and pathogen recognition in Toll-like receptors, *Trends Immunol 24*, 528-533.
72. Kobe, B., and Kajava, A. V. (2001) The leucine-rich repeat as a protein recognition motif, *Curr Opin Struct Biol 11*, 725-732.
73. Ferrero, E., Hsieh, C. L., Francke, U., and Goyert, S. M. (1990) CD14 is a member of the family of leucine-rich proteins and is encoded by a gene syntenic with multiple receptor genes, *J Immunol 145*, 331-336.
74. Stelter, F., Pfister, M., Bernheiden, M., Jack, R. S., Bufler, P., Engelmann, H., and Schutt, C. (1996) The myeloid differentiation antigen CD14 is N- and O-glycosylated - Contribution of N-linked glycosylation to different soluble CD14 isoforms, *European Journal of Biochemistry 236*, 457-464.
75. Kim, J. I., Lee, C. J., Jin, M. S., Lee, C. H., Paik, S. G., Lee, H., and Lee, J. O. (2005) Crystal structure of CD14 and its implications for lipopolysaccharide signaling, *J. Biol. Chem. 280*, 11347-11351.
76. Evdokimov, A. G., Anderson, D. E., Routzahn, K. M., and Waugh, D. S. (2001) Unusual molecular architecture of the Yersinia pestis cytotoxin YopM: a leucine-rich repeat protein with the shortest repeating unit, *J Mol Biol 312*, 807-821.
77. Bell, J. K., Botos, I., Hall, P. R., Askins, J., Shiloach, J., Segal, D. M., and Davies, D. R. (2005) The molecular structure of the Toll-like receptor 3 ligand-binding domain, *Proc Natl Acad Sci U S A 102*, 10976-10980.
78. Kim, H. M., Park, B. S., Kim, J. I., Kim, S. E., Lee, J., Oh, S. C., Enkhbayar, P., Matsushima, N., Lee, H., Yoo, O. J., and Lee, J. O. (2007) Crystal structure of the TLR4-MD-2 complex with bound endotoxin antagonist eritoran, *Cell 130*, 906-917.
79. Viriyakosol, S., and Kirkland, T. N. (1996) The N-terminal half of membrane CD14 is a functional cellular lipopolysaccharide receptor, *Infect Immun 64*, 653-656.
80. Liu, L., Botos, I., Wang, Y., Leonard, J. N., Shiloach, J., Segal, D. M., and Davies, D. R. (2008) Structural basis of toll-like receptor 3 signaling with double-stranded RNA, *Science 320*, 379-381.

81. Latz, E., Visintin, A., Lien, E., Fitzgerald, K. A., Monks, B. G., Kurt-Jones, E. A., Golenbock, D. T., and Espevik, T. (2002) Lipopolysaccharide rapidly traffics to and from the Golgi apparatus with the toll-like receptor 4-MD-2-CD14 complex in a process that is distinct from the initiation of signal transduction, *J Biol Chem 277*, 47834-47843.
82. Bella, J., Hindle, K. L., McEwan, P. A., and Lovell, S. C. (2008) The leucine-rich repeat structure, *Cell Mol Life Sci 65*, 2307-2333.
83. Choe, J., Kelker, M. S., and Wilson, I. A. (2005) Crystal structure of human toll-like receptor 3 (TLR3) ectodomain, *Science 309*, 581-585.
84. Park, B. S., Song, D. H., Kim, H. M., Choi, B. S., Lee, H., and Lee, J. O. (2009) The structural basis of lipopolysaccharide recognition by the TLR4-MD-2 complex, *Nature 458*, 1191-U1130.
85. Janeway, C. A., and Medzhitov, R. (2002) Innate immune recognition, *Annual Review of Immunology 20*, 197-216.
86. Thompson, A. J., and Locarnini, S. A. (2007) Toll-like receptors, RIG-I-like RNA helicases and the antiviral innate immune response, *Immunol Cell Biol 85*, 435-445.
87. Zipfel, C. (2008) Pattern-recognition receptors in plant innate immunity, *Curr Opin Immunol 20*, 10-16.
88. Zipfel, C., and Felix, G. (2005) Plants and animals: a different taste for microbes?, *Curr Opin Plant Biol 8*, 353-360.
89. Mizel, S. B., West, A. P., and Hantgan, R. R. (2003) Identification of a sequence in human toll-like receptor 5 required for the binding of Gram-negative flagellin, *J Biol Chem 278*, 23624-23629.
90. Jacchieri, S. G., Torquato, R., and Brentani, R. R. (2003) Structural study of binding of flagellin by Toll-like receptor 5, *J Bacteriol 185*, 4243-4247.
91. Andersen-Nissen, E., Smith, K. D., Bonneau, R., Strong, R. K., and Aderem, A. (2007) A conserved surface on Toll-like receptor 5 recognizes bacterial flagellin, *J Exp Med 204*, 393-403.
92. Bauer, Z., Gomez-Gomez, L., Boller, T., and Felix, G. (2001) Sensitivity of different ecotypes and mutants of Arabidopsis thaliana toward the bacterial elicitor flagellin correlates with the presence of receptor-binding sites, *J Biol Chem 276*, 45669-45676.
93. Cunningham, M. D., Shapiro, R. A., Seachord, C., Ratcliffe, K., Cassiano, L., and Darveau, R. P. (2000) CD14 employs hydrophilic regions to "capture" lipopolysaccharides, *J. Immunol. 164*, 3255-3263.
94. Shapiro, R. A., Cunningham, M. D., Ratcliffe, K., Seachord, C., Blake, J., Bajorath, J., Aruffo, A., and Darveau, R. P. (1997) Identification of CD14 residues involved in specific lipopolysaccharide recognition, *Infect Immun 65*, 293-297.
95. Nakata, T., Yasuda, M., Fujita, M., Kataoka, H., Kiura, K., Sano, H., and Shibata, K. (2006) CD14 directly binds to triacylated lipopeptides and facilitates recognition of the lipopeptides by the receptor complex of Toll-like receptors 2 and 1 without binding to the complex, *Cell Microbiol 8*, 1899-1909.

96. Triantafilou, M., Gamper, F. G., Haston, R. M., Mouratis, M. A., Morath, S., Hartung, T., and Triantafilou, K. (2006) Membrane sorting of toll-like receptor (TLR)-2/6 and TLR2/1 heterodimers at the cell surface determines heterotypic associations with CD36 and intracellular targeting, *J Biol Chem 281*, 31002-31011.
97. Dziarski, R., Tapping, R. I., and Tobias, P. S. (1998) Binding of bacterial peptidoglycan to CD14, *J. Biol. Chem. 273*, 8680-8690.
98. Elass, E., Coddeville, B., Guerardel, Y., Kremer, L., Maes, E., Mazurier, J., and Legrand, D. (2007) Identification by surface plasmon resonance of the mycobacterial lipomannan and lipoarabinomannan domains involved in binding to CD14 and LPS-binding protein, *FEBS Lett 581*, 1383-1390.
99. Brodskyn, C., Patricio, J., Oliveira, R., Lobo, L., Arnholdt, A., Mendonca-Previato, L., Barral, A., and Barral-Netto, M. (2002) Glycoinositolphospholipids from Trypanosoma cruzi interfere with macrophages and dendritic cell responses, *Infect Immun 70*, 3736-3743.
100. Schroder, N. W., Opitz, B., Lamping, N., Michelsen, K. S., Zahringer, U., Gobel, U. B., and Schumann, R. R. (2000) Involvement of lipopolysaccharide binding protein, CD14, and Toll-like receptors in the initiation of innate immune responses by Treponema glycolipids, *J Immunol 165*, 2683-2693.
101. Levitz, S. M. (2004) Interactions of Toll-like receptors with fungi, *Microbes Infect 6*, 1351-1355.
102. Kirkland, T. N., Finley, F., Leturcq, D., Moriarty, A., Lee, J. D., Ulevitch, R. J., and Tobias, P. S. (1993) Analysis of lipopolysaccharide binding by CD14, *J. Biol. Chem. 268*, 24818-24823.
103. Cunningham, M. D., Seachord, C., Ratcliffe, K., Bainbridge, B., Aruffo, A., and Darveau, R. P. (1996) Helicobacter pylori and Porphyromonas gingivalis lipopolysaccharides are poorly transferred to recombinant soluble CD14, *Infect Immun 64*, 3601-3608.
104. Lee, H. K., Dunzendorfer, S., Soldau, K., and Tobias, P. S. (2006) Double-stranded RNA-mediated TLR3 activation is enhanced by CD14, *Immunity 24*, 153-163.
105. Kurt-Jones, E. A., Popova, L., Kwinn, L., Haynes, L. M., Jones, L. P., Tripp, R. A., Walsh, E. E., Freeman, M. W., Golenbock, D. T., Anderson, L. J., and Finberg, R. W. (2000) Pattern recognition receptors TLR4 and CD14 mediate response to respiratory syncytial virus, *Nat Immunol 1*, 398-401.
106. Kol, A., Lichtman, A. H., Finberg, R. W., Libby, P., and Kurt-Jones, E. A. (2000) Cutting edge: heat shock protein (HSP) 60 activates the innate immune response: CD14 is an essential receptor for HSP60 activation of mononuclear cells, *J Immunol 164*, 13-17.
107. Viriyakosol, S., and Kirkland, T. N. (1995) A region of human CD14 required for lipopolysaccharide binding, *J Biol Chem 270*, 361-368.
108. McGinley, M. D., Narhi, L. O., Kelley, M. J., Davy, E., Robinson, J., Rohde, M. F., Wright, S. D., and Lichenstein, H. S. (1995) CD14: Physical Properties and

Identification of an Exposed Site That Is Protected by Lipopolysaccharide, *J. Biol. Chem. 270*, 5213-5218.
109. Juan, T. S. C., Hailman, E., Kelley, M. J., Busse, L. A., Davy, E., Empig, C. J., Narhi, L. O., Wright, S. D., and Lichenstein, H. S. (1995) Identification of a Lipopolysaccharide Binding Domain in CD14 between Amino Acids 57 and 64, *J. Biol. Chem. 270*, 5219-5224.
110. Stelter, F., Bernheiden, M., Menzel, R., Jack, R. S., Witt, S., Fan, X. L., Pfister, M., and Schutt, C. (1997) Mutation of amino acids 39-44 of human CD14 abrogates binding of lipopolysaccharide and *Escherichia coli*, *European Journal of Biochemistry 243*, 100-109.
111. Voss, S., Welte, S., Fotin-Mleczek, M., Fischer, R., Ulmer, A. J., Jung, G., Wiesmuller, K. H., and Brock, R. (2006) A CD14 domain with lipopolysaccharide-binding and -neutralizing activity, *Chembiochem 7*, 275-286.
112. Means, T. K., Lien, E., Yoshimura, A., Wang, S., Golenbock, D. T., and Fenton, M. J. (1999) The CD14 ligands lipoarabinomannan and lipopolysaccharide differ in their requirement for Toll-like receptors, *J Immunol 163*, 6748-6755.
113. Campos, M. A., Almeida, I. C., Takeuchi, O., Akira, S., Valente, E. P., Procopio, D. O., Travassos, L. R., Smith, J. A., Golenbock, D. T., and Gazzinelli, R. T. (2001) Activation of Toll-like receptor-2 by glycosylphosphatidylinositol anchors from a protozoan parasite, *J Immunol 167*, 416-423.
114. Brandenburg, K., and Wiese, A. (2004) Endotoxins: relationships between structure, function, and activity, *Curr Top Med Chem 4*, 1127-1146.
115. Seydel, U., Oikawa, M., Fukase, K., Kusumoto, S., and Brandenburg, K. (2000) Intrinsic conformation of lipid A is responsible for agonistic and antagonistic activity, *European Journal of Biochemistry 267*, 3032-3039.
116. Sugiyama, T., and Wright, S. D. (2001) Soluble CD14 mediates efflux of phospholipids from cells, *J. Immunol. 166*, 826-831.
117. Gregory, C. D. (2000) CD14-dependent clearance of apoptotic cells: relevance to the immune system, *Curr. Opin. Immunol. 12*, 27-34.
118. Otting, G. (1993) Experimental NMR techniques for studies of protein-ligand interactions, *Curr. Opin. Struct. Biol. 3*, 760-768.
119. Garcia-Mayoral, M. F., Perez-Canadillas, J. M., Santoro, J., Ibarra-Molero, B., Sanchez-Ruiz, J. M., Lacadena, J., Martinez del Pozo, A., Gavilanes, J. G., Rico, M., and Bruix, M. (2003) Dissecting structural and electrostatic interactions of charged groups in alpha-sarcin. An NMR study of some mutants involving the catalytic residues, *Biochemistry 42*, 13122-13133.
120. Grinna, L. S., and Tschopp, J. F. (1989) Size Distribution and General Structural Features of N-Linked Oligosaccharides from the Methylotrophic Yeast, Pichia-Pastoris, *Yeast 5*, 107-115.
121. Meng, J., Parroche, P., Golenbock, D. T., and McKnight, C. J. (2008) The differential impact of disulfide bonds and N-linked glycosylation on the stability and function of CD14, *J Biol Chem 283*, 3376-3384.
122. Raetz, C. R. H., Garrett, T. A., Reynolds, C. M., Shaw, W. A., Moore, J. D., Smith, D. C., Ribeiro, A. A., Murphy, R. C., Ulevitch, R. J., Fearns, C., Reichart,

D., Glass, C. K., Benner, C., Subramaniam, S., Harkewicz, R., Bowers-Gentry, R. C., Buczynski, M. W., Cooper, J. A., Deems, R. A., and Dennis, E. A. (2006) Kdo(2)-Lipid A of *Escherichia coli*, a defined endotoxin that activates macrophages via TLR-4, *Journal of Lipid Research 47*, 1097-1111.

123. Shnyra, A., and Lindberg, A. A. (1995) Scavenger receptor pathway for lipopolysaccharide binding to Kupffer and endothelial liver cells in vitro, *Infection and Immunity 63*, 865-873.
124. Reynolds, C. M., and Raetz, C. R. (2009) Replacement of lipopolysaccharide with free lipid A molecules in Escherichia coli mutants lacking all core sugars, *Biochemistry 48*, 9627-9640.
125. Brade, L., Rietschel, E. T., Kusumoto, S., Shiba, T., and Brade, H. (1986) Immunogenicity and antigenicity of synthetic Escherichia coli lipid A, *Infect Immun 51*, 110-114.
126. Loppnow, H., Brade, H., Durrbaum, I., Dinarello, C. A., Kusumoto, S., Rietschel, E. T., and Flad, H. D. (1989) IL-1 Induction-capacity of defined lipopolysaccharide partial structures, *J. Immunol. 142*, 3229-3238.
127. Wu, S. X., and Letchworth, G. J. (2004) High efficiency transformation by electroporation of Pichia pastoris pretreated with lithium acetate and dithiothreitol, *Biotechniques 36*, 152-154.
128. De Backer, M. D., Maes, D., Vandoninck, S., Logghe, M., Contreras, R., and Luyten, W. H. M. L. (1999) Transformation of Candida albicans by electroporation, *Yeast 15*, 1609-1618.
129. Galanos, C., Luderitz, O., and Westphal, O. (1969) A New Method for the Extraction of R Lipopolysaccharides, *European Journal of Biochemistry 9*, 245-249.
130. Perdomo, R., and Montero, V. (2006) Purification of *E. coli* 055:B5 lipopolysaccharides by size exclusion chromatography, *Biotecnología Aplicada 23*, 124-129.
131. Fischer, W. (1990) Purification and fractionation of lipopolysaccharide from gram-negative bacteria by hydrophobic interaction chromatography, *Eur J Biochem 194*, 655-661.
132. Kiang, J., Szu, S. S. C., Wang, L. X., Tang, M., and Lee, Y. C. (1997) Determination of 2-keto-3-deoxyoctulosonic acid (KDO) with high-performance anion-exchange chromatography (HPAEC): Survey of stability of KDO and optimal hydrolytic conditions, *Anal. Biochem. 245*, 97-101.
133. Kanipes, M. I., Lin, S., Cotter, R. J., and Raetz, C. R. (2001) Ca2+-induced phosphoethanolamine transfer to the outer 3-deoxy-D-manno-octulosonic acid moiety of Escherichia coli lipopolysaccharide. A novel membrane enzyme dependent upon phosphatidylethanolamine, *J Biol Chem 276*, 1156-1163.
134. Juan, T. S. C., Hailman, E., Kelley, M. J., Wright, S. D., and Lichenstein, H. S. (1995) Identification of a Domain in Soluble CD14 Essential for Lipopolysaccharide (LPS) Signaling but Not LPS Binding *J. Biol. Chem. 270*, 17237-17242.

135. Majerle, A., Kidric, J., and Jerala, R. (1999) Expression and refolding of functional fragments of the human lipopolysaccharide receptor CD14 in *Escherichia coli* and *Pichia pastoris*, *Protein Expression and Purification 17*, 96-104.
136. Guha, M., and Mackman, N. (2001) LPS induction of gene expression in human monocytes, *Cellular Signalling 13*, 85-94.
137. Nomura, S., Inamori, K., Muta, T., Yamazaki, S., Sunakawa, Y., Iwanaga, S., and Takeshige, K. (2003) Purification and characterization of human soluble CD14 expressed in *Pichia pastoris*, *Protein Expression and Purification 28*, 310-320.
138. Dziarski, R., Ulmer, A. J., and Gupta, D. (2000) Interactions of CD14 with components of gram-positive bacteria, in *Cd14 in the Inflammatory Response*, pp 83-107.
139. Cleveland, M. G., Gorham, J. D., Murphy, T. L., Tuomanen, E., and Murphy, K. M. (1996) Lipoteichoic acid preparations of grain-positive bacteria induce interleukin-12 through a CD14-dependent pathway, *Infection and Immunity 64*, 1906-1912.
140. Weidemann, B., Brade, H., Rietschel, E. T., Dziarski, R., Bazil, V., Kusumoto, S., Flad, H. D., and Ulmer, A. J. (1994) Soluble peptidoglycan-induced monokine production can be blocked by anti-CD14 monoclonal antibodies and by lipid A partial structures, *Infection and Immunity 62*, 4709-4715.
141. Delude, R. L., Savedra, R., Zhao, H. L., Thieringer, R., Yamamoto, S., Fenton, M. J., and Golenbock, D. T. (1995) CD14 enhances cellular responses to endotoxin without imparting ligand-specific recognition, *Proceedings of the National Academy of Sciences of the United States of America 92*, 9288-9292.
142. Yu, B., and Wright, S. D. (1996) Catalytic properties of lipopolysaccharide (LPS) binding protein - Transfer of LPS to soluble CD14, *J. Biol. Chem. 271*, 4100-4105.
143. Weigelt, J. (1998) Single scan, sensitivity- and gradient-enhanced TROSY for multidimensional NMR experiments, *Journal of the American Chemical Society 120*, 10778-10779.
144. Li, H., Nooh, M. M., Kotb, M., and Re, F. (2008) Commercial peptidoglycan preparations are contaminated with superantigen-like activity that stimulates IL-17 production, *J Leukoc Biol 83*, 409-418.
145. Girardin, S. E., Boneca, I. G., Viala, J., Chamaillard, M., Labigne, A., Thomas, G., Philpott, D. J., and Sansonetti, P. J. (2003) Nod2 is a general sensor of peptidoglycan through muramyl dipeptide (MDP) detection, *J Biol Chem 278*, 8869-8872.
146. Dziarski, R., and Gupta, D. (2005) Peptidoglycan recognition in innate immunity, *Journal of Endotoxin Research 11*, 304-310.
147. Anas, A., van der Poll, T., and de Vos, A. F. (2010) Role of CD14 in lung inflammation and infection, *Crit Care 14*, 209.
148. Golenbock, D. T., Hampton, R. Y., Qureshi, N., Takayama, K., and Raetz, C. R. H. (1991) Lipid-A-like molecules that antagonize the effects of endotoxins on human monocytes, *J. Biol. Chem. 266*, 19490-19498.

149. Schromm, A. B., Brandenburg, K., Loppnow, H., Moran, A. P., Koch, M. H. J., Rietschel, E. T., and Seydel, U. (2000) Biological activities of lipopolysaccharides are determined by the shape of their lipid A portion, *European Journal of Biochemistry 267*, 2008-2013.
150. Schromm, A. B., Brandenburg, K., Loppnow, H., Zahringer, U., Rietschel, E. T., Carroll, S. F., Koch, M. H. J., Kusumoto, S., and Seydel, U. (1998) The charge of endotoxin molecules influences their conformation and IL-6-inducing capacity, *J. Immunol. 161*, 5464-5471.
151. Albright, S., Chen, B., Holbrook, K., and Jain, N. U. (2008) Solution NMR studies provide structural basis for endotoxin pattern recognition by the innate immune receptor CD14, *Biochemical and Biophysical Research Communications 368*, 231-237.
152. Ribeiro, A. A., Zhou, Z. M., and Raetz, C. R. H. (1999) Multi-dimensional NMR structural analyses of purified Lipid X and Lipid A (endotoxin), *Magnetic Resonance in Chemistry 37*, 620-630.
153. Gangloff, S. C., Zahringer, U., Blondin, C., Guenounou, M., Silver, J., and Goyert, S. M. (2005) Influence of CD14 on ligand interactions between lipopolysaccharide and its receptor complex, *J Immunol 175*, 3940-3945.
154. Obst, S., Kastowsky, M., and Bradaczek, H. (1997) Molecular dynamics simulations of six different fully hydrated monomeric conformers of Escherichia coli re-lipopolysaccharide in the presence and absence of Ca2+, *Biophysical Journal 72*, 1031-1046.
155. Ohto, U., Fukase, K., Miyake, K., and Satow, Y. (2007) Crystal structures of human MD-2 and its complex with antiendotoxic lipid IVa, *Science 316*, 1632-1634.
156. Zidek, L., Novotny, M. V., and Stone, M. J. (1999) Increased protein backbone conformational entropy upon hydrophobic ligand binding, *Nat Struct Biol 6*, 1118-1121.
157. Opal, S. M., and Cohen, J. (1999) Clinical gram-positive sepsis: does it fundamentally differ from gram-negative bacterial sepsis?, *Crit Care Med 27*, 1608-1616.
158. Girardin, S. E., Boneca, I. G., Carneiro, L. A. M., Antignac, A., Jehanno, M., Viala, J., Tedin, K., Taha, M. K., Labigne, A., Zahringer, U., Coyle, A. J., Bertin, J., Sansonetti, P. J., and Philpott, D. J. (2003) Nod1 detects a unique muropeptide from Gram-negative bacterial peptidoglycan, *Science 300*, 1584-1587.
159. Girardin, S. E., Travassos, L. H., Herve, M., Blanot, D., Boneca, I. G., Philpott, D. J., Sansonetti, P. J., and Mengin-Lecreulx, D. (2003) Peptidoglycan molecular requirements allowing detection by Nod1 and Nod2, *J Biol Chem 278*, 41702-41708.
160. Heinzmann, S., Entian, K. D., and Stein, T. (2006) Engineering Bacillus subtilis ATCC 6633 for improved production of the lantibiotic subtilin, *Appl Microbiol Biotechnol 69*, 532-536.

161. Seo, H. S., Cartee, R. T., Pritchard, D. G., and Nahm, M. H. (2008) A new model of pneumococcal lipoteichoic acid structure resolves biochemical, biosynthetic, and serologic inconsistencies of the current model, *J Bacteriol 190*, 2379-2387.
162. Delaglio, F., Grzesiek, S., Vuister, G. W., Zhu, G., Pfeifer, J., and Bax, A. (1995) NMRPipe: a multidimensional spectral processing system based on UNIX pipes, *J Biomol NMR 6*, 277-293.
163. Marintchev, A., Frueh, D., and Wagner, G. (2007) NMR methods for studying protein-protein interactions involved in translation initiation, *Methods Enzymol 430*, 283-331.
164. Dunning, F. M., Sun, W., Jansen, K. L., Helft, L., and Bent, A. F. (2007) Identification and mutational analysis of Arabidopsis FLS2 leucine-rich repeat domain residues that contribute to flagellin perception, *Plant Cell 19*, 3297-3313.
165. Markwick, P. R., Malliavin, T., and Nilges, M. (2008) Structural biology by NMR: structure, dynamics, and interactions, *PLoS Comput Biol 4*, e1000168.
166. Santoro, M. M., Liu, Y., Khan, S. M., Hou, L. X., and Bolen, D. W. (1992) Increased thermal stability of proteins in the presence of naturally occurring osmolytes, *Biochemistry 31*, 5278-5283.
167. Matthews, S. J., and Leatherbarrow, R. J. (1993) The use of osmolytes to facilitate protein NMR spectroscopy, *J. Biomol. NMR 3*, 597-600.
168. Henzler-Wildman, K. A., Lei, M., Thai, V., Kerns, S. J., Karplus, M., and Kern, D. (2007) A hierarchy of timescales in protein dynamics is linked to enzyme catalysis, *Nature 450*, 913-916.
169. Cordier, F., and Grzesiek, S. (2002) Temperature-dependence of protein hydrogen bond properties as studied by high-resolution NMR, *J Mol Biol 317*, 739-752.
170. Krishna Mohan, P. M., and Hosur, R. V. (2007) NMR insights into dynamics regulated target binding of DLC8 dimer, *Biochem Biophys Res Commun 355*, 950-955.
171. Frederick, K. K., Marlow, M. S., Valentine, K. G., and Wand, A. J. (2007) Conformational entropy in molecular recognition by proteins, *Nature 448*, 325-329.
172. Wang, M., Prorok, M., and Castellino, F. J. (2010) NMR backbone dynamics of VEK-30 bound to the human plasminogen kringle 2 domain, *Biophys J 99*, 302-312.
173. Bahar, I., Lezon, T. R., Yang, L. W., and Eyal, E. (2010) Global dynamics of proteins: bridging between structure and function, *Annu Rev Biophys 39*, 23-42.
174. Gillespie, J. R., and Shortle, D. (1997) Characterization of long-range structure in the denatured state of staphylococcal nuclease. I. Paramagnetic relaxation enhancement by nitroxide spin labels, *J Mol Biol 268*, 158-169.
175. Carlomagno, T. (2005) Ligand-target interactions: what can we learn from NMR?, *Annu Rev Biophys Biomol Struct 34*, 245-266.
176. Battiste, J. L., and Wagner, G. (2000) Utilization of site-directed spin labeling and high-resolution heteronuclear nuclear magnetic resonance for global fold determination of large proteins with limited nuclear overhauser effect data, *Biochemistry 39*, 5355-5365.

177. Jahnke, W. (2002) Spin labels as a tool to identify and characterize protein-ligand interactions by NMR spectroscopy, *Chembiochem 3*, 167-173.
178. Jain, N. U., Venot, A., Umemoto, K., Leffler, H., and Prestegard, J. H. (2001) Distance mapping of protein-binding sites using spin-labeled oligosaccharide ligands, *Protein Science 10*, 2393-2400.
179. Albright, S., Agrawal, P., and Jain, N. U. (2009) NMR spectral mapping of Lipid A molecular patterns affected by interaction with the innate immune receptor, *Biochemical and Biophysical Research Communications 378*, 721-726.
180. Bretscher, L. E., Buchaklian, A. H., and Klug, C. S. (2008) Spin-labeled lipid A, *Anal. Biochem. 382*, 129-131.
181. Molinaro, A., Silipo, A., Lanzetta, R., Parrilli, M., Malvagna, P., Evidente, A., and Surico, G. (2002) Determination of the structure of the lipid a fraction from the lipopolysaccharide of Pseudomonas cichorii by means of NMR and MALDI-TOF mass spectrometry, *European Journal of Organic Chemistry*, 3119-3125.
182. Murphy, R. C., Raetz, C. R. H., Reynolds, C. M., and Barkley, R. M. (2005) Mass spectrometry advances in lipidomica: collision-induced decomposition of Kdo(2)-lipid A, *Prostaglandins & Other Lipid Mediators 77*, 131-140.
183. Janzen, E. G. (1972) ESR studies of thermal decomposition mechanisms. II. Electron spin resonance study of the SO2- formation in the thermal decomposition of sodium dithionite, sodium and potassium metabisulfite, and sodium hydrogen sulfite, *J. Phys. Chem. 76*, 157-162.
184. Rogacheva, S. M., Kuntcheva, M. J., Panchev, I. N., and Obretenov, T. D. (1995) L-ascorbic acid in nonenzymatic reactions. I. Reaction with glycine, *Z Lebensm Unters Forsch 200*, 52-58.
185. Lalikainen, T., Joslyn, M. A., and Chichester, C. O. (1958) Mechanism of browning of ascorbic acid-citric acid-glycine systems, *J. Agric. Food Chem. 6*, 135-139.
186. Hodgson, W. G., Neaves, A., and Parker, C. A. (1956) Detection of free radicals in sodium dithionite by paramagnetic resonance, *Nature (London, U. K.) 178*, 489.
187. Cavanagh, J., Fairbrother, W. J., Palmer III, A. G., Rance, M., and Skelton, N. J. (2007) *Protein NMR spectroscopy : principles and practice*, 2nd ed., Academic Press, Amsterdam ; Boston.
188. Hackley, V. A., and Clogston, J. D. (2011) Measuring the hydrodynamic size of nanoparticles in aqueous media using batch-mode dynamic light scattering, *Methods Mol Biol 697*, 35-52.
189. Tidswell, M., Tillis, W., Larosa, S. P., Lynn, M., Wittek, A. E., Kao, R., Wheeler, J., Gogate, J., and Opal, S. M. Phase 2 trial of eritoran tetrasodium (E5564), a toll-like receptor 4 antagonist, in patients with severe sepsis, *Crit Care Med 38*, 72-83.

APPENDICES

A.1 ^{1}H and ^{13}C NMR ASSIGNMENTS FOR *Escherichia coli* Kdo_2-LIPID A

Table A1. ^{1}H and ^{13}C NMR assignments for *E. coli* Kdo_2-Lipid A

Resonance	Assignment (ppm)[a]	
	^{1}H	^{13}C
C1-H1	5.22	95.31
C2-H2	3.89	53.22
C3-H3	4.99	75.24
C4-H4	3.42	68.76
C5-H5	3.92	72.65
C6-H6a/b	3.81/3.60	69.4
C1'-H1'	4.34	103.08
C2'-H2'	3.63	55.16
C3'-H3'	4.89	74.59
C4'-H4'	3.73	73.94
C5'-H5'	3.3	74.5
C6'-H6'	3.68/3.50	64.88
K1C2-K1H2a/b	1.53/1.88	36.39
K1C3- K1H3	3.72	72.68
K1C4- K1H4	3.53	65.52
K1C5- K1H5	3.56	71.48
K1C6- K1H6	3.68	67.47
K1C7- K1H7	3.49	64.96
K2C2-K2H2	1.71	35.09
K2C3- K2H3	3.89	69.41
K2C4- K2H4	3.9	65.52
K2C5- K2H5	3.57	72.65
K2C6- K2H6	3.47	75.89
K2C7- K2H7	3.30/3.58	63.58
Acyl chains		
αI	2.08	44.8
αII	2.18	44.16
αIII	2.31	42.86
αIV	2.1	37.03

αV	2.48	40.92
αVI	2.09	35.09
βI	3.67	70.7
βII	3.72	71.35
βIII	4.94	72.65
βIV	1.31	26.67
βV	4.97	71.33
βVI	1.37	25.38
γI	1.19	38.33
γII	1.26	38.98
γIII	1.32	35.74
γIV	1.06	26.67
γV	1.4	36.39
γVI	1.18	27.32
$(CH_2)n$	1.01, 1.04, 1.05	24.08, 34.44, 30.56
$Ω(-CH_3)$	0.65	15.02

a ^{1}H and ^{13}C chemical shifts at 17 ºC in $CDCl_3$:CD_3OD:D_2O (2:3:1, v/v) relative to DSS.

A.2 WESTERN BLOT PROCEDURES FOR ANALYSIS OF *Pichia pastoris* EXPRESSED SOLUBLE CD14

For western blot analysis pure sCD14 samples (~1 μg) were mixed with 2x SDS sample buffer and boiled for 10 minutes. A 15-well Novex 18% tris–glycine gel (Invitrogen, Carlsbad, CA) was then loaded in duplicate with 15 μl/well of boiled sCD14 sample, and 8 μl/well of pre-stained broad range protein molecular weight (Promega, Madison, WI). The gel was then run in tris-glycine SDS running buffer at 125 V for 90 minutes at 4 ºC, using a SureLock Xcell mini-cell electrophoresis unit (Invitrogen). After the separation, half the gel was stained in Coomassie-blue overnight, and de-stained the following morning. The other half of the gel was transferred overnight onto a PVDF membrane (Pierce, Rockford, IL) at 4 ºC using the Xcell II blotting module (Invitrogen) with a constant current of 25 V. All buffers used in the separation and transfer steps were prepared following the Invitrogen's recommendations, the lone exception being the tris-glycine transfer buffer was prepared containing only 10% methanol rather than the standard 20%. The transfer of higher weight molecular proteins onto the PVDF membrane was significantly improved by reducing the methanol content of the transfer buffer.

Following the transfer the PVDF membrane was incubated in blocking buffer, 5% powdered milk in TBST (10 mM Tris (pH 7.4), 150 mM NaCl, 0.1% Tween-20), for 1 hour at room temperature. The membrane was washed three times with 25 ml of TBST, and then incubated for three hours in 8 ml of blocking buffer containing the monoclonal CD14 antibody MEM-18 (Abcam, Cambridge, MA), diluted 1:1000. This was followed

by two 15 minute, 25 ml TBST washes, next 8 ml of blocking buffer containing a 1:2000 dilution of the secondary antibody, anti-mouse IgG conjugated to horseradish peroxidase (HRP) (Abcam). The membrane was incubated in the secondary antibody for 1 hour. After three 25 ml washes in TBST the blot was either developed using the colorimetric reagent metal-enhanced DAB (Pierce) or was developed in SuperSignal West Pico chemiluminescent substrate (Pierce), and visualized by exposing the membrane to x-ray film. Both development reagents were used per the manufacturer's directions.

An alternative single antibody development procedure followed the same development steps, but required no secondary antibody incubation, and skips straight to the washing and visualization steps after the primary antibody incubation. This abbreviated protocol used a monoclonal anti-6xHis tag antibody directly conjugated to HRP (BD Bioscience, San Jose, CA). After the transfer and two TBSt wash steps, the membrane was incubated for 1 hour in 8 ml of anti-6xHis tag antibody diluted 1:300 in blocking buffer. Visualization of the blot was carried out as described above.

Alternatively, the PVDF membrane was developed using Millipore's Snap i.d. system. The Snap i.d. was used following the manufacturer's directions, the membrane was blocked using 30 ml of 0.5% powdered milk in TBST, and incubated for 10 minutes in 3 ml of MEM-18, diluted 1:2500 in blocking buffer, followed by a 30ml wash with TBST, and a 10 minute incubation with 3 ml of anti-mouse IgG conjugated to HRP, diluted 1:5000. The anti-6xHis-HRP conjugated antibody was diluted 1:800 in 3 ml of 0.5% powdered milk blocking buffer. Final visualization of the blot was carried out as described above using either the metal-enhanced DAB or the SuperSignal

chemiluminescent substrate.

VITA

Seth Andrew Albright, the son of Steve and Peggy Albright, was born in Knoxville, TN, on July 31, 1980. He graduated from Central High School in Knoxville in 1999. In May of 2003 he graduated from Carson Newman College in Jefferson City, Tennessee with a Bachelor of Arts in Biology. In August of 2004 he graduated with a Bachelor of Science in Biology with a concentration in Biochemistry, Cellular, and Molecular Biology (BCMB) from the University of Tennessee in Knoxville, Tennessee.

Seth was accepted to the BCMB graduate in the Fall of 2004, and joined the laboratory of Dr. Nitin Jain in April of 2005 where he applied the techniques of nuclear magnetic resonance to the innate immune receptor CD14 and its ligands lipopolysaccharide and lipoteichoic acid. In 2007 Seth was awarded a Joint Institute of Neutron Science graduate fellowship. In 2010 he won 2nd prize in the University of Tennessee Sigma Xi presentation competition, and was the recipient of the UT Knoxville, Science Alliance Award, Outstanding Scholarly Achievement by a Graduate Student. He was also involved in creation of a novel minimal expression media for the isotopic labeling of proteins in yeast systems for nuclear magnetic resonance studies, which is currently under patent consideration, and being marketed by the UT Research Foundation.